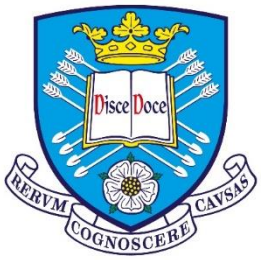

The University Of Sheffield.

Development of Magnesium Silicate Hydrate Binder System with the Addition of Alkali Carbonates

by

Han Zhao

A thesis submitted in fulfilment of the requirements for the degree of

Doctor of Philosophy

Department of Materials Science and Engineering

University of Sheffield

August 2023

Abstract

Portland cement is currently the most common globally used cement, responsible for most of the carbon dioxide emission in cement industries. Magnesium cement may become a potential alternative to the Portland cement, especially for some specific applications, and offers solutions to mitigate the carbon dioxide emission in traditional cement industries by reducing the energy requirements. One of the magnesium cement types is the magnesium silicate hydrate (M-S-H) cement. It obtains strength from M-S-H gel which corresponds to the calcium silicate hydrate (C-S-H) in the Portland cement. However, currently the application of M-S-H cement for construction is limited by its long setting time and relative insufficient strength at early stage. Thus, the development of the M-S-H gel needs to be investigated.

This project aims to investigate the development of the M-S-H gel, in order to obtain a reliable and feasible methodology to develop the M-S-H cement for general applications with acceptable period of hardening time. The effects of additives are studied, including sodium bicarbonate ($NaHCO_3$) and sodium carbonate (Na_2CO_3), aiming to change the pH of the system as well as sodium and carbonate ion concentration in the cement at batch preparation stage. The change of the pH is expected to influence the solubility of different materials in the batch, and the evolution of the M-S-H gel is investigated under different conditions. The effects of different ions in the additives are also studied on M-S-H evolution.

The development of the M-S-H gel is first tested by the addition of $NaHCO_3$ and Na_2CO_3 solutions with various concentrations. The obtained results show that the carbonate additives have the ability to aid the reaction, but the reaction rate is affected by the additives concentration to different extent. The maximum acceleration was achieved generally when the concentration equals to the saturation. The addition of $NaHCO_3$ resulted in the formation of intermediate hydromagnesite, which appeared to accelerate the reaction of $Mg(OH)_2$, while this intermediate phase was identified only in a limited amount in the Na_2CO_3 system. The final products are also affected by the concentration of the solutions, that some magnesium carbonate species appear in the $NaHCO_3$ samples when concentration equals to the saturation but disappeared when the concentration is reduced; talc or dolomite may appear in the Na_2CO_3 samples depending on the concentration of Na_2CO_3.

In the next step, alternative raw materials are used to test their feasibility to develop the M-S-H cement. The Mg dross from alloy industries is used as the alternative magnesium source and calcined clay is used as the alternative silicon source in the M-S-H formation. The results indicate that using the Mg dross is able to form M-S-H gel, and the reaction can be accelerated

by the presence of $NaHCO_3$, while the formation of M-S-H gel is limited when using calcined clay in the condition used. Additional phases are presented in final products for both systems due to the impurity contents of the raw materials. The compressive strength of the samples is limited, likely due to the too much water contained in the samples. The results suggest that the addition of the carbonate may also reduce the total strength.

To improve the strength of the M-S-H cement, the effect of water reduction and the effect of superplasticisers are tested in the final step. The M-S-H batches with same composition but different water-to-solid (w/s) ratio are tested. The results suggest that the addition of NaHMP as the superplasticisers effectively reduced the water requirements for making the paste but may retard the reaction. The reduction of water in the cement successfully increased the compressive strength of the cement and can also accelerate the reaction. However, the addition of $NaHCO_3$ may hinder the effect of NaHMP.

Table of Contents

List of Figures

Chapter 2

Chapter 3

Chapter 4

Chapter 5

Chapter 6

Chapter 7

List of Tables

Chapter 3

Chapter 4

Chapter 5

Chapter 6

Chapter 7

Chapter 1. Synopsis

Cement is one of the most important materials in the modern construction applications, and the growing requirements for new buildings increased the demand for this convenient and cost-efficient component of the concrete [1]. In recent years, as the second most used substance in the world after water, cement manufacturing became the largest human-made carbon dioxide emission source [1]. Since the environmental issue associated with the cement industries raised the concern, the industries are seeking solutions to mitigate the carbon dioxide emission [2]. Multiple methods are proposed, including the optimum design mix and production plan, recycling of the materials, heat recovery in the cement plants and so on [1]. The use of alternative cement binders is also motivated [2].

Magnesium silicate hydrate (M-S-H) cement is an alternative product to the Portland cement (PC)-based cementitious systems, which may offer a bright future for the cement industries with less pollution issues. The M-S-H cement requires less energy input than PC during manufacturing and may be able to sequestrate and store the carbon dioxide during their use [1], making the M-S-H cement an eco-friendly cement and potentially becomes carbon neutral. Compared to PC, M-S-H cement is having lower internal pH environment, which is not favoured in reinforced concrete applications where passivation of the steel is less effective, but the lower pH enables M-S-H cement to be used in the applications with aluminium involved for less corrosion issue [2]. Some nuclear waste immobilisation may also find M-S-H cement better than PC, such as the $Mg(OH)_2$-rich Magnox sludges from the U.K. nuclear industry [2].

To date, limited study has been done on the M-S-H cement, and its application is mainly constrained by its very slow setting time at ambient temperatures. To scale up for commercial application of M-S-H as a cementitious material, the potential improvements in mechanical properties and setting time are significant.

The main aim of this thesis is attempted to establish an effective and feasible method for M-S-H formation by changing the composition of the cement batches, and improve the behaviour of the M-S-H cement. Alkali carbonate solutions are investigated as the reaction accelerator in this thesis work, and the acceleration mechanism is discussed. The mechanical behaviour of the M-S-H cement with the presence of carbonate and superplasticisers are also studied. Furthermore, alternative raw materials are applied to the system and the corresponding reactions are investigated, such study can help to reduce the production cost of the M-S-H cement and reduce the overall carbon footprint of the industries.

Chapter 2 will outline the general information of the M-S-H cement currently available in the literature, including the structure of the binder phase, the advantages of the M-S-H cement and possible applications. The reaction mechanisms of the M-S-H are also discussed with the special interest in the effect of different additives in the M-S-H cement system.

Chapter 3 presents a preliminary investigation of the M-S-H cement formation, testing the effect of sodium bicarbonate ($NaHCO_3$) additive. This will include the comparison between samples with or without the additives, hypothesis of the acceleration effect of $NaHCO_3$ is also proposed.

Chapter 4 discusses the acceleration effects of $NaHCO_3$ on the M-S-H formation further, with a focus on the concentration of $NaHCO_3$. The mechanism of acceleration is further investigated, with an attempt to identify the optimal concentration of $NaHCO_3$.

Chapter 5 investigates the effects of Na_2CO_3 with various concentrations on the M-S-H formation. Because of high solubility of Na_2CO_3 in water, this system allows to study a wider concentration range of sodium and carbonate ions. This chapter, together with Chapter 4, assesses the performance of the additives and study the reason of the acceleration.

Chapter 6 investigates the formation of M-S-H gel by using alternative materials, including Mg dross from alloy industries and metakaolin obtained from natural clay. Using such materials help the sustainable development of the cement industries and potentially reduce the production cost.

Chapter 7 examines the strength development of the M-S-H cements by varying the water to solid ratio and the addition of superplasticizers. It is important to produce M-S-H cement with adequate strength and fluidity. This chapter will investigate the formation of M-S-H with different batch compositions, and examine their effects on the compressive strength.

Chapter 8 contains a series of concluding remarks, and suggestion for future work for commercial application of the M-S-H cement.

Chapter 2: Literature Review

2.1 Overview of the production of cement

Cement is one of the most important construction materials in human activities, large quantity of cement is consumed annually, making the cement industry becomes the largest employer of carbonate decomposition and responsible for 8% of human-made world carbon dioxide emissions [3, 4]. The carbon dioxide emission is mainly generated from two aspects regarding to the cement production. The first aspect is the thermal decomposition process of the carbonate compounds to produce the raw materials for cement production, for example, the calcination of the calcium carbonate ($CaCO_3$) to produce magnesia (CaO) in the Portland cement manufacture process. The by-product of the thermal decomposition, carbon dioxide, directly proportioned to the amount of carbon oxide produced by the industries [3]. The second aspect of carbon dioxide emission is the combustion of the fossil fuels to generate the energy used to heat the materials to specific temperature (usually around 1500°C) [5], which enables the formation of necessary mineral phases, consumes 12%-15% of total industry energy usage [4].

As the environmental problems associated with the greenhouse effect becoming increasingly serious in the recent years, the reduction of the carbon footprint of the cement industries are emphasized. One of the choices is using alternative binders in the Portland cement production to reduce the overall energy cost.

Magnesium based cement may become the possible substitution of the Portland cement to mitigate the carbon dioxide emission of the cement industries, which can be achieved from two aspects. On one hand, the temperature requirement for the production of the main raw materials of magnesium-based cement, magnesia (MgO), is around 650°C, which is much lower comparing to the CaO production in Portland cement manufacture [5]. On the other hand, some of the components in the magnesium based cement may even absorb the carbon dioxide during application which potentially makes the magnesium cement carbon neutral [2]. The ecological benefits of the magnesium-based cement encourage further research on this kind of cement, which may become the sustainable future of cement industry.

Magnesia (MgO) has been used as a cementitious material since hundreds of years ago. The cement industries were historically based on a wide range of materials suitable for local conditions and applications, followed by the predominant utilisation of Portland cement from latter half of 20^{th} century with other materials sidelined [2]. In recent years, the magnesium-

based cement again gets motivated driven by its environmental benefits. MgO can absorb carbon dioxide and form a cementitious material, combining with its low firing temperature, can possibly become “carbon neutral”, which is interested by both academic and commercial [2].

The two major types of Mg-based cements are magnesium phosphate cements and magnesium silicate hydrate (M-S-H) cements. The magnesium phosphate cements are commonly produced by reacting ammonium/potassium phosphate with MgO, forming a hardened binder similar to the zinc based phosphate cements [2, 6]. The magnesium phosphate cement is able to set rapidly, can be used for rapid repair of cracked, damaged and pot-holed road surfaces [7, 8]. It can also been described as a prospective encapsulation matrix for general waste streams, especially for the reactive metals unsuitable for conventional Portland cement blends [2, 9]. However, the application of magnesium phosphate cements is constrained by its too-low internal pH values and relatively expensive production cost [2]. The concept for the other major type of Mg-based cements, M-S-H cement, has been existing since 1889 but relatively unresearched for over 50 years, the first major systematic studies of the M−S−H cement was at the late 1980s [2]. The properties of the M-S-H cement will be further investigated in following sections.

2.2 The structure of M-S-H gel

The strength of the M-S-H cement is mainly obtained from its binder phase, M-S-H gel, which corresponding to the calcium silicate hydrate (C-S-H) in the Portland cement. The formation of the M-S-H gel are typically generated by the reaction between magnesium oxide (MgO) and reactive silica (e.g. silica fume) respecting to the formula of $MgO + mSiO_2 + nH_2O \rightarrow MgO{\cdot}mSiO_2{\cdot}nH_2O$ [10]. By the reaction between the magnesium oxide and a soluble source of silica at room temperature, the M-S-H product formed is usually in the form of poorly crystallized gel with Mg/Si ratio vary from 0.25 to 1.5, and the final composition of the product is sensitive to the aging conditions. The local ordering of the formed M-S-H gel will be improved with the higher aging temperature and longer aging time [2, 10-14]. Water is also able to be bounded with the M-S-H gel physically, which its amount strongly dependent on the relative humidity of the environment and the drying methods [15].

Although M-S-H and C-S-H gel are having similar compositions, their chemical are studied in detail and showing they are incompatible [16]. It is not applicable to produce the M-S-H cement by simply substitute the CaO with the MgO in existing Portland cement industries. The comparison of the respective (MgO, CaO)−Al_2O_3−SiO_2 ternary phase diagrams are presented in Figure 1, showing distinct chemistry and phase formation [2]. Specifically, the circled region

in Figure 1 (b), showing the key hydraulic phases in Portland cement, is not having magnesian analogues in the same position at Figure 1 (a). Therefore, different starting materials and processing design will be required for the development of M-S-H cement.

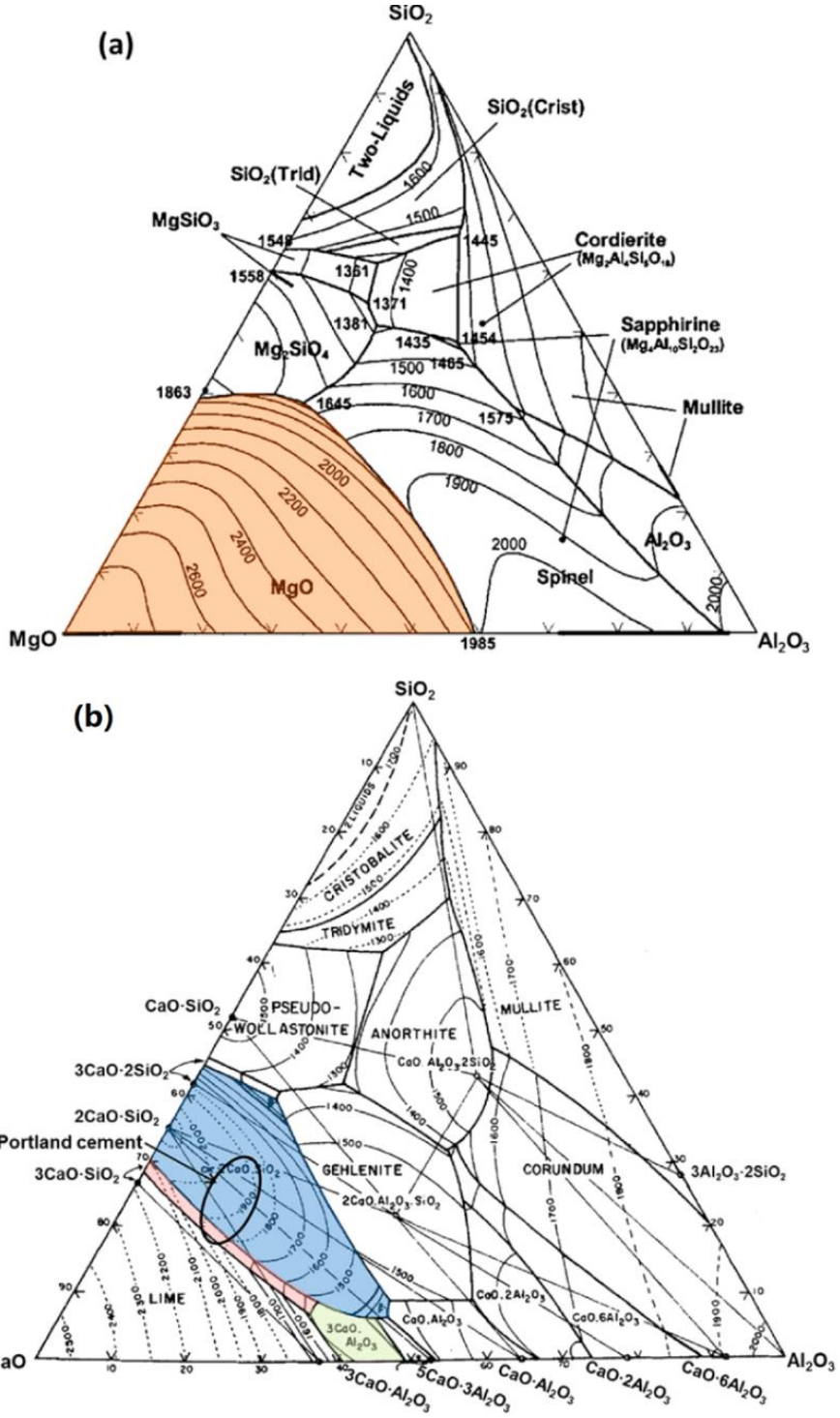

Figure 1. Ternary phase diagrams, in units of weight percent, for the systems (a) $MgO–SiO_2–Al_2O_3$ and (b) $CaO–SiO_2–Al2O_3$ [2].

It is reported that in the Magnesium-rich environment, the raw materials mixture in the MgO-SiO_2 system is able to form a cryptocrystalline solid with maximum Mg/Si ratio of 1.5. This product is able to be process continuing to react with the residual silica in the system, form solids with progressively lower magnesium content down to the Mg/Si ratio equal to that of the initial mixture [17]. However, the excess MgO content, which amount exceed the 1.5 Mg/Si ratio, will appear as brucite in the system when water is enough, while unreacted silica will remain in the solution when Mg/Si ratio is smaller than the lower limit [10, 17, 18].

The M-S-H synthesised at room temperature is showing a poorly crystalline structure containing a series of silicate sheets. The interlayer distance between silicate sheets is relatively large when synthesised at ambient temperature but able to be reduced with the elevated temperature. The interlayer distance will also be smaller at high Mg/Si ratio compared to low Mg/Si ratio [10]. The arrangement of the silicates are in tetrahedral layers with the magnesium in the octahedral layers comparable to 2:1 or 1:1 phyllosilicates, the schematically drawing of the structure is presented in Figure 2 [19], the poorly ordered structure of M-S-H has been related to sepiolite ($Mg_4Si_6O_{15}(OH)_2 \cdot 6H_2O$), hydrated nanoparticles of talc ($Mg_3Si_4O_{10}(OH)_2$), hydrated talc or hydrated antigorite ($(Mg, Fe)_3Si_2O_5OH_4$), lizardite ($Mg_3(Si_2O_5)(OH)_4$), stevensite ($(Ca,Na)_xMg_{3-x}(Si_4O_{10})(OH)_2$) or saponite ($Ca_{0.25}(Mg,Fe)_3((Si,Al)_4O_{10})(OH)_2 \cdot n(H_2O)$).

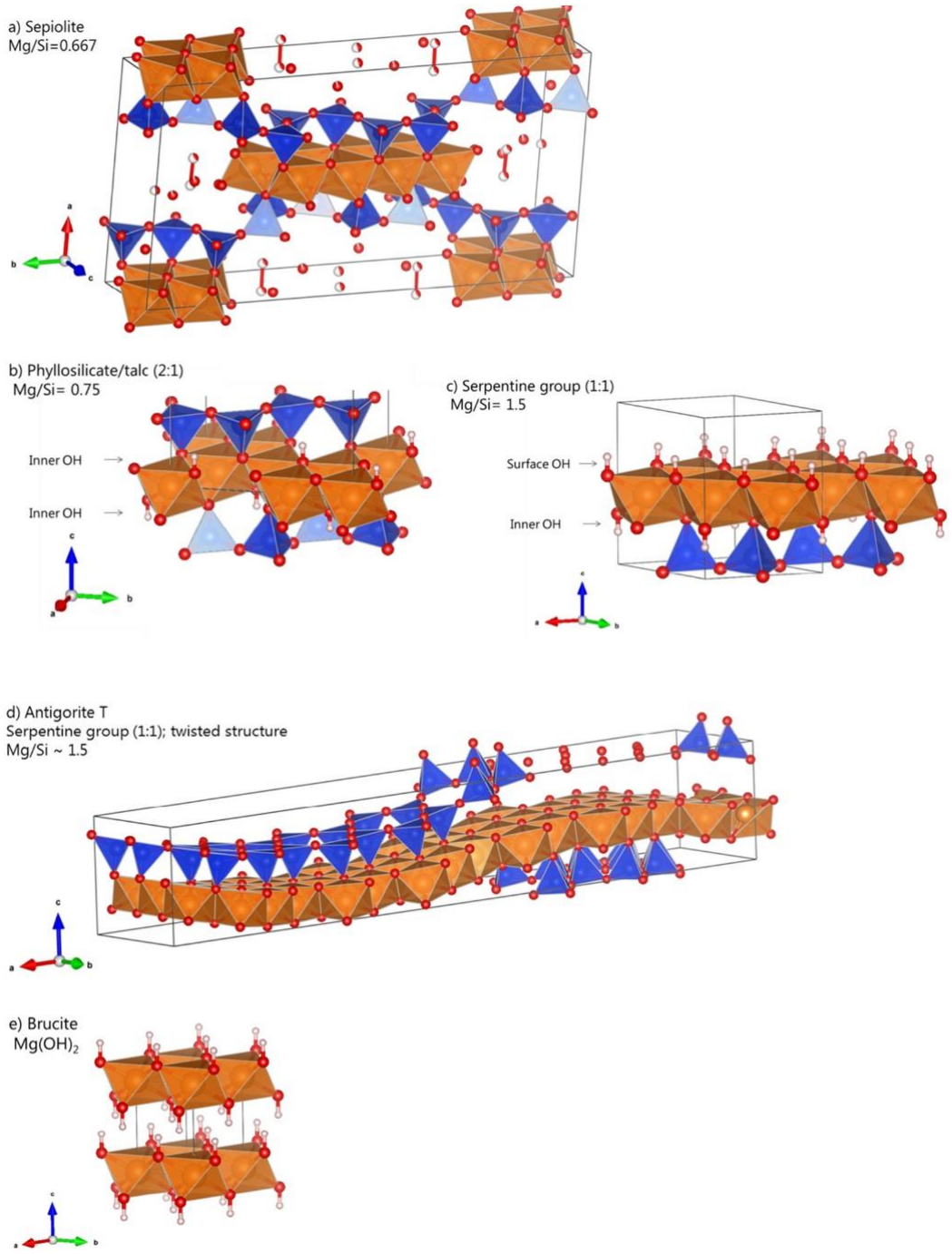

Figure 2. Schematic sketches of the structure of (a) sepiolite; (b) 2:1 phyllosilicates structure (talc); (c) 1:1 phyllosilicate structure (serpentine group); (d) antigorite; (e) brucite. (orange: octahedral magnesium site, blue: tetrahedral silicate site, red: Oxygen).

The M-S-H gel is having negative surface charge due to its deprotonated silanol groups at the edges and/or in vacancies of the silicate layers, increase in pH will cause a more negatively charged surface as more silanol groups are deprotonated. The negative charge makes the gel potentially able to absorb cation ions in the absence of alkalis and absorption amount is increasing at higher pH values. Some of the alkalis may also be replaced by the absorbed

cations at exchangeable sites. However, the negatively charged surfaces will hinder the growth or assembly of the M-S-H sheets. In addition, the absorption is only present at the surface or interlayer of M-S-H but not significant within the magnesium and silicate sheets, in the absence of other alkali, only approximately 2% of the total magnesium was bound at the exchangeable sites, which indicates the absorption amount may be small [20].

There are two phases of M-S-H after aging in the temperature range of 100°C-300°C, which are $3MgO_2{\cdot}SiO_2{\cdot}2H_2O$ (phase I) and $3MgO{\cdot}4SiO_2{\cdot}H_2O$ (phase II) [18]. This phase I is a white, powdery and hydrophilic material. And phase II is a white, loose powder, waxy and hydrophobic material. Phase I can be formed by reagents over a wide range of Mg/Si ratios, as long as both components are present. It is formed more readily when the temperature is lower than 200°C (100°C-200°C). When phase I is under heating, it starts to loss structural water in the temperature range between 550°C to 600°C, and then a metastable amorphous phase can be present. As the temperature increased above 600°C, the crystallinity of the product will be improved and forsterite ($2MgO{\cdot}SiO_2$) can be detected readily by using X-ray diffraction measurements. The enstatite ($MgO{\cdot}SiO_2$) starts to appear when the temperature is increased to 750°C. The proportion of enstatite to forsterite keep increasing with the temperature up to 1000°C and the quantity of amorphous silica remained in the system reduced accordingly, which indicates that the enstatite was formed as the result of the solid-state reaction between the forsterite and the amorphous silica. Phase II can be prepared in well-characterised form only when the Mg/Si ratio of the precursor is less than 1.5. It is more easily to be formed when the temperate is in the range of 200°C -300°C. The crystal lattice of phase II will be broken down when temperature is above 890°C -900°C with the simultaneous releasing of structural water, while enstatite and α-cristobalite (polymorph of silica) starts to form correspondingly. [18]

2.3 The applications of magnesium silicate hydrate cement

The varied properties of different types of cements enable them to gradually replace the general-purpose Portland cement in different utilisations. M-S-H cement is one of the magnesium-based cements which are potentially able to substitute the Portland cement in some application areas. M-S-H cements are having low corrosiveness, high temperature resistance, good surface gloss, low internal pH, light weight and good mechanical properties. A wide range of applications of the M-S-H cement has been studied recently, including contaminant immobilisation, metal-containing waste treatment, refractory castable, as well as construction materials [14, 15, 21, 22].

Other than general construction applications, cements are currently widely used for waste encapsulation [23]. The advantage of using magnesium-based cements as substitution for encapsulation of some specific kind of wastes is that it can provide better stability and integrity. As some of the nuclear wastes already contained magnesium element in them, the waste itself is able to form stable matrix for encapsulation, which helps to save the space for external cement matrix and achieve higher integrity. For example, the UK nuclear waste Magnox sludge already embodied magnesium oxide in the waste, which is able to react with the reactive silica directly to form hardened M-S-H cement matrix [24].

The substitution of Portland cement into M-S-H cement also brings advantages in durability due to the high resistance of the hydration and carbonation in aggressive environment. It can also provide a relative low pH environment compared to Portland cement and having low sensitivity to impurities, enabling the utilization of waste and by-products from industrial. These advantages make M-S-H cement ideally to be used as the immobilisation agent for the disposal of heavy metal wastes [22, 25]. For Portland cement, the relatively high pH values of the pore solution may cause the passivating or corrosion of metal inside the cement, which either be used as supporting matrix or the waste capsulated. For comparison, the lower pH environment of the M-S-H cement will cause less corrosion, since the solubility of most of the heavy metals is low at the pH range of M-S-H cement. This effect potentially able to mitigate the corrosion of the heavy metals which used as supporting matrix or contained in the waste, and hence increase the long-time durability of concrete and extend the usage time [26]. Moreover, this relatively low pH environment of the M-S-H cement facilitates aluminium being in the passive state, so that the aluminium will not get corrode to the same degree as it would when traditional Portland cement is used [27, 28]. The relatively low pH values of the M-S-H cement can also help to reduce the dissolution of the clays in construction materials and improve overall cement–clay compatibility and the overall stability [2].

However, certain limitations regarding to the manufacture and implementation of the M-S-H cement also exist, which include the unfamiliarity, insufficient documentation and record of reliability, low market confidence compared to existing high validation Portland cement, relatively low availability of the raw materials and proximity to the existing production facilities [25]. Moreover, for both construction and waste encapsulation applications of the cement, the early strength and setting time are often taken into consider, usually a short setting time and high early strength are desired, but the application of M-S-H cement is highly restricted by its slow setting time at room temperature, which may require 28 days to reach 130 Mpa compressive strength [29]. This relatively low setting time is not favoured in the construction applications but it is desired for nuclear applications, providing enough strength are reached under 48 hours [2].

The information of the structure and properties of the M-S-H gel is also limited due to it is a relative new kind of material. However, the approved properties for M-S-H gel show it has a good heat resistant up to 1500°C and relatively good compression resistance (up to 130 Mpa), which makes the M-S-H cement potentially useful for construction of refractory purposes. [30, 31].

2.4. The formation of the M-S-H cement

2.4.1 Formation mechanism of M-S-H

By using magnesia and silica fume as the starting materials, the overall process of the reaction can be concluded into four steps. Firstly, the MgO will dissolve and $Mg(OH)_2$ will formed while OH^- and Mg^{2+} will appear in the solution. The presence of OH^- will encourage the dissolution of the silica source into silicate ions, and the formation of M-S-H will be carried out by the charge transfer, which is the exchange of basic hydroxide and acidic oxide [32]. After the silica dissolved, the Mg^{2+} ions will be able to react with the hydrated silica to form the M-S-H gel. At last, the consumption of Mg^{2+} ions and silicate ions will promote the dissolution of brucite and silica continuously and progress the reaction until all raw materials are completely reacted [14].

In this project, the starting materials used is brucite (Magnesium hydroxide, $Mg(OH)_2$) instead of the lime (Magnesium oxide, MgO). The commercial supplied MgO powders are usually containing some proportion of calcium oxide (CaO) as impurity, which able to form C-S-H with the silica source and may also change the pH of the cement solution strongly. The undesired CaO can therefore affect the reactions in the cement solution and influence the observation of the formed M-S-H gel [26]. Also, the use of MgO as starting material for M-S-H formation will need extra time for the brucite formation at first, and then the formed brucite will be able to encourage the formation of M-S-H gel [14]. Thus, in the aspect of shorten M-S-H gel formation period, using brucite as starting material directly could be a better choice. Another concern of using lime as starting material is the production method of the lime is not eco-friendly. The common method for lime production in industries usually involves the thermal decomposition of magnesium carbonate minerals, which requires external heat and approximately 52 wt% of the magnesium carbonate will be released in the form of carbon dioxide [33].

It is known that the formation of the M-S-H gel will be affected by the pH value of the reaction solution, the changing of the pH value will change the concentration of different ions in the solution. For the solubility of the magnesium hydroxide, it follows the solubility product of

itself, which $K_{sp} = [Mg^{2+}] [OH^-]^2$. For saturated pure $Mg(OH)_2$ solution, the pH value will be approximately close to 10.5. When pH value of the cement solution is lower than 10.5, the concentration of OH^- is relatively low, the amount of Mg^{2+} ions in the solution will be able to increase and the solubility of the brucite will be high. The high concentration of the Mg^{2+} ions in the solution will able to promote the formation rate of the M-S-H gel [34].

The solubility of silica will also be affected by the changing of the pH simultaneously. The formation rate of the M-S-H gel will be depressed when the concentration of the dissolved silicate ions is not sufficient compared to the Mg^{2+} ions [15].

When pH value of the solution is above 9, the silicon atoms are able to be ionised into $SiO(OH)^{3-}$ and $SiO_2(OH)_2^{2-}$, and then the anions formed will be able to react with the metallic cation in the solution [21]. The solubility of the silica will be determined by the concentration of OH^- per unit surface area of silica, that the bonding between the silicon and oxygen atoms will be weaken by the attached OH^- ions [35]. Therefore, at higher pH values, the solution is having higher OH^- ions concertation and hence increase the solubility of the silica. The solubility of the silica is able to increase from 138 (mg/L) to 876 (mg/L) when the pH value change from 9 to 10.6 [21]. The higher solubility can also be achieved without changing the pH by increasing the total surface area of the silica, which is usually achieved by using silica source with small particle size.

The reverse behaviour of the solubility of the $Mg(OH)_2$ and silicon would result a balance point between the concentration of Mg^{2+} and silicate ions, which available for the solution to achieve highest reaction rate and/or the Mg-Si ratio. An illustration of the relationship between the solubility of silica and brucite and Mg/Si ratio in the M-S-H gel as a function of pH is shown in Figure 3 [10], the two dashed lines in Figure 3 represents the solubility of amorphous silica and brucite respectively. From the graph it can be seen that when pH value is close to 10, both silica and brucite achieved a relatively high solubility, implies a suitable region for the formation of M-S-H gel.

One example of evolution of pH during M-S-H formation with the changing concentration of Mg^{2+} and hydrated silica is presented in Figure 4 [14]. The pH is raised by the releasing of OH^- from the brucite and then enhance the dissolution of silica, the dissolution of brucite is then hindered and OH^- are consumed so that pH value drops back, finally an equilibrium is achieved during the reaction. The initial present work of this project is trying to control the starting pH value of the cement batches in order to manipulate the formation of the M-S-H gel by the addition of additives.

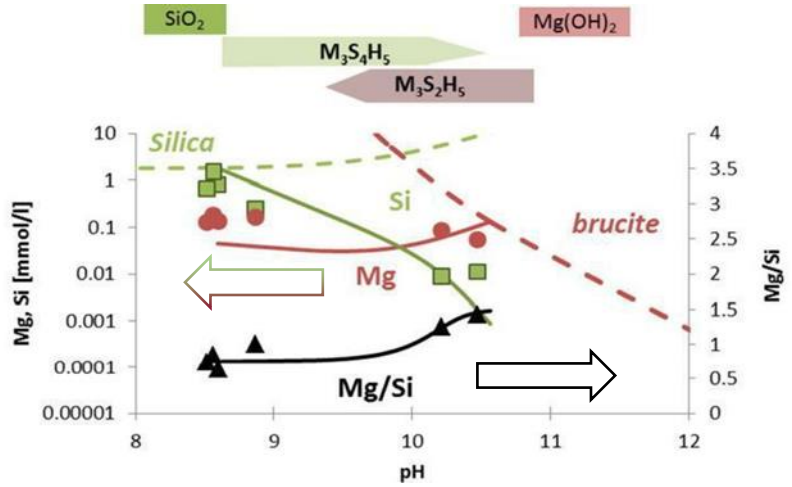

Figure 3. Si (■) and Mg (●) concentrations displayed on the primary y-axis as function of the pH. Mg/Si ratio (◢) displayed on the secondary y-axis. [10] The dashed lines are the solubility of amorphous SiO_2 and brucite.

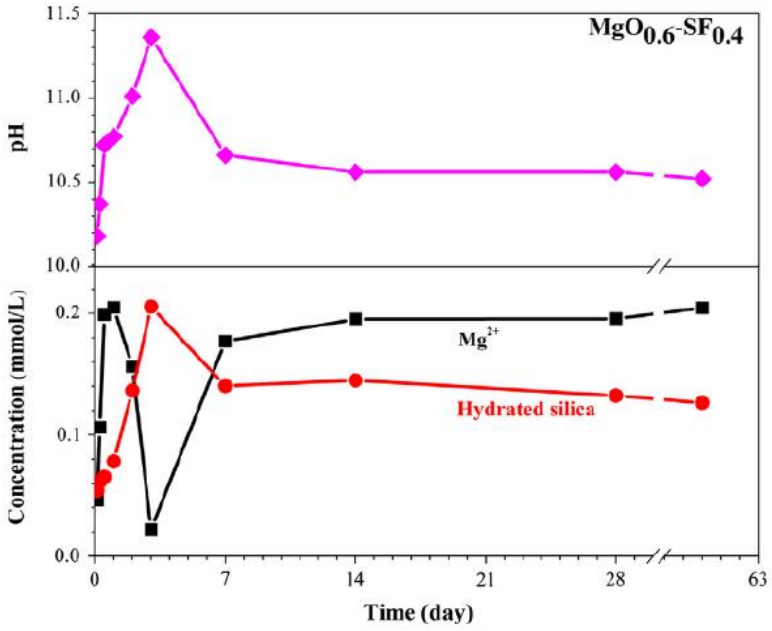

Figure 4. Mg^{2+} and hydrated silica concentrations and the pH evolution of the pore solution of a MgO-Silica fume paste [14].

To control the pH of the cement, and trying to use the cement as source for carbon capture storage, sodium carbonate and sodium bicarbonate are used as the additives to varying the pH of the cement. In previous research, it stated that in MgO – hydrated magnesium carbonate system, the addition of magnesium carbonate will help to accelerate the hydration of MgO

significantly, as well as the strength of the MgO aggregate samples and CO_2 sequestration rates [37]. These results imply the carbonate ions will not impede the formation of the M-S-H gel, but the effect of the sodium ions needs to be investigated further in the project.

However, the hydration of magnesia to form brucite and the dissolution of brucite may retarded by the presence of dissolved silicon. When the concentration of silicon in the solution in high, the dissolution of brucite is hindered, which consequently reduces the concentration of magnesium ions in the solution and limits the formation of M-S-H [13]. Brucite will precipitate on the surface of magnesia and react to form M-S-H, which create a poorly crystalline layer surrounds the magnesia grains and hindered the further hydration process of magnesia [36].

The protection of the magnesia from hydration is beneficial for the refractory castable applications. The refractory materials are able to maintain its magnesia nature, so that maintain the high melting point nature and eliminates the volumetric expansion problems caused by the hydration. M-S-H gel also provides a new binding phase in the refractory castable without any loss of strength or refractory properties. The setting time and flowability can also be influenced by the addition of silica [34].

On the other hand, for the effort of manufacturing M-S-H based cement or concrete, the hydration of the magnesia needs to be fast for a relatively short setting time. To avoid the hinder of the hydration, either using the brucite as the starting materials or add hydrated magnesium carbonates (HMCs) to the precursor can be applied. The addition of the HMCs provides the alternative surfaces for the brucite to be precipitate on, so that the M-S-H gel will have less opportunity to form the shell on the surfaces of magnesia particles [37].

M-S-H gel is also able to form at the surface of the silica particles in the shell shape with cavity. The silica will then be gradually consumed by the diffusion of solution through the M-S-H shell. The growth of the M-S-H gel is in the direction outwards the shell but not filling the gaps between the shell and particles, which may cause the shrinkage of the M-S-H products [15].

The formation rate of the M-S-H gel also depends on the curing temperature of the reaction significantly. For same sets of samples curing at 20°C and 40°C separately, the 20°C curing sample at 30 days shows similar XRD pattern to the 40°C curing sample at 3 days [34]. This phenomenon means that the time required for the formation of M-S-H gel is able to decrease for a factor of 10 at the elevated temperature. The large factor of decreasing in reaction time need to be considered carefully that, although the increasing of the curing temperature will help to save the time cost, some of the early stage reactions may become too short and not

able to be observed in the experiment when the temperature is too high. Also, the increasing temperature may affect the solubility of various raw materials differently and therefore will not linearly influence the formation rate of the M-S-H gel.

2.4.2 The effect of the raw materials

Both brucite and magnesia are able to be used as the precursors for the formation of M-S-H gel, however it is reported that using magnesia as the magnesium source will react with the silica more intensively than using brucite in same ambient conditions [12, 38]. This could be attributed to that the newly formed brucite phases from magnesia hydration is highly reactive due to its relatively large specific surface area, facilitating the formation of M-S-H phases [17, 38].

The properties of magnesia will affect the formation of M-S-H significantly, it is usually produced from the decomposition of magnesium-based minerals or from the precipitation of seawater, well and lake brines [4, 21]. The chemical and physical properties of the magnesia can be grouped into four grades based on its calcination temperature, which are light-burned (700°C -1000°C), hard-burned (1000°C-1400°C), dead-burned (1400°C-2000°C) and fused (over fusion temperature 2800°C). With the increasing of calcination temperature and/or the calcination duration, the specific surface area of the magnesia and distortion of the crystal lattice decreased, and the particle size increased, resulted in decrease in activity of the magnesia but increase in strength, abrasion resistance and chemical stability. Higher activity of magnesia is preferred for the formation of M-S-H, which determined the amount of brucite available for reaction, but properties of magnesia varied significantly even in same grade, it should be take into consideration when making the precursors for M-S-H [21, 39].

As another part of the precursors, the properties of silica are also not consistent. The crystallinity of silica determines the solubility of the amorphous silica in water, which with the increasing in crystallinity its solubility will reduce [39].

The hydration water also has an essential role when the magnesium source is reacted with silica, the brucite is barely react with the silica without the presence of water in the condition of mechanical milling [38]. Water enhances the alkaline nature of the magnesium hydroxide particles' surfaces, helps the dissolution of the silica and encourages the charge transfer between the materials [12].

The impurities in the raw materials can also affect the formation of M-S-H. The pH of the MgO solution can increase to 12.5 by the presence of CaO impurities [26]. Only 0.078 wt% of CaO

will increase the pH of MgO solution from 10.5 to 11.3 at solution density of 100 g/L, which able to affect the dissolution of brucite and silica accordingly [39].

2.4.3 The carbonation of the M-S-H cement

Since water will progressively be used to form the hydration products in the cement, the water content of the cement can cause the presence of porosity after aging. The large water demand of magnesia required for the hydration leads to a relatively high porosity level in the final products, which enables the diffusion of atmosphere gases [25, 40]. The hydration product of magnesia, brucite, is able to be carbonated when expose to CO_2 gas. The CO_2 gas will dissolve in the pore water of the cement and react with the brucite, which forms several hydrated magnesium carbonates (HMCs), including nesquehonite ($MgCO_3 \cdot 3H_2O$), hydromagnesite ($Mg_5(CO_3)_4(OH)_2 \cdot 4H_2O$) and dypingite ($Mg_5(CO_3)_4(OH)_2 \cdot 5H_2O$) etc., a ternary phase diagram of the HMCs is presenting in Figure 5 [41]. The kind of HMCs formed will depend on the carbon dioxide partial pressure, relative humidity, time, and temperature [41].

The formation of HMCs in the magnesium-based cement leads to the permanent sequestration of CO_2 and accompanied with the rapid strength development (increase in the toughness and stiffness). The strength development is gained by reducing porosity of the cement, that converted from brucite to nesquehonite can have a raise in solid volume. Only 5% of CO_2 gas in the atmosphere is sufficient for the cement to reach necessary strength requirement for blocks [4, 25, 42].

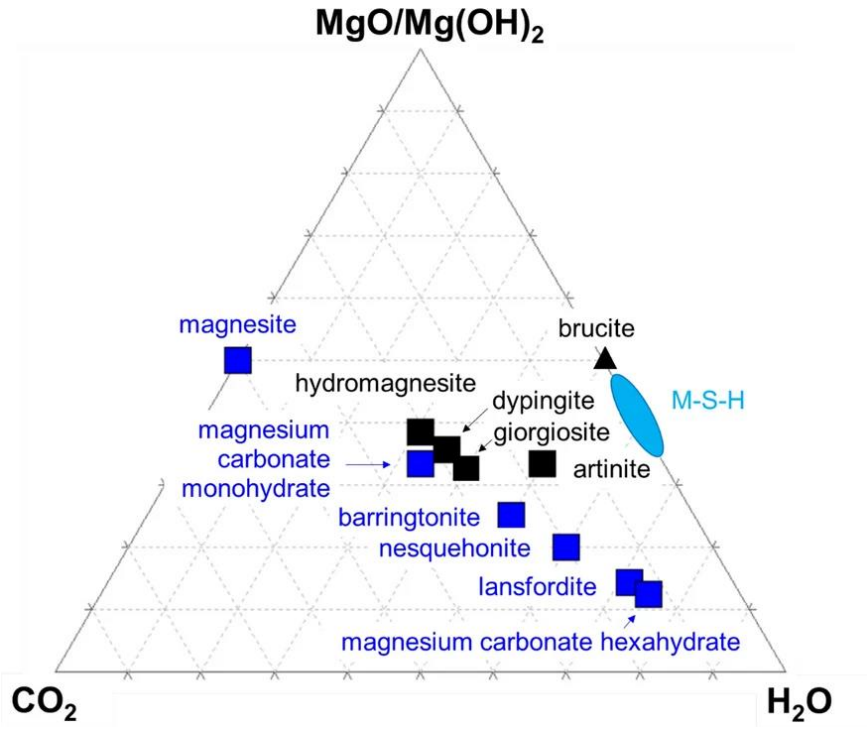

Figure 5. MgO-CO_2-H_2O ternary phase diagram with M-S-H (silica is only present in M-S-H) [41].

2.4.4 The incorporation of aluminosilicates from metakaolin

The synthesis of M-S-H cement are commonly used silica fume as the raw materials due to its relatively high reactivity [15, 41]. However, the cost of silica fume is expensive and alternatives need to be used to scaleup the production of M-S-H cement. Metakaolin is one of the substitutions for the silica fume in cement formation, which has the reactive aluminosilicates phases and having low environmental impact [43].

Reactive alumina and silica are contained in the metakaolin, the binder phase formed between metakaolin, magnesium source and water will possibly become magnesium (alumino-)silicate hydrates (M-(A-)S–H). The M-(A-)S–H phases are hydrated nano-crystalline phyllosilicates with variable Mg/Si and Al/Si ratios, which is having similar structure to M-S-H phases.

Metakaolin is alkali-activated materials, typically requires high pH environment to initiate the reaction. This can be done by adding Na_2CO_3 into the cement batches, which can raise the pH and accelerate the M-S-H formation in same time [44]. A hydrotalcite-like phase can also be formed during the reaction, and at low pH values, less M-A-S-H structure will be formed while more hydrotalcite will be produced [45]. However, the formation of the hydrotalcite like phase can lowering the porosity and improve the mechanical properties of the cement [43, 44].

2.4.5 The addition of superplasticisers

Using of the superplasticisers potentially able to improve the mechanical behaviour of the cement by reducing the water content and thus the porosity of the cement. The application of inorganic phosphate salts into the MgO-Si systems can significantly improve the fluidity of the cement [46].

Sodium hexametaphosphate (Na-HMP) is a hexamer of sodium metaphosphate, and is proved to be effectively used in the M-S-H cement for making the product with high strength [47, 48]. According to the literature, the optimum composition of the Na-HMP used in MgO/SF system is 1 wt.%, which allows the water to solid ratio of the cement down to 0.4 [47]. However, the addition of Na-HMP may inhibit the formation of $Mg(OH)_2$ from MgO.

2.5 literature review conclusion

The M-S-H cement is able to bring advantages in several applications as the substitution of the Portland cement, but currently restricted by its formation limitations. However, due to the amorphous nature of the M-S-H gel, the composition and structure of the M-S-H gel formed at ambient conditions remained unclear. The factors affecting the formation of the M-S-H cement also need to be considered carefully including temperature, pH and aging conditions etc. The materials used for M-S-H formation can be adjust to obtain desired products, making the cement more eco-friendly or cost effective. The overall aim of this project is trying to understand the formation mechanism of the M-S-H cement and establish an effective method to reduce its setting time and improve its compressive strength.

Chapter 3. Acceleration of M-S-H gel formation through the addition of alkali carbonates

Han Zhao, Theodore Hanein, Nabaichuan Li, Abdullah Alotaibi, Ang Li, Samuel Walling, Hajime Kinoshita

This work was presented at 15th International Congress on the Chemistry of Cement and published as the conference paper. Han Zhao is responsible for samples preparation, complete the experimental works, obtaining the data, data analysis.

Abstract

The varied properties of different cements enable the cement industry to shift towards the manufacture of application-specific cements rather than a general-purpose binder. M-S-H cements could offer a good alternative for specialist application, and could potentially have a lower carbon footprint as they require much lower temperatures for their production compared with Portland cement (PC). M-S-H cements harden with M-S-H gel as a binding phase, which is the equivalent of calcium silicate hydrate (C-S-H) gel in PC. However, the development of M-S-H is much slower than that of C-S-H, resulting in insufficient strength development of the product; thus, limiting the applications of M-S-H cement. The present study investigates the effects of an additive to enhance the development of M-S-H gel. Sodium bicarbonate was tested, and its impacts on the evolution of M-S-H gel were studied. The obtained results indicate that sodium bicarbonate has the ability to aid the development of M-S-H by promoting the reaction of $Mg(OH)_2$ and SiO_2, which resulted in the accelerated development of M-S-H gel.

3.1 Introduction

3.1.1 Background

Magnesia-based cements are generally produced from a mixture of magnesium oxide MgO (or hydroxide $Mg(OH)_2$) and reactive silica SiO_2 (e.g. silica fume). Upon reaction with water, the system forms magnesium silicate hydrate (M-S-H) gel as a “binding” phase, which is the equivalent of calcium silicate hydrate (C-S-H) gel in Portland cement.

One of the key challenges for wider application of magnesia-based cements is obtaining the raw material MgO or $Mg(OH)_2$. Although MgO has a much lower firing temperature (~650 °C), compared with the generally employed Portland cement, for its production from MgCO3 in

conventional kilns [5], it is still carbon-intensive because ~52 wt.% of $MgCO_3$ is CO_2 and the reaction is endothermic. $MgCO_3$ is also scarce itself. Further developing carbon-efficient technologies to extract MgO or $Mg(OH)_2$ from these rocks would help to establish magnesia-based eco-cements [33]. Magnesia-based cements can still have a great potential to be used for specialist application, for example, encapsulation of nuclear wastes such as Magnox sludge [24], where the embodied magnesium oxide in the waste can be directly utilised together with reactive silica to form the hardened M-S-H cement matrix; thus, encapsulating the radioactive components without a need of conventional cement matrix. M-S-H gel is also shown to be an excellent material to stabilize the heavy metals in contaminated sediment [49]. These ecological benefits of using magnesia-based cements encourage further research in the field. The application of M-S-H cement is currently restricted by its relatively slow setting time and strength development. Unfortunately, information related to the structure and properties development of M-S-H gel is still limited, as it is a relatively new kind of binder system. Therefore, the present study investigates the effects of additive to in order to enhance the development of M-S-H gel. Sodium bicarbonate is tested, with the positive utilisation of carbonate ions in mind, and their impacts on the evolution of M-S-H gel were studied.

3.1.2 Formation of M-S-H gel

M-S-H is typically formed by the reaction between magnesium oxide, reactive silica (e.g. silica fume), and water: $MgO + mSiO_2 + nH_2O \rightarrow MgO{\cdot}mSiO_2{\cdot}nH_2O$ [10]. The reaction of MgO with a soluble source of silica at room temperature generally forms a gel with a varying Mg/Si ratio [2, 10, 14, 49]. It is known that the pH of the reaction solution can affect the formation of M-S-H gels. The pH of a saturated $Mg(OH)_2$ solution is approximately 11, and the solubility of $Mg(OH)_2$ increases when the pH value is below 11 (Figure 1). This is expected because the solubility of Mg^{2+} ions follows the solubility product constant of $[Mg^{2+}][OH^-]_2$, thus, the solubility of Mg^{2+} ions decreases with increasing alkalinity of the mixture. This implies that lower pH is favourable in terms of Mg contribution to M-S-H formation, as a high Mg^{2+} concentration promotes the formation rate of M-S-H [14]. The solubility of the silica also affects the formation of M-S-H, and the rate of formation is depressed when the concentration of silicate in the solution is not sufficient. The solubility of the silica depends on the concentration of OH^- per unit surface area of silica, and the OH^- ions are able to weaken the bonds between the silicon and oxygen atoms [50]. The solubility of silica increases from 138 mg/L to 876 mg/L when the pH changes from 9 to 10.6 [21]. Therefore, the higher pH is favourable in terms of silica contribution to M-S-H formation. The reverse change in the solubility of $Mg(OH)_2$ and SiO_2 would lead to a balance point between Mg and Si concentrations available to produce M-S-H gel. The dashed lines in Figure 1 [10] represent the solubility of amorphous SiO_2 and brucite. The region of pH ~10 demonstrates a relatively high

solubility both for brucite and silica, which suggest that higher pH than neutral pH=7 is more beneficial for M-S-H formation. In the present work, as a preliminary investigation, the initial pH conditions are varied via the addition $NaHCO_3$ to the distilled water used for the reaction.

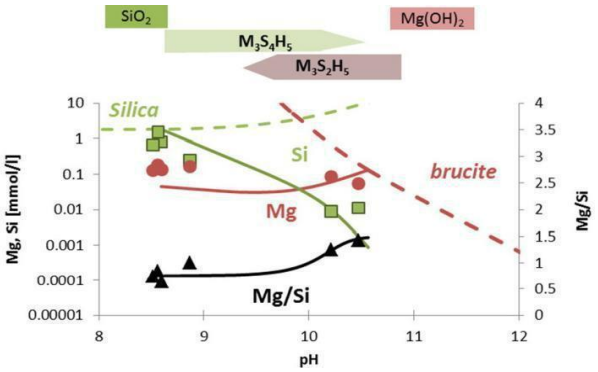

Figure 1. Concentration of Mg and Si in M-S-H at different pH [10]. Si (■) and Mg (●) concentrations are presented together with Mg/Si ratio (◢). The dashed lines are the solubility of amorphous SiO_2 and brucite.

3.2 Experimental

3.2.1 Materials and sample preparation

To study the effect of sodium bicarbonate on the evolution of M-S-H gel, cement pastes were prepared with two different initial water solutions and characterised at different curing times. Samples were prepared by mixing $Mg(OH)_2$ powder with silica fume and one of the solutions as shown in Table 1 for ~10 minutes. 200 mL of distilled water was used to prepare each solution: distilled water and saturated $NaHCO_3$ solution. The amount of $NaHCO_3$ added was set by its solubility at room temperature. The details of the raw materials used are listed in Table 2.

Table 1. Composition and initial pH of solutions for the systems studied

	Solution			Solid	
	Water (mL)	Carbonate (g)	pH at 20°C	$Mg(OH)_2$ (g)	Silica fume (g)
Distilled water	200	N/A	6.2	100.1	100.0
$NaHCO_3$ solution	200	19.2	8.8	100.1	100.0

Table 2. Information of the materials used

	$Mg(OH)_2$	Microsilica 940-U	$NaHCO_3$
Supplier	Sigma-Aldrich	Elkem	Sigma-Aldrich
Purity	≧ 95%	90%	≧ 99.0%

Samples were allowed to cure in closed 50 mL centrifuge tubes in an oven at 35°C for 3, 7, 14, 28, 56 and 112 days. The cured samples were then crushed (if hardened) and washed with approximately 100 mL of acetone in order to arrest the hydration reaction. The washed mixture was then recovered from the acetone using filter paper and a vacuum pump assisted Büchner funnel for approximately 30 minutes, after which the solid component was collected. The powder was then dried in a desiccator under vacuum for more than 3 hours and then stored in sealed tubes until characterisation.

3.2.2 Characterisation

X-ray diffraction (XRD) was used to assess the materials consumption and M-S-H evolution in the different samples. A benchtop Bruker D2 PHASER apparatus armed with a Cu-Kα radiation source running at 30kV and 10mA was used. A one mm divergence slit was used, and the upper and lower discriminators were set at 0.11 and 0.25 V respectively. Diffraction patterns were collected over 5 – 80° 2θ with an increment of 0.02. All samples rotated at 15 rpm during measurements.

X-Ray Fluorescence (XRF) was used to determine oxide composition of the silica fume and the 56 day cured samples for each formulation to check the purity of the microsilica and to determine the amount of sodium remaining in the produced solid after being washed with acetone. A Claisse LeNeo Fluxer was used to make beads, and the XRF measurement was conducted using PANalytical's Zetium operated using PANalytical SuperQ software. The PANalytical WROXI (wide-ranging oxides) calibration was used to determine the oxide concentrations in wt.%. The fused 40 mm beads used for measurements were made by mixing 10 g of lithium tetraborate (with 0.5%) flux with 1 g of sample. The specimen was heated in 5 steps before being poured and cooled: 1) 4 min at 1065°C, 2) 3 min at 1065°C rocking at 10 rpm and an angle of 15°, 3) 6 min at 1065°C rocking at 30 rpm and an angle of 40°, 4) 1 min at 1000°C, 5) 4 min at 1000°C rocking at 25 rpm and an angle of 45°. Measurements were taken in triplicates and the average values used.

The pH was measured to investigate sample pH evolution over time. A Mettler Toledo pH/Cond bench meter SE S470-K equipped with an expert proISM probe (error = ±0.01) was used to carry out all pH measurements; the probe was calibrated each day before use. The pH value at 0 day was measured right after mixing the cement paste; a small portion of the sample was separated, and the probe inserted into the paste directly. For the hardened samples, the pH was measured via the ex-situ leaching method [51]. A crushed powder sample of 1 g was added to 80 mL of distilled water (excess of solid material) and stirred with a magnetic stirrer. The pH reading was taken by inserting the testing probe into the solution, after 15 minutes of stirring to ensure that the measured solution was saturated and pH value became stable.

Thermogravimetric analysis (TGA) was also carried out to support the identification of species within the hardened cement that undergo thermal decomposition. Analysis was carried out on approximately 40 mg of sample in a PerkinElmer TGA 4000 heated from 30 °C to 990 °C at a heating rate of 10 °C/min under a nitrogen flow of 40 mL/min; a 5 min isothermal hold was also applied at the start and end temperatures. A Hiden mass spectrometer (HPR-20 GIC EGA) was used to record the signals for H_2O, CO_2, O_2, CO, and H_2.

3.3 Results and discussion

3.3.1 M-S-H evolution: XRD

The XRD patterns of the samples with different initial water solutions are shown in Figures 2 a and b. According to the literature, amorphous broad humps at 10-13°, 20-30°, 35-39° and 58-62° 2θ stem from the produced M-S-H [38], and the broad hump at 18–25° 2θ represents the unreacted silica fume [26]. The brucite pattern consists of sharp peaks at approximately 18.6°, 38.0°, 50.8° and 58.6° 2θ [38]. In the samples prepared with distilled water (Figure 2a), the intense peaks of brucite persist up to 56 days, indicating a slow consumption of brucite in this system. Accordingly, the formation of M-S-H appears to be slow, and peaks of M-S-H become apparent only at ≥ 28 days. A broad hump at 6-10° 2θ is slightly different from the expected range of 10-13° 2θ, but the increase in the peak intensity with the consumption of brucite suggests that this peak also represents M-S-H but in a slightly different from.

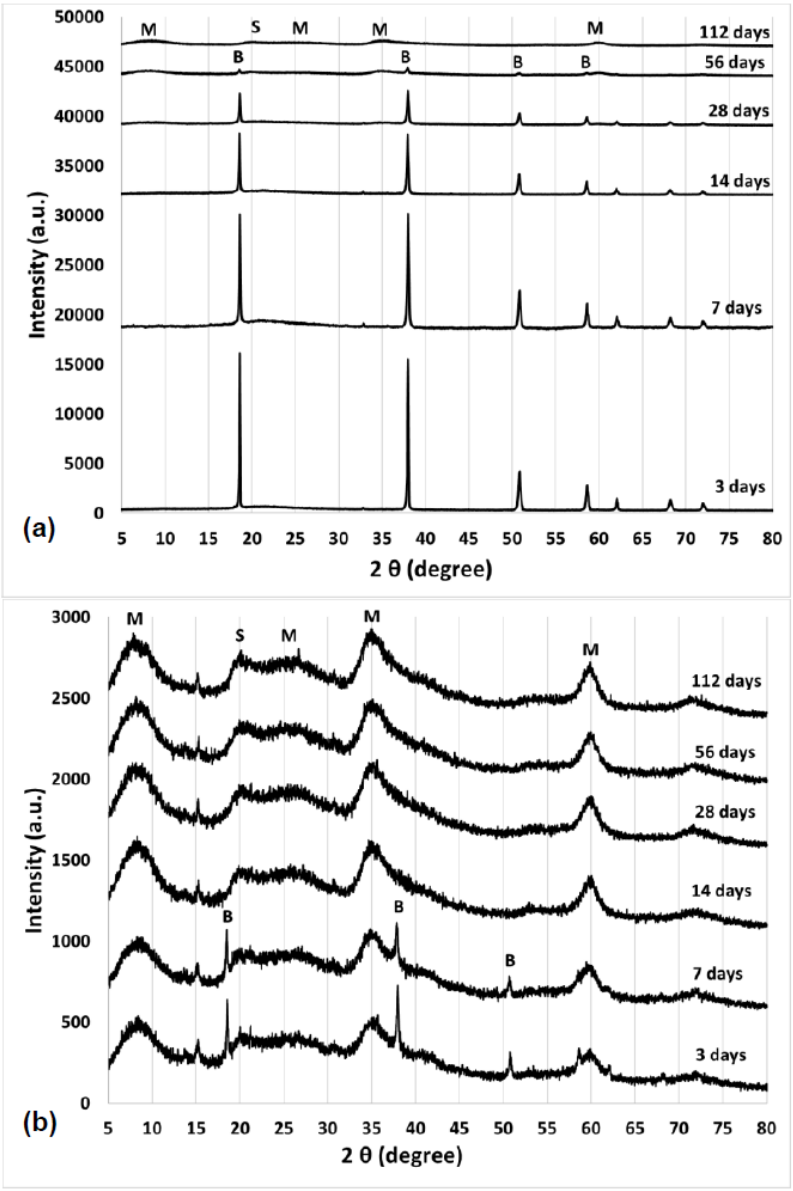

Figure 2. The XRD patterns showing the consumption of brucite (B) and silica fume (S), and the formation of M-S-H gel (M) over time in the samples prepared with: (a) distilled water and (b) $NaHCO_3$ solution.

The samples with $NaHCO_3$ addition (Figure 2b) showed much faster brucite reaction as the peaks of brucite disappeared within 14 days, while the M-S-H peaks can be clearly identified even after 3 days. The small peak observable at ~15° 2θ is likely to indicate the presence of hydromagnesite $Mg_5(CO_3)_4(OH)_2{\cdot}4H_2O$ [52]. The consumption of silica fume is difficult to discuss in these samples due to the possible overlapping of the main hump at 18–25° 2θ with a M-S-H hump. At 112 days, both systems have similar XRD patterns with exception of small peaks of minor phases in $NaHCO_3$ containing systems. This indicates that M-S-H formation using distilled water sample has likely completed within 112 days. The addition of $NaHCO_3$ did

not appear to significantly change the final M-S-H product. The XRD patterns clearly show that the M-S-H formation can be accelerated in the presence of $NaHCO_3$.

3.3.2 Mass balance: XRF

The oxide composition of the silica fume used in this work, derived through XRF analyses, and the loss on ignition (LOI) is shown in Table 3. Only oxides with >0.1 wt.% are presented in the Table. For the 100g of silica fume used, about 5.64g of other components are introduced into the sample. These impurities could be one of the reasons for the shift of the M-S-H hump at 10-13° 2θ to 6-10° 2θ observed in XRD data.

Table 3. Oxide composition of the silica fume

Element	SiO_2	K_2O	MgO	Fe_2O_3	Al_2O_3	Na_2O	CaO	ZnO	LOI
Weight %	94.36	1.12	0.71	0.61	0.50	0.32	0.22	0.20	1.82

XRF analyses was also carried out on the 56 days samples, and the results are shown in Table 4. Using these data, mass balance of the key elements was compared with the initial balance shown in Table 1, and the results are presented in Table 5. It is shown that the Mg/Si ratio in both samples remained approximately constant with small discrepancies probably arising from experimental error. This proves that the batch preparation was correct and that neither Mg nor Si were not lost in considerable amounts during washing with acetone. The Na/Mg ratios suggest that in the $NaHCO_3$ sample, the sodium remained in the sample, although the exact form of the sodium requires further investigation.

Table 4. The main element composition of the 56 days testing sample

	MgO (wt.%)	SiO_2 (wt.%)	Na_2O (wt.%)
Distilled water	30.15	39.87	-
$NaHCO_3$	26.21	34.64	3.40

Table 5. Elemental mass ratio between the initial mixtures and 56 day cured samples

	Initial (t=0)		t = 56 days	
	Mg/Si ratio	Na/Mg ratio	Mg/Si ratio	Na/Mg ratio
Distilled water	0.945	0.008	0.972	0.008
$NaHCO_3$	0.946	0.134	0.973	0.160

3.3.3 Progress of reaction: pH

The pH evolution for both sets of sample over 112 days is shown in Figure 3. The variation of the pH generally represents the change of the OH^- concentration in the solution. The dissolution of brucite will increase the pH of the solution, but only up to a maximum of ~10.5, which is the pH of saturated $Mg(OH)_2$ solution [14]. Therefore, in the $NaHCO_3$ samples, the pH values higher than 10.5 are likely due to the presence of alkaline element ions. The pH in this system decreases in the first 14 days and remains constant, consistent with pH evolution reported for similar systems [14, 21], and can be attributed to the consumption of OH^- ions for the dissolution of silica and formation of $H_4SiO_4(aq)$, $[H_3SiO_4]^-$ and $[H_2SiO_4]^{2-}$ [53].

For the paste made with distilled water, pH was 9.48 at t = 0 and increased to 10.01 by 14 days; the pH then decreased slightly to 9.9 towards 112 days. In the first 14 days, the production of OH^- from the dissolution of $Mg(OH)_2$ appears more significant than the consumption of OH^- in the dissolution of SiO2. After 14 days, these effects appear to be balanced. Since dissolution of $Mg(OH)_2$ should be continuing as the pH is below 10.5, this is likely due to the increased solubility of silica at a higher pH.

The $NaHCO_3$ sample had a relatively low pH value of 8.79 at day 0, which sharply increased to 10.59 by 3 days, then dropped to 10.22. The initial pH must be corresponding to that of the saturated $NaHCO_3$ solution (Table 1). The presence of $NaHCO_3$ clearly increased the pH of the mixture. The production of OH^- by dissolution of $Mg(OH)_2$ was much larger than the OH^- consumption rate in the first 3 days, but the high pH also encouraged the dissolution of silica and consumption of OH^-, resulting in the reduction of pH. The stable pH value after 14 days implies that majority of the reactions of the system, including M-S-H formation was completed, which is in agreement with XRD data.

The obtained results suggest that the availability of sodium and/or carbonate ions promote the reaction of $Mg(OH)_2$ and SiO_2, encouraging the M-S-H formation. Further research is required to elucidate the accelerated M-S-H development.

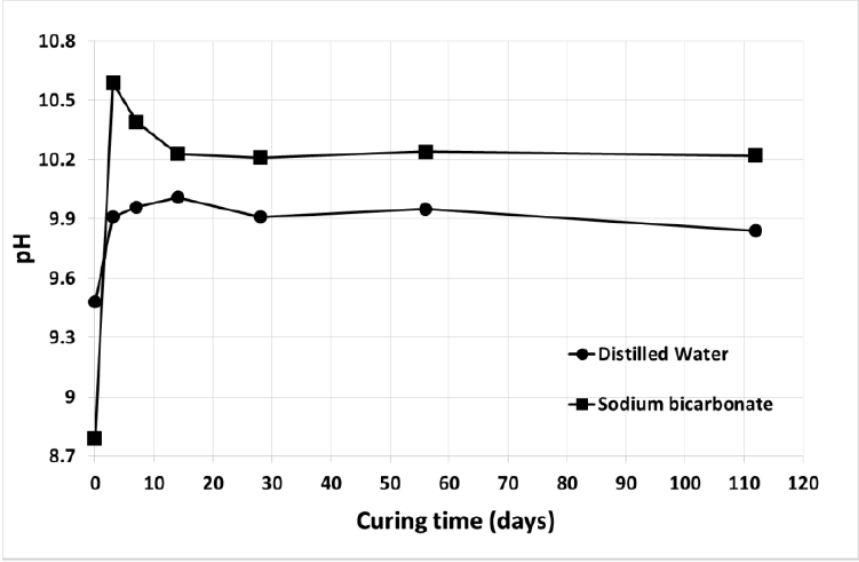

Figure 3. The results of pH test for all samples

3.3.4 Development of phases: TGA

The differential thermogravimetric (DTG) curves obtained from TGA are shown in the Figure 4. For the samples with $NaHCO_3$ the 28 days and 56 days samples were not tested as little progress of the reaction was suggested by XRD and pH data, but the 112 days samples were tested to compare the long-term behaviour.

The DTG peaks at 80-200 °C in the distilled water samples (Figure 4a) represent the loss of free water as well as water from M-S-H, while the decomposition of the brucite is represented by the peaks at around 400 °C. The broad responses peaked at 500-600 °C are also caused by the loss of coordinated water in M-S-H [21]. It also clearly shows that, with the increase of curing time, the amount of M-S-H increased while the amount of Mg(OH)2 decreased. This is evidence of the continued consumption of brucite to form M-S-H. A minor discrepancy is observed between 3 day and 7 days data with regard to the amount brucite; but, as the variation is relatively small, this may be due to experimental error.

The $NaHCO_3$ sample (Figure 4b) indicated similar peaks associated with M-S-H and $Mg(OH)_2$; more M-S-H and less $Mg(OH)_2$ compared with the distilled water samples. The mass loss at around 450°C in the $NaHCO_3$ sample may be explained by the presence of magnesite or hydromagnesite. Both of them are known to have TG responses at ~250 °C and 450 °C [52, 54, 55].

The $NaHCO_3$ samples have a fast reaction rate in the first 3 days as demonstrated from the amount of brucite remaining in the samples as well as the increased formation of M-S-H. The weight loss around 100°C associated with M-S-H does not show a clear trend. This may be explained in three ways: (1) the presence of sodium and/or carbonate ions influenced the retention and bonding of molecular water in M-S-H, (2) this DTG peak also include the water loss from sodium carbonate hydrates or bicarbonate [56], or (3) the experimental error associated with a small quantity of tested materials.

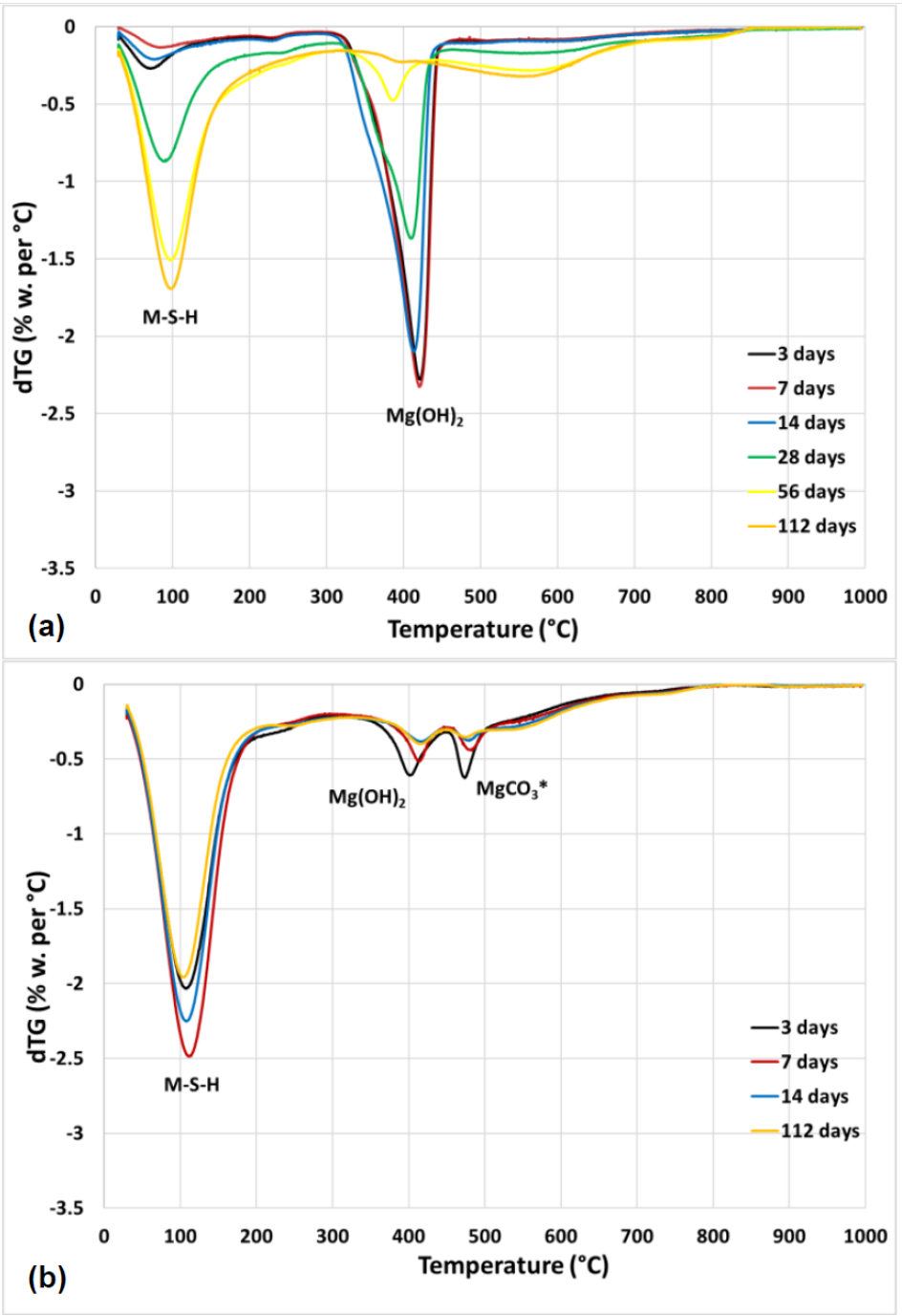

*Figure 4. The DTG data obtained from TG analysis for: (a) distilled water sample and (b) $NaHCO_3$ samples. The symbol * implies possible contribution of these species.*

3.4 Conclusion

The addition of $NaHCO_3$ promoted the reaction of $Mg(OH)_2$ and SiO_2 and resulted in the accelerated development of M-S-H gel. A higher pH of the mixing solution at ~10.2 appears to be beneficial to increase the dissolution of silica and formation of M-S-H. Further work is required to delineate these observations. Presence of carbonate ions in the system resulted in possible precipitation of hydromagnesite. The addition of $NaHCO_3$ also improved the fluidity of the paste and can allow for the production of magnesia-based concrete with a lower water/solid ratio without the addition of dispersants; thus, improving the strength. The availability of $NaHCO_3$ is also not foreseen an issue as sodium is one of the most abundant elements in the earth's crust. This work will reignite keen research interest into M-S-H cements.

Chapter 4. Effect of sodium bicarbonate ($NaHCO_3$) on the development of magnesium silicate hydrate (M-S-H) cement

Han Zhao, Theodore Hanein, Hajime Kinoshita

This work was submitted to Cement and Concrete Research as Research paper. Han Zhao is responsible for samples preparation, complete the experimental works, obtaining the data, data analysis.

Abstract

Magnesium silicate hydrate (M-S-H) cement is an alternative to Portland cement with potential benefits in certain conditions. The application of M-S-H cement is currently constrained by its slow formation; however, the acceleration of M-S-H formation by the addition of $NaHCO_3$ has been confirmed in previous study. The present work further investigates the addition of $NaHCO_3$, aiming for the optimisation of its quantity, and the quantitative study in the reaction kinetics. Although the acceleration was enhanced with increasing $NaHCO_3$ concentration up to saturation, it was possible to gain a significant acceleration of M-S-H formation even with decreased amount of $NaHCO_3$. The study also found that larger amounts of $NaHCO_3$ resulted in larger amounts of $Mg(OH)_2$ remaining in the system without reacting. The reaction kinetics in the presence of $NaHCO_3$ were likely nucleation controlled, and the H_2O/MgO molar ratio of the M-S-H remained approximately to throughout its development in the systems investigated.

4.1 Introduction

Cement is one of the most important construction materials, but their large annual production and consumption makes the cement industry responsible for 8 % of world man-made carbon dioxide emissions [3, 4]. The carbon dioxide emission is mainly associated with the two aspects in the cement production. The first aspect is the thermal decomposition of the carbonate compounds in the raw materials i.e., the calcination of limestone (mostly composed of calcium carbonate) to generate calcium oxide in the Portland cement manufacture process [3]. The second aspect is the combustion of the fossil fuels to heat the materials to specific temperature (usually around 1500°C) [5], enabling the formation of necessary mineral phases, which consumes 12 % - 15 % of total industry energy usage [4]. As the environmental problems associated with the greenhouse effect becoming increasingly serious in the recent years, the reduction of the carbon footprint became an important task for the cement industries.

Magnesium based cement may be a possible alternative to the Portland cement, to mitigate the carbon dioxide emission of the cement industries. The temperature requirement for the production of magnesia (MgO), the main raw material of magnesium based cement is around 650°C, which is much lower compared to the CaO production in aforementioned Portland cement manufacture [5]. Some of the components in the magnesium based cement may also be able to absorb carbon dioxide during applications, which reduces the carbon footprint of the cement through their service life [2]. The potential ecological benefits of the magnesium based cement encourage further research on this type of cements to support the sustainable future of cement industry.

Magnesium silica hydrate (M-S-H) cement is one of the magnesium based cements. which has been studied increasingly in recent years for a wide range of applications, including contaminant immobilisation, metal-containing waste treatment, refractory castable and construction materials [14, 15, 21, 22]. This is owing to its characteristics e.g., high resistance in aggressive environment, low pH environment compared to Portland cement and high temperature resistance [22, 25, 34].

Unfortunately, the practical application of M-S-H cement is currently constrained by its slow setting time and low early-strength development. It has been reported that a significant length of time is required for the formation of M-S-H up to 2 years to completely react to M-S-H depending on the Mg/Si ratio [13]. It may take few months for the M-S-H cement to achieve the desired strength [22]. Reaction at elevated temperatures has been attempted to increase the reaction kinetics with a certain level of success [11, 34].

M-S-H gel is typically generated through the reaction of magnesium compounds such as MgO or $Mg(OH)_2$ with soluble source of SiO_2 such as silica fume in the presence of water. It is known that a high Mg^{2+} concentration in the reacting solution promotes the formation of M-S-H [14]. Because the solubility of MgO and $Mg(OH)_2$ in water both decreases at higher pH [57], the lower pH environment appears to be favourable to increase the Mg^{2+} contribution to the M-S-H formation. On the other hand, the solubility of SiO_2 increases at higher pH, as OH^- ions weaken the bonds between the silicon and oxygen atoms [35]. This suggests that the higher pH environment is favourable for the availability of silica component and its contribution to M-S-H formation. Therefore, the pH of the reaction environment is one of the important factors to assure the effective formation of M-S-H gel, and sufficient strength development of the system.

Numbers of admixtures have also been studied for M-S-H cement systems, to improve their properties, most notably sodium hexametaphosphate $(NaPO_3)_6$ [5, 47]. These additives are primarily introduced to the system as a dispersant, improving the fluidity of the paste and/or allowing to reduce the water to solid ratio, which usually result in the reduced porosity and improved mechanical strength of the products. Other sodium-based phosphates such as trimetaphosphate and orthophosphate have also been studied [58] and their plasticising effect and promoted formation of M-S-H are reported, while dipotassium hydrogen phosphate ($K_2HPO_4 \cdot 3H_2O$) has been shown to improve the fluidity with a higher water reduction efficiency than $(NaPO_3)_6$ [59]. Although some of these dispersants, e.g. sodium hexametaphosphate [48] and orthophosphate [58], have been reported to promote the formation of M-S-H, their amount possibly introduced to the systems is restricted as the nature of the dispersant, since the excess amount of dispersant tends to have negative impact on the fluidity and setting of the paste [24]. If the system is to be improved further, additional additive would have to be introduced.

Our previous study demonstrated that addition of sodium bicarbonate ($NaHCO_3$) to the batch could accelerate the formation of the M-S-H binder [60] . The introduction of $NaHCO_3$ resulted in the accelerated consumption of $Mg(OH)_2$, while the pH of the system was increased to 10.2 from 9.9 of the reference system without inclusion of $NaHCO_3$ [60]. Differing from the phosphate dispersants mentioned above, the amount of $NaHCO_3$ to be introduced to the system does not have any restrictions because it is not introduced as a dispersant. Sodium bicarbonate is low cost and readily available, which makes the applications more suitable and sustainable. However, our previous study was only qualitative, and the accelerated formation of M-S-H still requires further study, including the effects of $NaHCO_3$ content on the reaction kinetics to optimise the amount of $NaHCO_3$.

To gain further insight into the acceleration by $NaHCO_3$, the present study examined the formation of M-S-H gel with the addition of $NaHCO_3$ solutions at different levels of concentrations along with the involved reaction mechanisms and kinetics. In our preliminary study [60], only saturated $NaHCO_3$ solution was used to maximise the increase in the pH level of the system, while solutions with reduced $NaHCO_3$ concentration were also used in the present investigation to elucidate the effects of $NaHCO_3$ concentration and associated pH levels. Such information is crucial for optimisation of $NaHCO_3$ concentration for the accelerated formation of M-S-H.

4.2 Material and methods

4.2.1 Materials

The raw materials used in this work are brucite from Sigma-Aldrich with purity ≥95%, microsilica 940-U from Elkem, sodium bicarbonate from Sigma-Aldrich with purity ≥99.0% and laboratory distilled water. The X-ray fluorescence (XRF) data of the microsilica used in listed in Table 1, presenting the oxide composition (constituents with >0.1 wt.% only) and loss on ignition (LOI).

Table 1． Oxide composition of the silica fume

Element	SiO_2	K_2O	MgO	Fe_2O_3	Al_2O_3	Na_2O	CaO	ZnO	LOI	Total
Weight %	94.36	1.12	0.71	0.61	0.50	0.32	0.22	0.20	1.82	99.86

4.2.2 Sample mix design

Cement paste is prepared by mixing brucite and silica fume with $NaHCO_3$ solutions of various concentrations; sample information is listed in Table 2. The distilled water (DW) sample is without any $NaHCO_3$ addition and taken from previous work together with the 1H sample [60]. The mass of sodium bicarbonate is determined by its solubility in water at 20°C, which is 9.6 g/l00ml [61]. The 1H notation represents the mass of $NaHCO_3$ equal to its solubility (saturated water solution); the ½ H and ¼ H are half and quarter the mass of saturation. These samples with different $NaHCO_3$ concentration were prepared in centrifuge tube for characterisation.

Table 2. Composition design of the systems together with DW and 1H sample taken from previous work [60] for comparison.

	Solution		**Solid**	
Sample ID	**Water (mL)**	**$NaHCO_3$ (g)**	**$Mg(OH)_2$ (g)**	**Silica fume (g)**
DW	200	0	100	100
1H	200	19.2	100	100
½ H	200	9.6	100	100
¼ H	200	4.8	100	100

4.2.3 Experimental procedure

In all samples, the solution was prepared first by dissolving the $NaHCO_3$ in the distilled water with magnetic stirrer for approximately 15 minutes at lab temperature (~20°C) until the solution becomes colourless. The $NaHCO_3$ solution was placed into a mixer (Heidolph RZR2020, 400rpm) and then all the brucite powder was added over approximately 5 minutes of mixing. Silica fume was then slowly added into the mixer with approximately 20 % of total mass every minute (total of 5 minutes). This methodology is undertaken to achieve homogeneous mixing and minimise dust loss from the microsilica, especially in samples with lower W/S ratio. After mixing, the cement paste was poured into 50 mL centrifuge tubes, and the tubes were then sealed with the lid and parafilm.

The samples were then cured in a 35°C oven and taken out at 3, 7, 14, 28, 56, and 112 days. After curing in the centrifuge tubes, the samples were crushed into small pieces and washed in approximately 200 mL of acetone for 5 minutes. Then, the washed samples were separated from the acetone by using filter paper and a Büchner funnel assisted with vacuum pump for approximately 5 minutes. The separated materials are immersed into approximately 200 mL of acetone again and kept for 48 hours in order to remove the free water. The samples were separated from acetone again by using filter paper and Büchner funnel for 15 minutes. The dried samples are stored in sealed centrifuge tubes with parafilm until further analysis.

4.2.4 Characterisation methods

4.2.4.1 X-ray diffraction

The X-ray diffraction (XRD) machine used was benchtop Bruker D2 PHASER apparatus armed with a Cu-Kα radiation source running at 30 kV and 10 mA. The divergence silt used was 1 mm, the upper and lower discriminators were 0.11 and 0.25 V respectively. The scanning angle range was from 5° to 80° 2θ with an increment of 0.02°. The sample was rotating at 15 rpm during scanning to avoid uneven distribution of microstructure. The samples are crushed and ground into powders before measurement.

4.2.4.2 Thermogravimetric analyses

Thermogravimetric analyses (TGA) was carried out by using PerkinElmer TGA 4000. Approximately 40 mg of samples were used for testing each time. The sample was heated from 30°C to 990°C at a rate of 10 °C/min under a nitrogen flow of 40 mL/min. Ten minutes of isothermal hold was used at both the start and end of the heating programme.

4.2.4.3 pH measurement

The apparatus used for pH measurements was a Mettler Toledo pH/Cond bench meter SE S470-K equipped with an expert proISM probe (error = ±0.01). The probe was calibrated each day before use by immersing into standard buffer solutions with known pH values. Two methods are used for measuring the samples at different reaction stage. The pH of the sample at 0 days (initially prepared batch) was measured right after the batch was mixed properly; a small portion of the batch was separated and then the testing probe was immersed directly into the paste to take the readings. For the cured samples, Ex-situ leaching method [51] was used for the pH measurement. For these tests, 1 g of powder sample was added into 80 mL of distilled water and then stirred with a magnetic stirrer, and then the testing probe was inserted into the solution. The pH reading was recorded after > 15 minutes of stirring when the pH reading of the solution stabilised. The amount of cement added was decided by a preliminary experiment, in which 0.2 g, 0.6 g, and 1.0 g of cement sample was added into 80 mL of distilled water separately. These preliminary tests showed that the pH readings for >0.6g addition are the same, and signifies that the solution is already saturated. However, using this method to measure the pH of the samples in the project assumes the pore solution of the cement is in over saturated state.

4.2.4.4 Fourier transform infrared (FTIR) spectroscopy

The apparatus used for Fourier transform infrared (FTIR) spectroscopy was Perkin Elmer Frontier Mid FT-IR spectrometer equipped with a deuterated triglycine sulfate (DTGS) detector and KBr beam splitter optical system. The measurements were made by scanning 32 times for each formulation at a resolution of 4 cm^{-1}. The samples were prepared by mixing and grinding 2 mg cement samples with 200 mg of potassium bromide (KBr) powders for over 5 minutes, and pressing into a pellet using hydraulic press under 1 tonne and 10 tonnes of pressure for 1 minute respectively.

4.3 Results and discussion

4.3.1 Phase formation and consumption of $Mg(OH)_2$

The XRD patterns of ½ H and ¼ H samples are compared with those of DW and 1H samples from previous work [3, 60] in Figure 1 (a)-(d). According to the literature, the broad humps at 10-13°, 20-30°, 35-39°, and 58-62° 2θ can be attributed to M-S-H [21], and the broad hump at 18–25° 2θ is attributed to unreacted silica fume [26]. These are observed in the data presented in Figure 1. The sharp peaks at 18.6°, 38.0°, 50.8°, and 58.6° 2θ are for brucite [21]. A broad peak at 6-10° 2θ also shows a similar trend to the M-S-H peaks, which is increasing in intensity with the decreasing of brucite peaks. This is slightly different from expected position (10-13° 2θ), but may also represent the formation of M-S-H gel [60]. Small reflection peaks are observed at approximately 15° 2θ for the 1H and 1/2H systems. This was previously attributed to the presence of hydromagnesite, $Mg_5(CO_3)_4(OH)_2{\cdot}4H_2O$ [52] forming because of the significant presence of carbonate ions in the system.

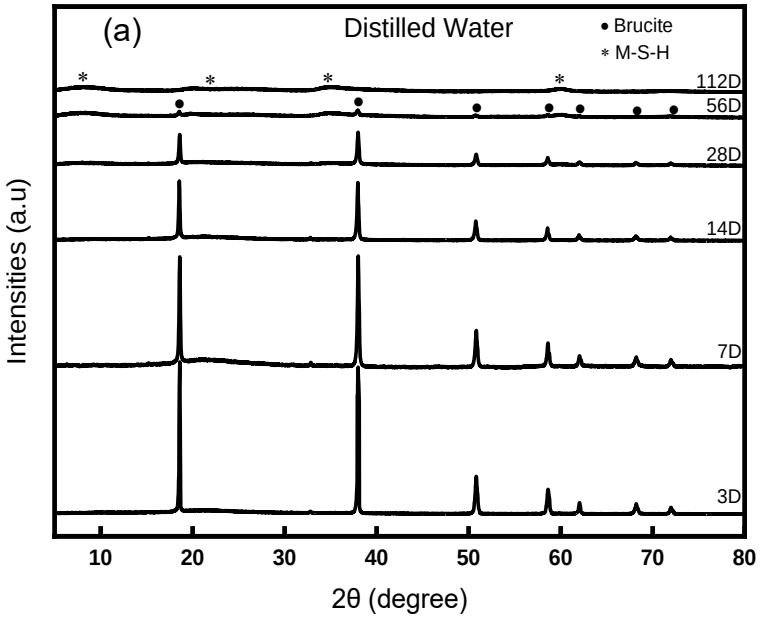
(a)
Distilled Water
• Brucite
∗ M-S-H
112D
56D
28D
14D
7D
3D
Intensities (a.u)
10
20
30
40
50
60
70
80
2θ (degree)

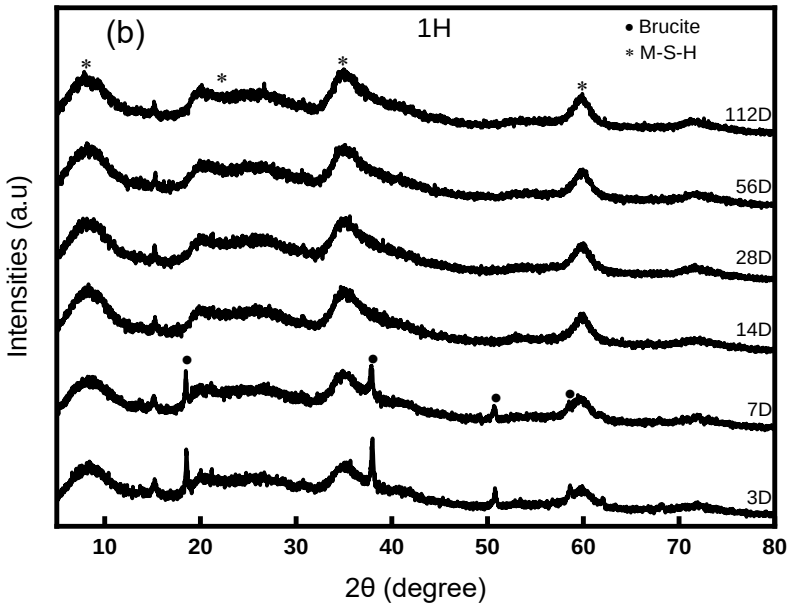
(b)
1H
• Brucite
∗ M-S-H
112D
56D
28D
14D
7D
3D
Intensities (a.u)
10
20
30
40
50
60
70
80
2θ (degree)

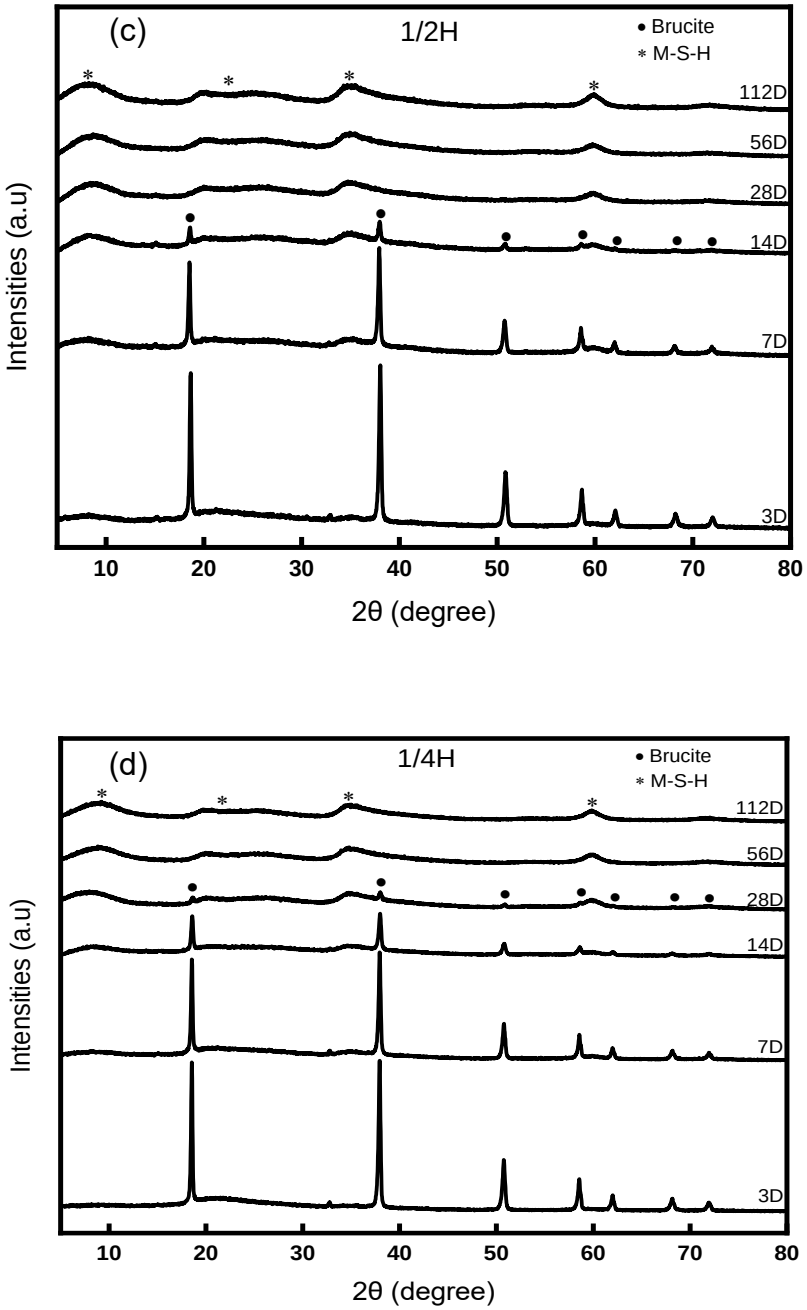

Figure 1. The XRD pattern of samples at different dates: (a) DW system [60]; (b) 1H system [60]; (c) ½ H system; (d) ¼ H system.

The X-ray patterns reveal the gradual formation of M-S-H and consumption of brucite in all the samples, and the concentration of $NaHCO_3$ has a clear impact on the reaction rate. The addition of $NaHCO_3$ allows for the acceleration of M-S-H formation, with less acceleration at lower concentration of $NaHCO_3$ (1H > ½H > ¼H). The XRD data of the 1H samples no longer show the reflection peaks of brucite at 14 days of curing time while the ½H samples still show the brucite peaks at 14 days, and the ¼H samples have reflection peaks for the unconsumed brucite in the system at 28 days, which eventually disappeared by 56 days. It should be noted, however, that the ¼H samples still show a faster reaction compared with DW samples with no $NaHCO_3$ addition which appear to require 112 days for brucite to react lower than the detention limit of XRD [60].

4.3.2 Influence of pH

The results of the pH measurement for the ½ H and ¼ H samples are shown in Figure 2 together with those for DW and 1H samples [60]. The variation of the pH represents the change in the concentration of OH^- ions in the solution, which can increase with the dissolution of brucite. However, the dissolution of brucite can increase the pH only up to the maximum of ~10.5 at saturation of $Mg(OH)_2$ [14].

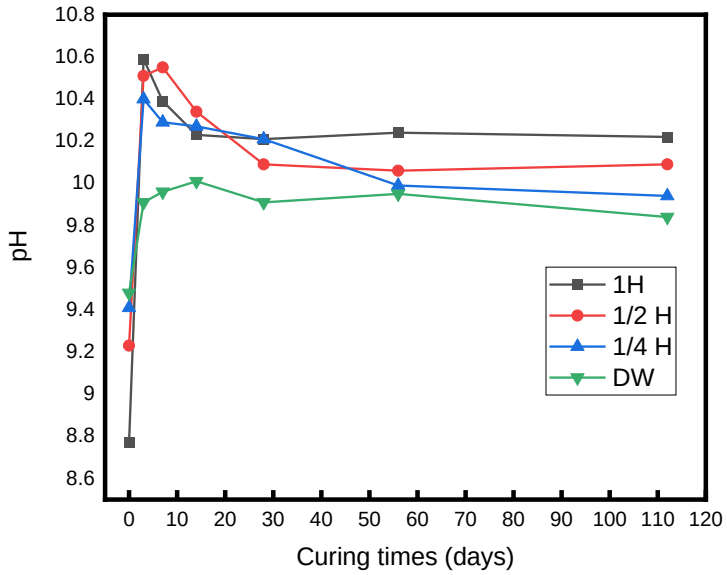

Figure 2. The pH measurements over time for cements with different starting solutions. The data of DW and 1H samples are from previous work [60].

For the 1H, ½ H, and ¼ H samples, the initial pH is reduced compared with the distilled water, with the increasing $NaHCO_3$ concentration. The pH of these samples increased in the first 3 days (also 7 days for ½H sample) to a value close to the pH of 10.5 for the saturated $Mg(OH)_2$ solution. This implies that the brucite is able to dissolve freely in the initial stage of the reaction, which is also supported by the fast consumption of brucite suggested in the XRD patterns. This relatively high pH caused by the dissolution of $Mg(OH)_2$ then encourages the dissolution of silica fume and the formation of silicate ions, by increasing the concentration of the OH^- ions per unit surface area of silica fume while consuming the OH^- ions, resulting in the gradual decrease in the pH [35]. This level of initial pH in the early age (3-7 days) may be necessary for accelerated formation of M-S-H. The highest pH values of the accelerated systems are close to 10.5 as mentioned above, where the reasonable dissolution of both brucite and silica are maintained as reported by Nied et al. [10].

The pH values are eventually stabilised as the reaction progresses, with the final pH value being higher with the higher concentration of $NaHCO_3$ solution. The period where the pH value stabilizes appears to be consistent with that when the brucite peaks are no longer observed in the XRD data, which are 14 days for 1H, 28 days for ½H, and 56 days for ¼H samples. This suggests that majority of brucite is consumed, corresponding amount of silica is dissolved and the reaction in the system has mostly completed at this stage. It is interesting that the pH of the ¼H system was initially similar to the other $NaHCO_3$ containing systems, but shifted more towards the DW system without $NaHCO_3$ in the later period.

4.3.3 Quantification of phases

The TG data of the samples are shown in Figure 3 together with the differential thermogravimetric (DTG) curves derived from the TG data. There are three regions of distinctive weight loss events observable on the DTG curves: region (I) is 80 – 250 °C, mainly caused by the loss of poorly bound water in M-S-H which should generally increase with the time of curing [21, 62] and possibly free water; Region (II) is in the range of 320 – 480 °C, corresponding to the amount of brucite remaining in the system but may overlap with the water loss from M-S-H [21]; Region (III) is the broad peaks in 500 – 600 °C which can be another indication of the formation of M-S-H, mainly caused by the loss of coordination water of M-S-H [21], more specifically, attributed to the loss of silanol hydroxyl group [10, 13, 63], increasing with curing time until the formation of M-S-H completed.

There are small peaks occurring around 500°C, which may be caused by the presence of magnesium carbonate species such as hydromagnesite, $Mg_5(CO_3)_4(OH)_2{\cdot}4H_2O$ [52, 55, 64], dypingite $Mg_5(CO_3)_4(OH)_2{\cdot}5H_2O$ [65], Nesquehonite ($MgCO_3{\cdot}3H_2O$) [55, 66], and/or eitelite, $Na_2Mg(CO_3)_2$ [47, 61, 66, 67]. All of these species can show a weight loss in this temperature range. The intensity of these peaks are reducing with the curing time, suggesting the carbonate species forming as an intermediate product in this system and being consumed during the formation of M-S-H. There is also an observable trend of continuous loss of water in the background between 200°C and 850°C, which signify the formation of hydrate phase. A similar water loss has been reported in a M-S-H or hydrated talc system[62], which is believe to become less when the structure of the M-S-H products becomes more crystallised [62].

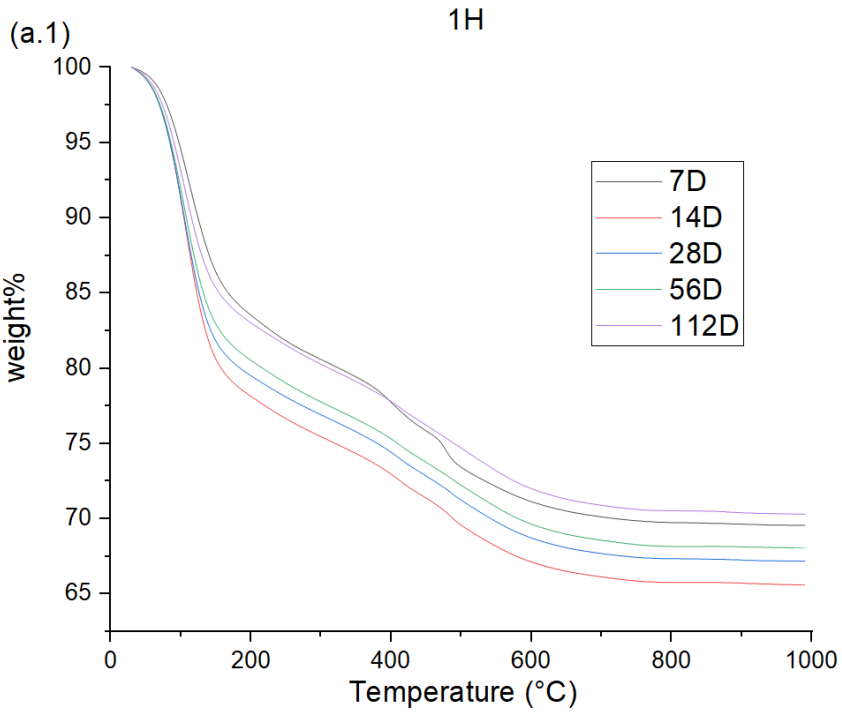
(a.1)
1H
100
95
90
85
80
75
70
65
weight%
0
200
400
600
800
1000
Temperature (°C)
7D
14D
28D
56D
112D

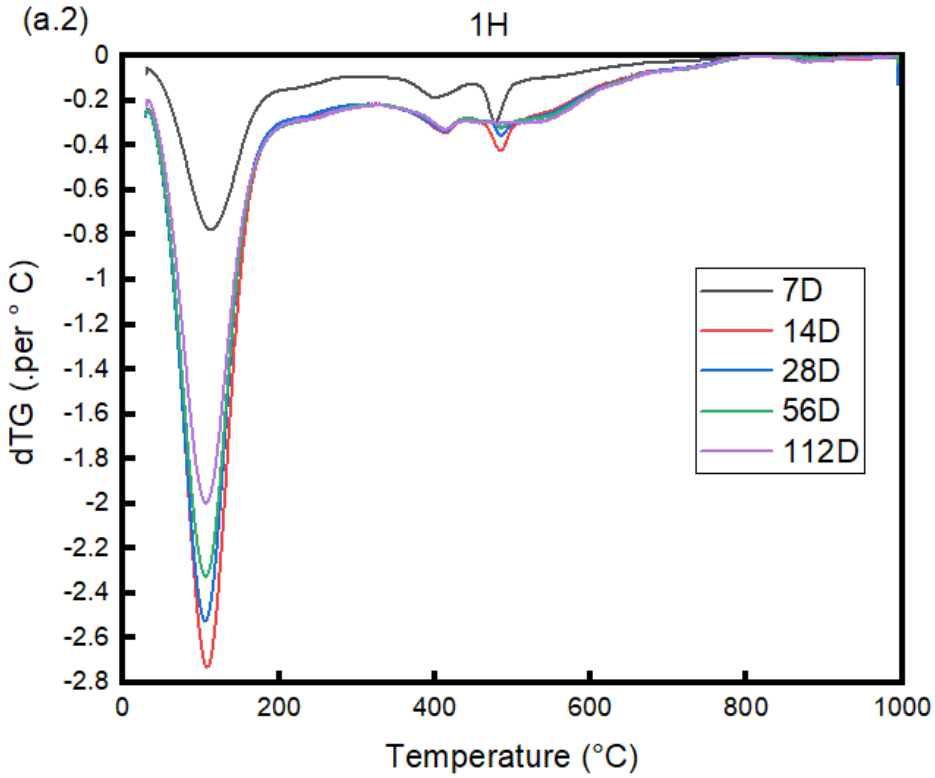
(a.2)
1H
0
-0.2
-0.4
-0.6
-0.8
-1
-1.2
-1.4
-1.6
-1.8
-2
-2.2
-2.4
-2.6
-2.8
dTG (.per ° C)
0
200
400
600
800
1000
Temperature (°C)
7D
14D
28D
56D
112D

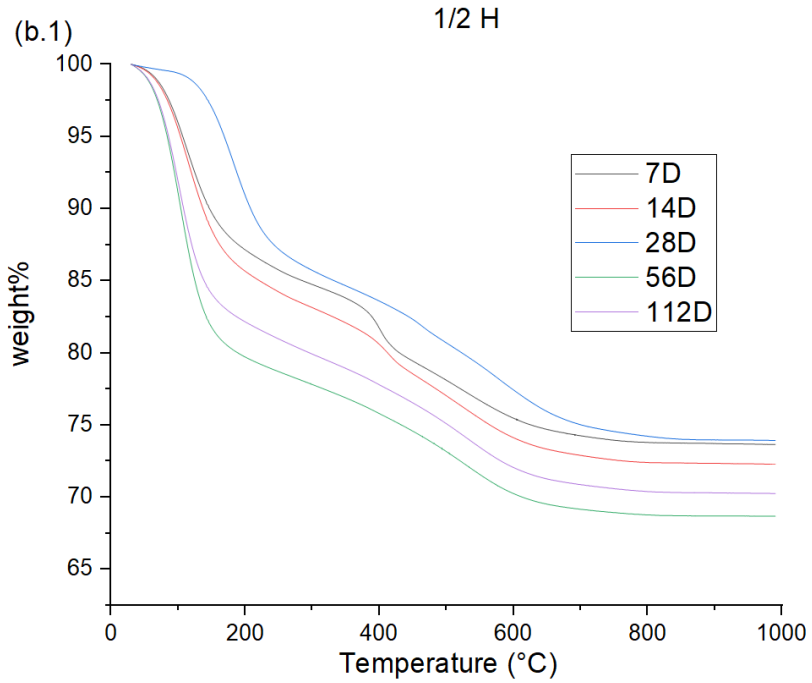
(b.1)
1/2 H
weight%
Temperature (°C)
7D
14D
28D
56D
112D

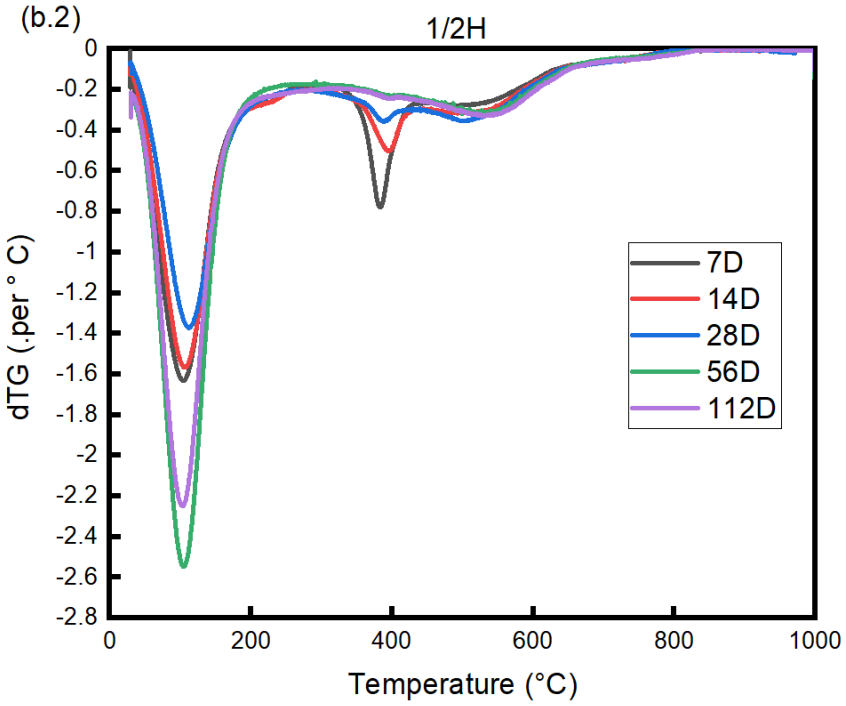
(b.2)
1/2H
dTG (.per ° C)
Temperature (°C)
7D
14D
28D
56D
112D

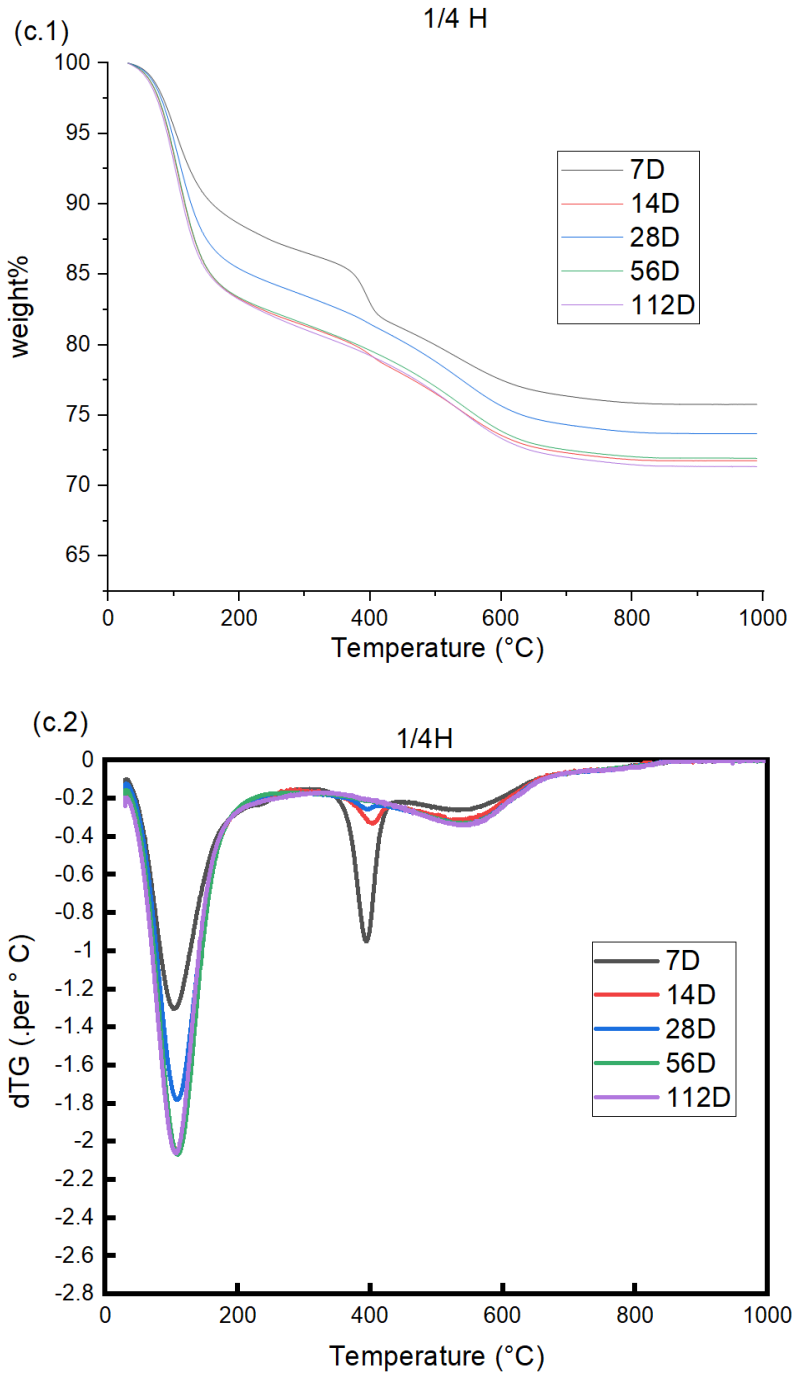

Figure 3. The TG (1) and DTG (2) of the three different sample series at different dates. (a) 1H

Based on the TG and DTG data, the amount of $Mg(OH)_2$ present in the system and water in M-S-H were estimated. The detailed summary of the estimation is presented in Appendix 1. The results of estimation are shown in Figure 4. The possible magnesium carbonate species mentioned above are ignored in the calculation, since the quantity of them are smaller than the detection limit of the XRD measurements, that no clear indication can be identified in the XRD patterns.

The addition of $NaHCO_3$ is able to accelerate the consumption of $Mg(OH)_2$, most notably in the 1H system up to 14 days (Figure 4 a). However, it is revealed that a small amount of $Mg(OH)_2$ remains in the 1H system despite its accelerated consumption, while more $Mg(OH)_2$ appears to be consumed when less amount of $NaHCO_3$ is introduced to the system at a longer ageing. The presence of $Mg(OH)_2$ was not identified in the XRD results in the older samples even for the 1H samples (Figure 1), likely because the quantity of remaining $Mg(OH)_2$ is below the detection limit of the XRD.

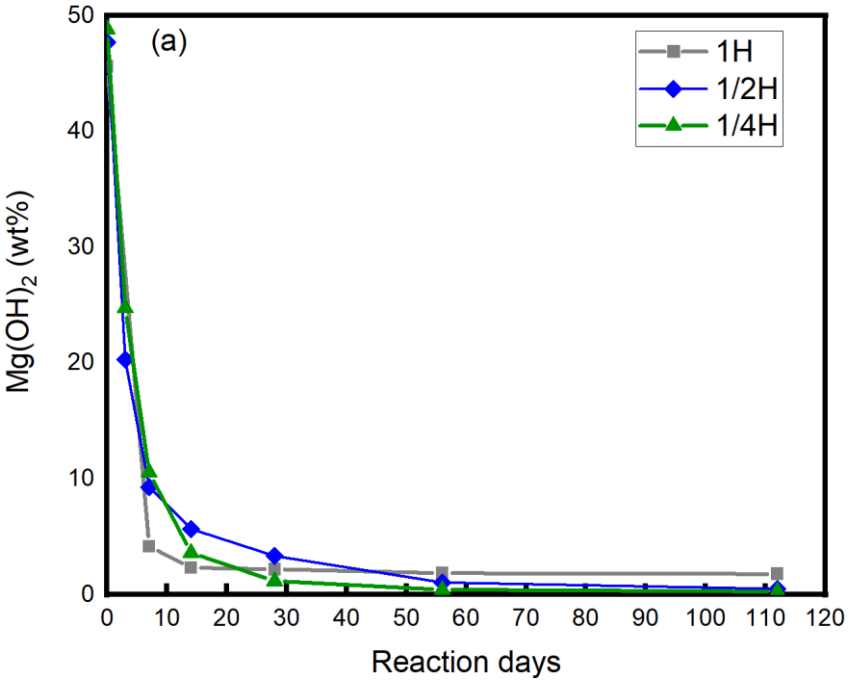

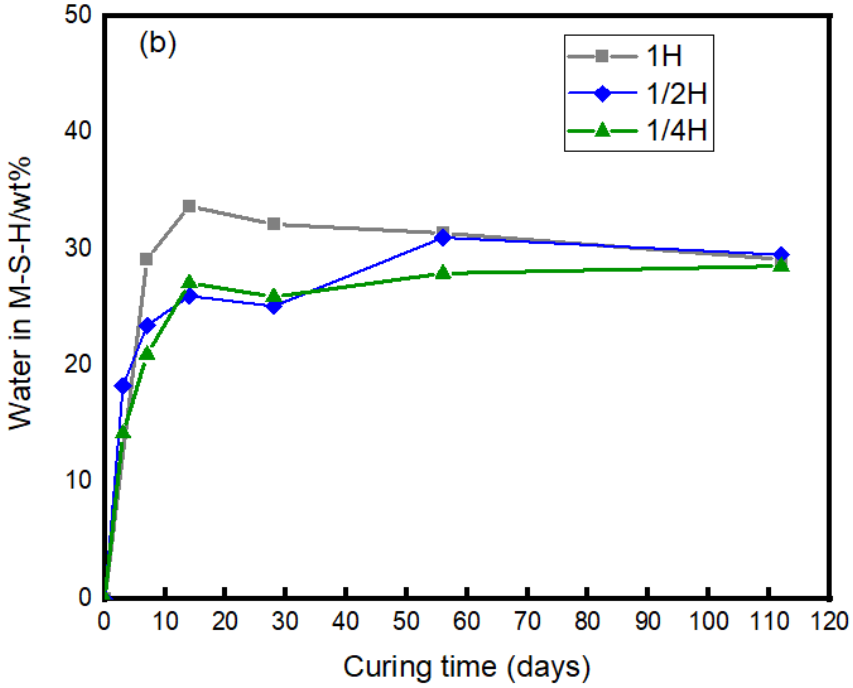

Figure 4. Estimation based on TG and DTG data: (a) amount of $Mg(OH)_2$ in the system and (b) amount of water in M-S-H.

The trend in the water loss from the M-S-H was similar in all systems containing $NaHCO_3$ (Figure 4 b). There is a decrease in the water in M-S-H in the 1H W/S = 1 sample after reaching the maximum at 14 days. Interestingly, all samples indicated a similar amount of water loss from M-S-H at 112 days, which implies that the quantity of M-S-H formed and associated water content at 112 days are similar. The estimated amount of water in M-S-H was compared with that of $Mg(OH)_2$ reacted in each of 1H, ½ H and ¼ H systems, and plotted in Figure 5. Because the 1H system reacted fast, it is harder to see the linear correlation, but the analysis suggests that the H_2O/MgO ratio in the M-S-H formed generally remains around 2 in the systems investigated. This is consistent with the H_2O/MgO ratio in the previously reported formula of $Mg_8Si_8O_{20}(OH)_8 \cdot 12H_2O$ [68]. The faster reaction with more inclusion of $NaHCO_3$ may have a slightly larger H_2O/MgO ratio.

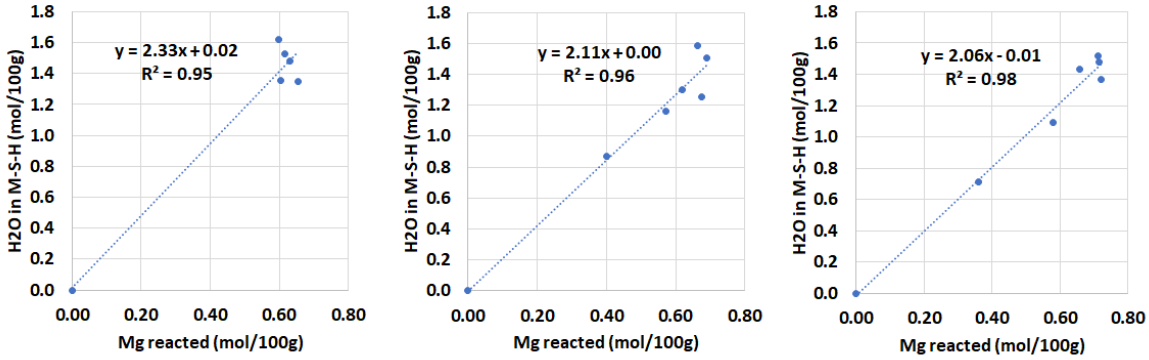

Figure 5. Comparison of water content in M-S-H and $Mg(OH)_2$ reacted: (a) 1H system, (b) ½ H system and (c) ¼ H system.

4.3.4 Phase identification by FT-IR spectroscopy

The FT-IR spectroscopy data of the 1H samples at different ages are shown in Figure 6. The absorption peaks can be mainly divided into high frequency region (4000 – 2500 cm^{-1}) and low frequency region (1600 – 400 cm^{-1}). The data provide information of the bond vibrations occurring in the samples by comparing with the value in literature [69-71] . The peaks in the high frequency region are generated by the bonds with relatively high polarity; a shoulder for the O-H hydrogen bonding at 3700 cm^{-1} attributes to the brucite [10, 19], confirming the presence of residual brucite suggested by the TGA data. The broad absorption peaks around 3500 cm^{-1} (shaded in grey) are due to the (Mg)-O-H stretching vibration of the hydroxyls, which can be assigned to the M-S-H formed [10, 13, 19, 69]. The broad peaks at 930 - 1130 cm^{-1} and

600 - 680 cm^{-1} (shaded in grey) also indicates the presence of M-S-H, corresponding to the Si–O stretching vibrations of Q_2 tetrahedral and Si–O–Si bending vibrations, respectively [10, 13, 19, 69]. The peaks at 1427 cm^{-1} and 1486 cm^{-1} correspond to the asymmetric stretching (v_3) of CO_3^{2-} ions in hydrated magnesium carbonates (hydromagnesite), with the formula of $MgCO_3,xH_2O$ [69, 72, 73]. The small peaks at 875 cm^{-1} are also due to the presence of CO_3^{2-} ions [69, 72, 73]. The peaks at 400 – 500 cm^{-1} correspond to the deformation of SiO_4 tetrahedral in the silica fume, which should show peak around 1130 cm^{-1} as well, but cannot be observed likely because of the overlap with the M-S-H peaks in the samples [69-71].

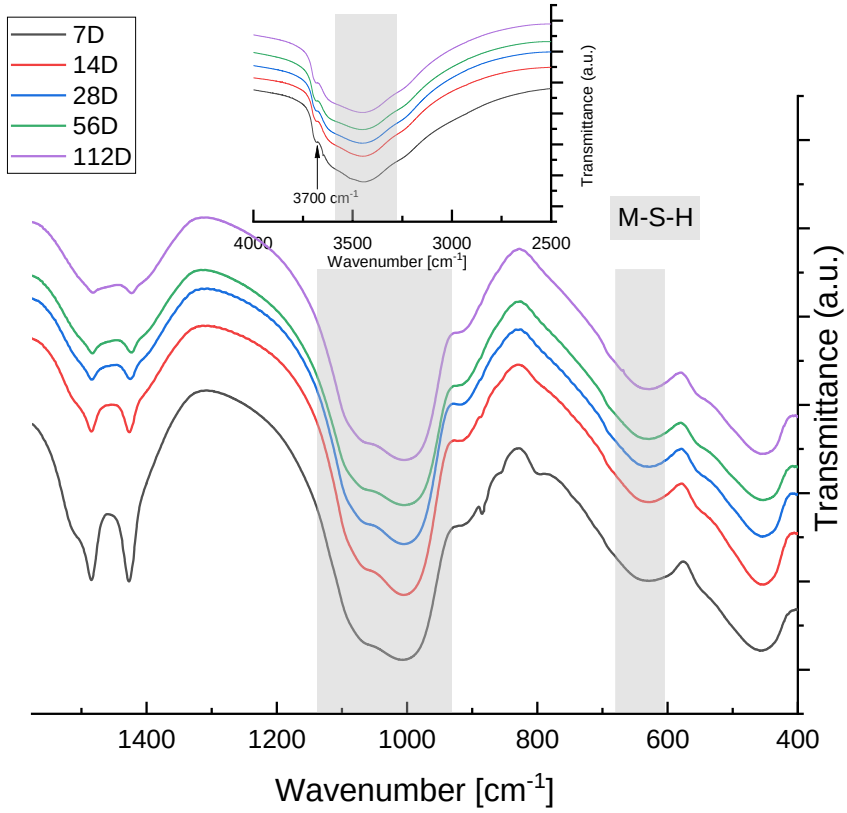

Figure 6. The FR-IR spectroscopy of 1H samples at different dates (with M-S-H region highlighted with grey shades)

The FT-IR data demonstrate the formation of the M-S-H as early as 7 days of curing and the presence of the residual brucite in 1H samples throughout the testing period of 112 days. The asymmetric peaks for M-S-H and brucite did not change in their intensities with time suggest that the reaction of the systems is fast, and the majority of the reaction occurs in the early stage. There are also significant peaks for silica, suggesting there was unreacted silica exist in this system.

The XRD and TG data suggest that the formation of intermediate carbonate species. Formation of such species has been reported in the $Mg(OH)_2$ slurry in the presence of carbonate and sodium ions at 45°C [74]. The spectroscopy data confirmed the formation of hydromagnesite in the samples, with the quantity decreasing with time. The reduction trend of hydromagnesite is same as the data in TG, which also confirms the hydromagnesite was formed as an intermediate product. The formation of hydromagnesite $Mg_5(CO_3)_4(OH)_2{\cdot}4H_2O$ is advantageous for the M-S-H formation. Although its solubility in water (1.8×10^{-4} mol/L at 25 ^oC [75]) is similar to that of brucite $Mg(OH)_2$ (2×10^{-4} mol/L at 25 ^oC [76], because it contains 5 times more of Mg^{2+} ions in the molecule, it can provide > 4 times more of Mg^{2+} ions in total. The positive impact of carbonate ions on the provision of Mg^{2+} ions in high pH environment has also been shown recently [77]. It has also been known that the presence of hydromagnesite can accelerate the dissolution of glass (mainly silica), which result in precipitation of magnesium silicate species [78].

4.3.5 Reaction Kinetics

Analysis of the reaction kinetic was attempted to further study the formation of the M-S-H phase in the samples. Assuming the magnesium content in the sample are either in the unreacted $Mg(OH)_2$ or formed M-S-H gel, the extent of reaction (α) can be estimated using the following equation.

$$\alpha = \frac{[Mg(OH)_2\ reacted]}{[Initial\ Mg(OH)_2\ in\ the\ system]} \qquad (1)$$

There are numbers of reaction models are available in the literature [79] that are usually expressed based on the extent of reaction (α), reaction constant (k) and reaction time (t). Three kinetic models commonly used to represent typical solid formation (equations 2, 3 and 4 [79]) were tested to examine the rate-limiting factor for the M-S-H formation.

Equation 2 represents the nucleation model, where the potential nucleation site is eliminated due to the ingestion of growing nucleus or the loss of reactant-product interface due to reaction zones of two or more growing nuclei merge. Equation 3 is for the contracting volume model, which assumes that the nucleation occurs immediately on the surface of the reactants, and the interface moves towards the centre of the sphere reactants, reducing the interface with the volume of the reactant. Equation 4 is diffusion model, which considers that the

movement of reactants to the reaction interface may be restricted by the layer of the product formed on the surface, acting as the limiting factor of the reaction.

$$\{-Ln(1-\alpha)\}^{\frac{1}{n}} = kt \qquad (2)$$

$$1-(1-\alpha)^{\frac{1}{3}} = kt \qquad (3)$$

$$\{1-(1-\alpha)^{\frac{1}{3}}\}^2 = kt \qquad (4)$$

Figures 7, 8 and 9 are the plots of these models for 1H, ½ H and ¼ H respectively, calculated using the extent of reaction estimated for each sample. It should be noted that, for the fitting purpose, Eq. 2 is rearranged into as following:

$$Ln\{-Ln(1-\alpha)\} = n \cdot Ln(k) + n \cdot Ln(t) \qquad (5)$$

The data used was up to 56 days for this analysis, as most of the reactions appeared to have completed by 56 days. The estimation of the extent of reaction is detailed in Appendix 2.

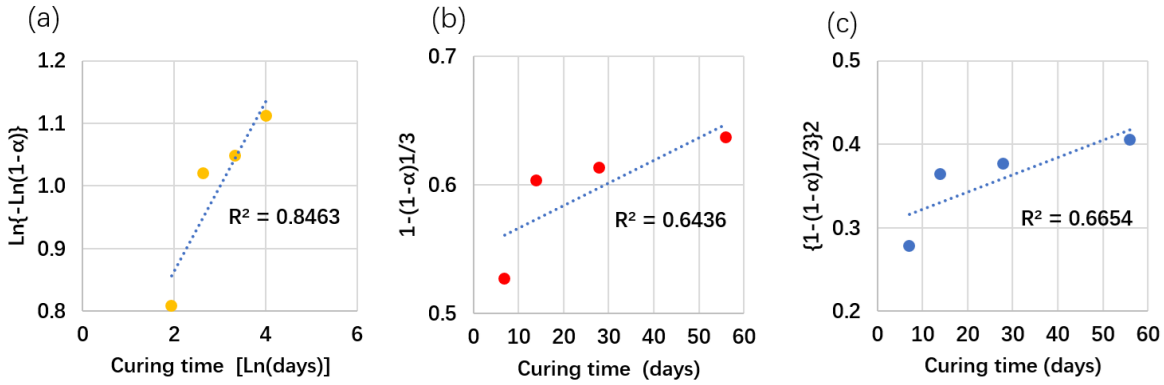

Figure 7. Kinetic models tested for 1H system up to 56 days: (a) nucleation model; (b) contracting model; (c) diffusion model.

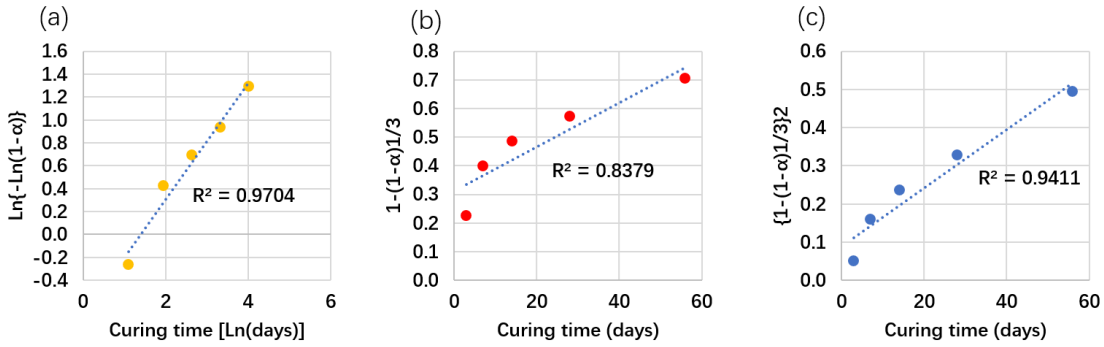

Figure 8. Fitting of the extent of reaction (α) for Mg in ½ H system up to 56 days. (a) nucleation model; (b) contracting model; (c) diffusion model.

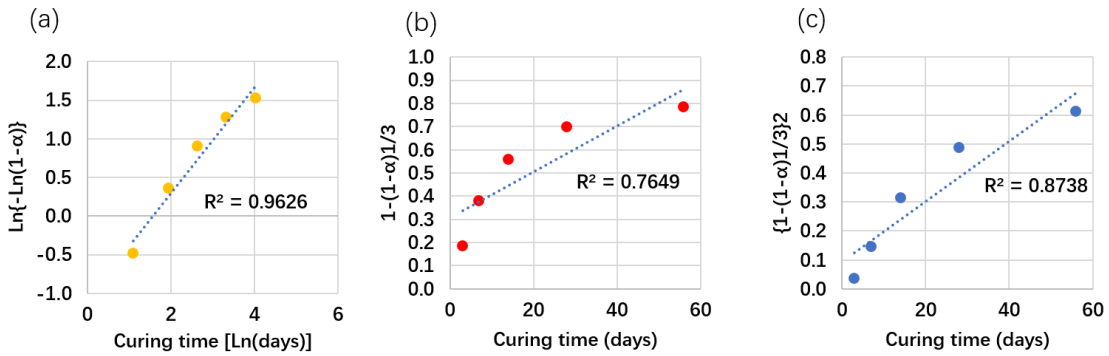

Figure 9. Fitting of the extent of reaction (α) for Mg in ¼ H system up to 56 days. (a) nucleation model; (b) contracting model; (c) diffusion model.

The goodness of fitting can be examined by the R^2 value; the closer the R^2 value is to 1, the better fitting is. In all the systems, nucleation model indicated the best fitting. The goodness of fitting is not very high in the 1H system, which is likely because the reaction reached the completion much faster than 56 days in the 1H system, so that the data used in the fitting were not be the best representative of the reaction for this system. These results imply that the addition of sodium bicarbonate helps the dissolution of the reactants, and the products are less likely to form the shell on the surface of the reactant to prevent further reaction. The pH analysis of the system also suggested that the solubility of the reactants is improved compared to the DW system. The reaction products identified in the studied systems are hydromagnesite and M-S-H. Since the formation and dissolution of hydromagnesite is not kinetically limited in the similar system [78], also the amount of its formation is limited, the entire reaction must be controlled by the precipitation of M-S-H.

4.4 Conclusions

The present study examined the formation of M-S-H gel with the addition of $NaHCO_3$ solutions at different levels of concentrations along with the involved reaction mechanisms and kinetics to elucidate the effects of $NaHCO_3$ concentration and associated pH levels. Such information is crucial for optimisation of $NaHCO_3$ concentration for the accelerated formation of M-S-H.

The increased $NaHCO_3$ concentration (e.g. at the $NaHCO_3$ solubility limit) favoured the acceleration of M-S-H formation, but it was also possible to gain a significant acceleration of M-S-H formation even with decreased amount of $NaHCO_3$ (e.g. 1/4 of the solubility limit). The

study also found that the higher $NaHCO_3$ concentration resulted in the larger amounts of $Mg(OH)_2$ remaining in the system without reacting. Thus, reducing the amount of $NaHCO_3$ content could be an option, if more consumption of $Mg(OH)_2$ ought to be beneficial.

The basic principle of the acceleration in the M-S-H formation was through the formation of hydromagnesite as an intermediate product, which can increase the Mg^{2+} ions and dissolution of silica in the system. The reaction kinetics were also assessed, and it is revealed that the systems studied are likely to be nucleation controlled, via the precipitation of M-S-H. The study also revealed that the molar H_2O/MgO ratio of the M-S-H remained approximately 2 in the systems investigated.

Acknowledgements

Hanein was funded by the Engineering and Physical Science Research Council (EPSRC) through grant: EP/R025959/1. This work was performed, in part, at the MIDAS facility at the University of Sheffield which was established with support from the department of energy and climate change. For the purpose of open access, the author has applied a Creative Commons Attribution (CC BY) licence to any Author Accepted Manuscript version arising.

Author Credit Statement

Han Zhao: Methodology, Validation, Formal analysis, Investigation, Data curation, Writing-Original draft, Visualization, Funding acquisition. Theodore Hanein: Conceptualization, Methodology, Formal analysis, Investigation, Data curation, Resources, Writing-Review & Editing, Supervision, Project Administration. Hajime Kinoshita: Conceptualization, Methodology, Formal analysis, Investigation, Data curation, Resources, Writing-Review & Editing, Supervision, Project Administration, Funding acquisition.

Chapter 4. Appendix 1

For the estimation of $Mg(OH)_2$, the weight loss associated with the dihydroxylation of $Mg(OH)_2$ in Region (II) was calculated by subtracting the background weight loss (attributed to the change in crystallinity of M-S-H) in this temperature region. The background weight loss in Region (II) was estimated based on the linear weight loss trend in 290 – 340 °C. The total water loss from M-S-H was also estimated from the total weight loss of the samples (from 30°C to 990°C) by excluding the weight loss due to the dihydroxylation of Mg(OH)2, assuming the weight loss from the free water and other phases such as hydromagnesite are minimal.

Table A1. Calculations from TG data for amount of water loss from $Mg(OH)_2$ and M-S-H. (a)1H system; (b) ½ H system; (c) ¼ H system.

a) 1H							
Curing time (days)	**Total wt. loss (30 – 990°C)**	**T range (°C) for $Mg(OH)_2$**	**Wt. loss in T range**	**Background wt. loss from M-S-H / 10°C (290 – 340°C)**	**wt. loss from $Mg(OH)_2$**	**$Mg(OH)_2$ (wt.%) calculated**	**Wt. loss from M-S-H**
0	N/A	N/A	N/A	N/A	N/A	45.62%	0
7	30.42%	345-450	3.71%	0.02%	1.29%	4.18%	29.13%
14	34.39%	345-450	3.08%	0.02%	0.72%	2.32%	33.67%
28	32.80%	345-445	2.91%	0.02%	0.68%	2.20%	32.11%
56	31.94%	350-445	2.73%	0.02%	0.57%	1.85%	31.37%
112	29.67%	355-445	2.63%	0.02%	0.55%	1.78%	29.12%

b) ½ H							
Curing time (days)	**Total wt. loss (30 – 970°C)**	**T range (°C) for $Mg(OH)_2$**	**Wt. loss in T range**	**Background wt. loss from M-S-H / 10°C (250 – 310°C)**	**wt. loss from $Mg(OH)_2$**	**$Mg(OH)_2$ (wt.%) calculated**	**Wt. loss from M-S-H**
0	N/A	N/A	N/A	N/A	N/A	47.71%	0
3	24.53%	310-440	8.17%	0.01%	6.27%	20.30%	18.26%
7	26.31%	320-470	5.60%	0.02%	2.87%	9.29%	23.44%
14	27.72%	330-460	4.40%	0.02%	1.75%	5.68%	25.97%
28	26.14%	340-450	3.29%	0.02%	1.0%	3.34%	25.10%
56	31.31%	360-425	1.48%	0.02%	0.32%	1.04%	30.99%
112	29.68%	370-420	1.20%	0.02%	0.15%	0.50%	29.52%

c) ¼ H							
Curing time (days)	**Total wt. loss (30 – 990°C)**	**T range (° C) for $Mg(OH)_2$**	**Wt. loss in T range**	**Background wt. loss from M-S-H / 10°C (280 – 320°C)**	**wt. loss from $Mg(OH)_2$**	**$Mg(OH)_2$ (wt.%) calculated**	**Wt. loss from M-S-H**
0	N/A	N/A	N/A	N/A	N/A	48.83%	0
3	21.84%	325-470	9.19%	0.01%	7.65%	24.76%	14.19%
7	24.22%	330-470	5.41%	0.02%	3.26%	10.55%	20.96%
14	28.21%	360-470	2.95%	0.02%	1.11%	3.61%	27.10%
28	26.28%	370-425	1.34%	0.02%	0.37%	1.18%	25.91%
56	28.04%	375-410	0.75%	0.02%	0.13%	0.43%	27.91%
112	28.63%	380-410	0.63%	0.02%	0.08%	0.27%	28.54%

The weight loss from $Mg(OH)_2$ (column 6) is calculated by subtract background water loss [(column 5) times temperature range in column 5] from the total weight loss in the brucite decomposition range (column 4).

Chapter 4. Appendix 2

The initial amount of $Mg(OH)_2$ was estimated based on the initial formulation of the sample and the TG data, assuming all H_2O are lost from the system when heated up to 990°C, leaving mostly MgO and SiO_2 with minor quantity of $Na2CO_3$. The amount of reacted $Mg(OH)_2$ was obtained from the initial amount of $Mg(OH)_2$ by subtracting remaining mass of $Mg(OH)_2$estimated from the TG data.

Table A2. Estimation of the extent of reaction: (a) 1H system; (b) ½ H system; (c) ¼ H system

a) 1H					
Curing Time	**Solid**	**Mg total**	**remaining Mg**	**reacted Mg**	**Extent α(Mg)**
(days)	(wt%)	(mol/100g)	(mol/100g)	(mol/100g)	
0	100.00	0.78	0.78	0.00	0.00
7	69.58	0.68	0.07	0.61	0.89
14	65.61	0.64	0.04	0.60	0.94
28	67.20	0.65	0.04	0.62	0.94
56	68.06	0.66	0.03	0.63	0.95
112	70.33	0.68	0.03	0.65	0.96

b) ½ H					
Curing Time	**Solid**	**Mg total**	**remaining Mg**	**reacted Mg**	**Extent α(Mg)**
(days)	(wt%)	(mol/100g)	(mol/100g)	(mol/100g)	
0	100.00	0.82	0.82	0.00	0.00
3	75.47	0.75	0.35	0.40	0.54
7	73.69	0.73	0.16	0.57	0.78
14	72.28	0.72	0.10	0.62	0.86
28	73.86	0.73	0.06	0.68	0.92
56	68.69	0.68	0.02	0.66	0.97
112	70.32	0.70	0.01	0.69	0.99

¼ H					
Curing Time	**Solid**	**Mg total**	**remaining Mg**	**reacted Mg**	**Extent α(Mg)**
(days)	(wt%)	(mol/100g)	(mol/100g)	(mol/100g)	
0	100.00	0.84	0.84	0.00	0.00
3	78.16	0.78	0.42	0.36	0.46
7	75.78	0.76	0.18	0.58	0.76
14	71.79	0.72	0.06	0.66	0.91
28	73.72	0.74	0.02	0.72	0.97
56	71.96	0.72	0.01	0.71	0.99
112	71.37	0.72	0.00	0.71	0.99

Chapter 5. The effect of sodium carbonate on the formation of magnesium silicate hydrate

Abstract

Practical application of magnesium silicate hydrate (M-S-H) cements is hindered due to their relatively slow setting time and low early strength development. Our previous study showed that the formation of the M-S-H binders can be accelerated by the addition of sodium bicarbonate ($NaHCO_3$) [60]. To further understand the effect of carbonate additives on the M-S-H formation, sodium carbonate (Na_2CO_3) is tested in this study. Aqueous solutions of Na_2CO_3 are used at different concentrations to hydrate a mixture of magnesium hydroxide ($Mg(OH)_2$) and microsilica. The products are analysed by X-ray diffraction (XRD), thermogravimetry (TG) and ex-situ pH measurements to track the evolution of M-S-H and other phases. The obtained results indicated that Na_2CO_3 introduced a significantly different effects on the consumption of brucite in the system, typically having a dormant period of initial ~7 days. The concentration of carbonate ions seems important, but the level of sodium concentration (or pH) appears to be in a certain range for the carbonate ions to work effectively.

5.1 Introduction

The demand for Portland cement substitutions keep increasing in recent years due to the high energy cost and carbon dioxide emission of the Portland cement. Magnesium-based cements can be a possible option to reduce the carbon dioxide emission from cement industries due to their lower temperature requirements for production [5]. However, the application of magnesium cements is constrained by their slow setting and early strength development. For example, magnesium silicate hydrate (M-S-H) is one of the interested binder phases of magnesium cements, but it may take few months to achieve desired strength at room temperature [22].

As shown in our previous study, the formation of M-S-H can be accelerated by the addition of $NaHCO_3$ into the batch [60]. Although the exact acceleration mechanism of the reaction remains unclear, a few possible factors can influence the formation of M-S-H: the addition of $NaHCO_3$ changes the pH of the batch, balancing the solubility of silicate and magnesium ions, leading to the pH of the solution approaching an optimum pH range for M-S-H formation and accelerates the reaction; the addition of Na^+, HCO_3^-, and/or CO_3^{2-} ions can possibly lead to the formation of intermediates that accelerate the overall M-S-H formation by providing another route of reaction.

To investigate the acceleration mechanism further, this work investigates the formation of M-S-H gel with the addition of Na_2CO_3 solutions. As our previous study revealed that the concentration of $NaHCO_3$ has an impact on the acceleration in the formation of M-S-H, the investigation was conducted focusing on the effects of Na_2CO_3 concentrations. Because Na_2CO_3 has a much higher solubility in water compared with $NaHCO_3$ [80], this system has a potential to provide larger amount of sodium and carbonate ions in the mixing solution of the cement pastes, which may offer a greater possibility to optimise the acceleration of M-S-H development.

The present work also envisages to study the importance of ions, including sodium and carbonate, through the comparison of the Na_2CO_3 system with the $NaHCO_3$ system or NaOH system. The Na_2CO_3 system would provide the balance between sodium and carbonate ions ($Na:CO_3$ = 2:1) different from $NaHCO_3$ system ($Na:CO_3$ = 1:1) or NaOH system ($Na:CO_3$ = 2:0).

5.2 Materials and Methods

5.2.1 Materials

The raw materials used in this work are brucite from Sigma-Aldrich with purity ≥95%, microsilica 940-U from Elkem, sodium carbonate from Sigma-Aldrich with purity ≥99.5% and laboratory distilled water. The X-ray fluorescence (XRF) data of the microsilica used in listed in Table 1, presenting the oxide composition (constituents with >0.1 wt.% only) and loss on ignition (LOI).

Table 1. Oxide composition of the silica fume

Element	SiO_2	K_2O	MgO	Fe_2O_3	Al_2O_3	Na_2O	CaO	ZnO	LOI	Total
Weight %	94.36	1.12	0.71	0.61	0.50	0.32	0.22	0.20	1.82	99.86

5.2.2 Sample mix design

M-S-H cement pastes were prepared by mixing brucite and microsilica with various concentrations of Na_2CO_3 solutions as shown in Table 2. The distilled water (DW) sample is has no additives, and data was adopted from previous work for comparison [60]. The concentration of Na_2CO_3 solutions was determined based on its solubility in water at 20°C [80], which is 21.5 g/100ml. 1C represent the concentration close to saturation, 1/2C is half of this concentration and so on. Two exceptions are 8.77pH-C and NaOH-C samples. 8.77pH-C represents the initial pH of 8.77 for the solution used, matching with the sample prepared in our previous work with $NaHCO_3$ solution [60]. In the NaOH-C sample, the quantity of NaOH was designed to have the same moles of Na^+ ions to the 1C, but no presence of carbonate ions. These additional formulations would allow us to examine the importance of the initial pH, Na^+ and CO_3^{2-} ions for accelerated development of M-S-H.

Table 2. Composition and initial pH of solutions for the systems studied

	solution		solid	
Sample ID	Water (mL)	Na_2CO_3 (g)	$Mg(OH)_2$ (g)	Silica fume (g)
DW	200	0	100.1	100.0
1.5C	200	64.5	100.1	100.0
1C	200	43.0	100.1	100.0
1/2C	200	21.5	100.1	100.0
1/4C	200	10.8	100.2	100.0
1/8C	200	5.4	100.0	100.0
1/16C	200	2.7	100.0	100.0
8.77pH-C	200	0.003	100.0	99.9
NaOH-C	200	(NaOH) 16.23	100.0	100.1

5.2.3 Experimental procedure

The experimental procedure is based on our previous study [60]. The solution for each sample was prepared first by dissolving Na_2CO_3 (or NaOH) in distilled water using magnetic stirrer for approximately 15 minutes at laboratory temperature (~20°C) until the solution becomes colourless. The solution was then placed into a mixer (Heidolph RZR2020, 400rpm), and all the brucite powder was added over approximately 5 minutes of mixing. Silica fume was then slowly added into the mixer with approximately 20 % of total mass every minute (total of 5

minutes) to allow homogeneous mixing. After mixing, the cement paste was poured into 50 mL centrifuge tubes, and the tubes were then sealed with the lid and parafilm.

The sealed pastes were cured in a 35° C oven, then taken out after 3, 7, 14, or 28 days of curing. The samples were crushed into powders and washed in approximately 200 mL of acetone for 5 minutes to arrest the hydration. The washed powders were then separated from the acetone by using filter paper and a Büchner funnel assisted with vacuum pump for approximately 5 minutes. The separated materials are immersed into approximately 200 mL of new acetone again and kept for 48 hours in order to remove the free water. The samples were separated from acetone again by using filter paper and Büchner funnel for 15 minutes. The dried samples are stored in sealed centrifuge tubes with parafilm until further analysis.

5.2.4 Characterisation methods

5.2.4.1 X-ray diffraction

The X-ray diffraction (XRD) was used for the phase analysis. The machine used was benchtop Bruker D2 PHASER apparatus armed with a Cu-Kα radiation source running at 30 kV and 10 mA. The divergence silt used was 1 mm, the upper and lower discriminators were 0.11 and 0.25 V respectively. The scanning angle range was from 5° to 80° 2θ with an increment of 0.02°. The sample was rotating at 15 rpm during scanning to avoid uneven distribution of microstructure. The samples are crushed and ground into powders before measurement.

5.2.4.2 Thermogravimetric analyses

Thermogravimetric analyses (TGA) was also used for the phase analysis. The tests were carried out by using PerkinElmer TGA 4000. Approximately 40 mg of samples were used for testing each time. The sample was heated from 30°C to 990°C at a rate of 10 °C/min under a nitrogen flow of 40 mL/min. Ten minutes of isothermal hold was used at both the start and end of the heating programme.

5.2.4.3 pH measurement

The apparatus used for pH measurements was a Mettler Toledo pH/Cond bench meter SE S470-K equipped with an expert proISM probe (error = ±0.01). The probe was calibrated each time before use by immersing into standard buffer solutions with known pH values. The pH of the samples at 0 day (initially prepared batch) was measured right after the batch was mixed properly; a small portion of the batch was separated, and then the testing probe was inserted directly into the paste to take the readings. For the cured samples, ex-situ leaching method [51] was used for the pH measurement. For each measurement, 1 g of powdered sample was

added into 80 mL of distilled water and then stirred with a magnetic stirrer, before the testing probe was immersed into the solution. The pH reading was recorded after > 15 minutes of stirring when the pH reading of the solution stabilised. For the ex-situ tests, preliminary tests were performed to determine the amount of cement to be added, in which 0.2 g, 0.6 g, or 1.0 g of a cured cement sample was added after powdered into 80 mL of distilled water These preliminary tests showed that the pH readings for > 0.6g addition are the same, implying that the solution is already saturated. It should be noted that this method to measure the pH of the samples assumes the pore solution of the cement is in over saturated state.

5.3 Results and discussion

5.3.1 Phase formation and consumption of $Mg(OH)_2$

5.3.1.1 Near saturation concentration (1C)

The XRD pattern of 1C sample is presented in Figure 1. According to the literature, the broad humps at 10-13°, 20-30°, 35-39°, and 58-62° 2θ can be attributed to M-S-H [21]. The hump at 10-13° was observed in slightly lower angle in these samples, as observed previously in the $NaHCO_3$ system [60] The broad hump at 18–25° 2θ is attributed to unreacted silica fume [26]. The sharp peaks at 18.6°, 38.0°, 50.8°, and higher angles attributed to brucite [21].

The data shows that the majority of brucite was consumed by 14 days in the 1C system. In our previous study, the system without addition of carbonate species indicated a similar level of brucite consumption at 56 days [60]. Therefore, the consumption of brucite is clearly accelerated by introducing Na_2CO_3 to the system at this level. However, the consumption of brucite appears to have occurred mostly between 7 and 14 days, as there is little change in the intensity of the reflection peaks for brucite up to 7 days. This is a significant difference from the system with $NaHCO_3$, as the consumption of brucite was clearly observed as early as 3 days when $NaHCO_3$ was introduced in our previous study [60].

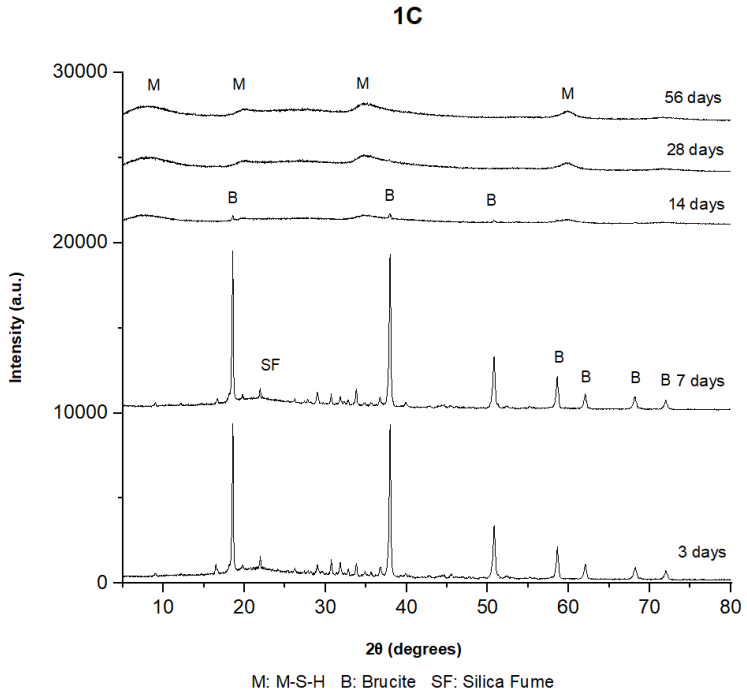

Figure 1. The XRD pattern of 1C sample at different ages (3-56 day). Reflection peaks are labelled as: brucite (B), silica fume (SF), M-S-H gel (MSH).

The data also shows number of small reflection peaks in the lower angles up to ~40° 2θ. Hydromagnesite $Mg_5(CO_3)_4(OH)_2{\cdot}4H_2O$, identified as an intermediate phase in the $NaHCO_3$ system was not observed in the current Na_2CO_3 system. As shown in Table 3, other carbonate phases considered did not show good match with the obtained data, except eitelite which has a main reflection peak at ~34 ° 2θ. These small peaks could also be attributed to magnesium silicate phases, and forsterite Mg_2SiO_4, enstatite $MgSiO_3$ and talc $Mg_3Si_4O_{10}(OH)_2$ have reasonably good match as shown in Table 4.

Table 3. Potential carbonate phases considered

Phase	Formula	Typical position ° 2θ of peaks (weaker peaks)	Reference
Hydromagnesite	$Mg_5(CO_3)_4(OH)_2{\cdot}4H_2O$	(14), 15, (20), 21, 31	[52]
Dypingite	$Mg_5(CO_3)_4(OH)_2{\cdot}5H_2O$	8, (14), 15, (20), 21, 31	[81]
Magnesite	$MgCO_3$	32, 43, 54	[82]
Eitelite	$Na_2Mg(CO_3)_2$	(23.5), (33), 34, (36), (40)	[67]
Natrite	Na_2CO_3	27, 30, (38), (40.5)	[83]
Nahcolite	$NaHCO_3$	18, 30.5, 34.5	[84]

Table 4. Potential magnesium silicate phases considered

Phase	Formula	Mg/Si ratio	Typical position ° 2θ of peaks (weaker peaks)	Reference
Forsterite	Mg_2SiO_4	Mg/Si = 2	(17.5), 23, 32, 36, 37, 40	[85]
Lizardite	$Mg_3Si_2O_5(OH)_4$	Mg/Si = 1.5	12 (19), 24, 26, (42)	[86]
Enstatite	$MgSiO_3$	Mg/Si = 1	(20), 28, (30), 31, 36	[47]
Talc	$Mg_3Si_4O_{10}(OH)_2$	Mg/Si = 0.75	9, 19, 28.5, 34, 36	[87]
Sepiolite	$Mg_4Si_6O_{15}(OH)_2{\cdot}6H_2O$	Mg/Si = 0.67	7.5, 19.5, 20.5, 26, 35, 40	[88]

5.3.1.2 Over saturation concentration (1.5C)

For the 1.5C samples, the XRD patterns shown in Figure 2 are having similar peak positions and intensities to those for the 1C samples (Figure 1). The broad peaks for M-S-H are almost fully developed at 14 days, while the peaks intensities for brucite peaks remain large until 7 days and almost disappeared at 14 days. The addition of sodium carbonate accelerates the M-S-H formation, but with the limit up to the saturation in the water, as the excess amount of Na^+ and/or CO_3^{2-} ions do not appear to enhance the M-S-H formation further. The 1.5C system does not follow the trend of the gradual consumption of brucite as in the sodium bicarbonate system [60], but consume majority of brucite between 7 and 14 days, also observed in the 1C system. A difference from the 1C system is the small reflection peaks observable at 56 days, which suggests likely formation (re-precipitation) of talc $Mg_3Si_4O_{10}(OH)_2$ in 1.5C samples.

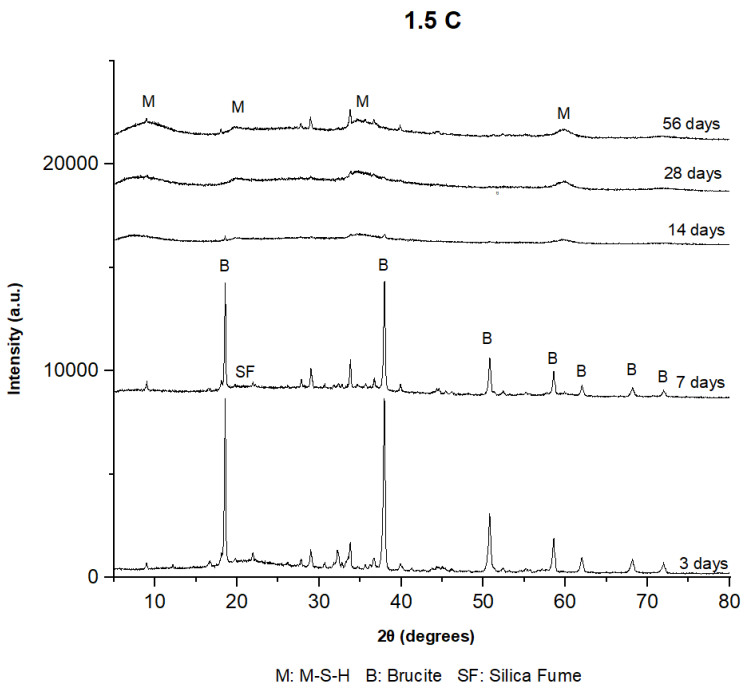

Figure 2. The XRD pattern of 1.5C sample at different ages (3-56 day). Reflection peaks are labelled as: brucite (B), silica fume (SF), M-S-H gel (MSH).

5.3.1.3 Reduced concentrations (1/2C, 1/4C, 1/8C, 1/16C)

When the concentration of Na_2CO_3 is reduced, the reaction of the systems appears to gradually slow down except the 1/2C sample. As shown in Figure 3 (a), in the 1/2C system, the reaction of brucite is very limited even at 28 days, as if the dormant period of brucite consumption, observed in the first 7 days for 1C system is extended. On the other hand, in 1/4C (Figure 3 (b)), 1/8C and 1/16C samples (Figures 4 (a) and (b) respectively), with the decreasing of sodium carbonate concentration, the acceleration trend of M-S-H formation reduced accordingly. The 1/4C samples show the full consumption of brucite at 28 days, while 1/8C and 1/16C still have small amount of brucite remained at 28 days. These samples, including 1/2C system, show a faster reaction compared with the system with no addition of carbonate which requires 112 days for brucite to react lower than the detention limit of XRD [68].

The XRD data for 1/2C system was inconsistent with other systems. The inconclusive trend of the Na_2CO_3 concentration may suggests that the reaction is not completely depending on the concentration of Na_2CO_3.

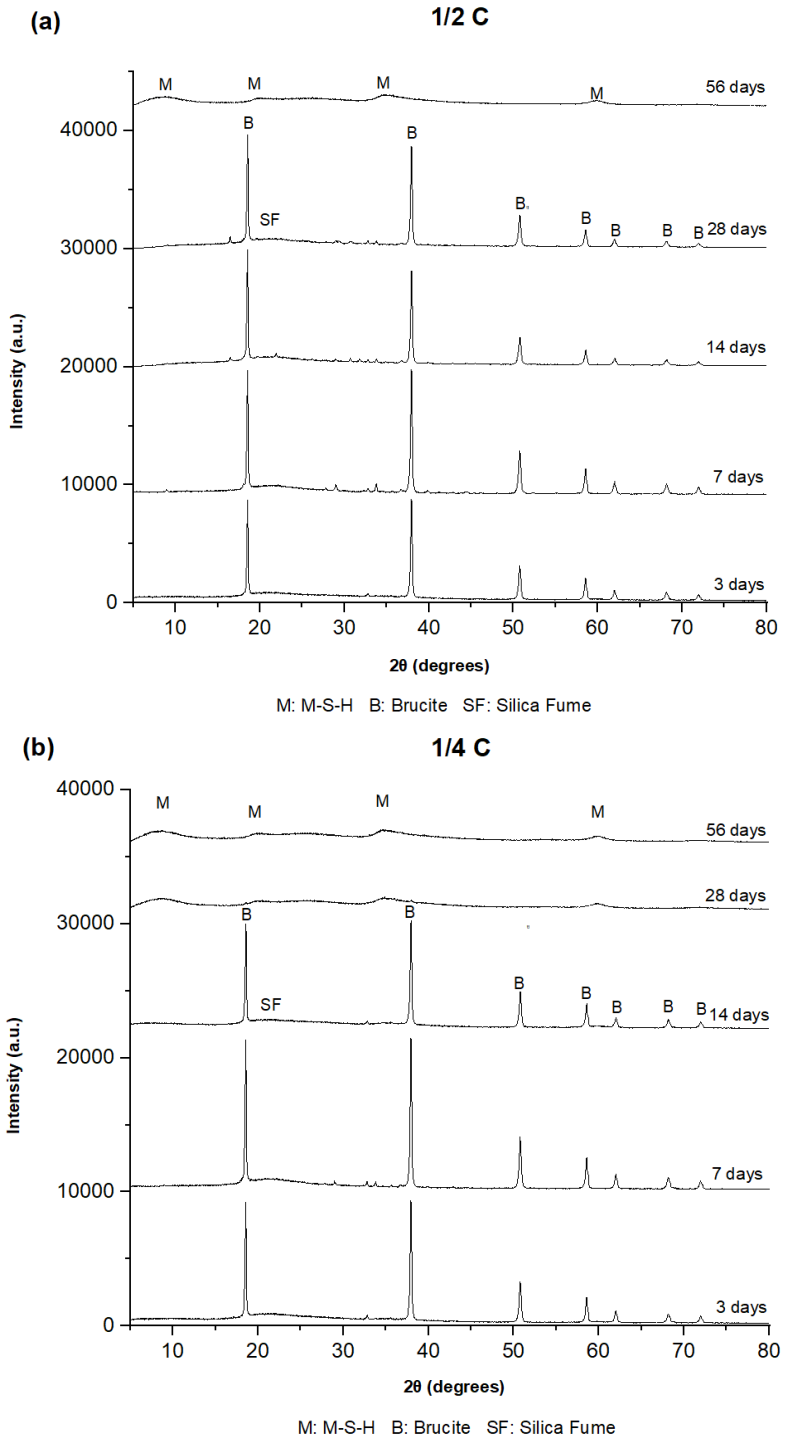

Figure 3. The XRD pattern of samples at different ages: (a) 1/2C, (b) 1/4C samples. Reflection peaks are labelled as: brucite (B), silica fume (SF), M-S-H gel (MSH).

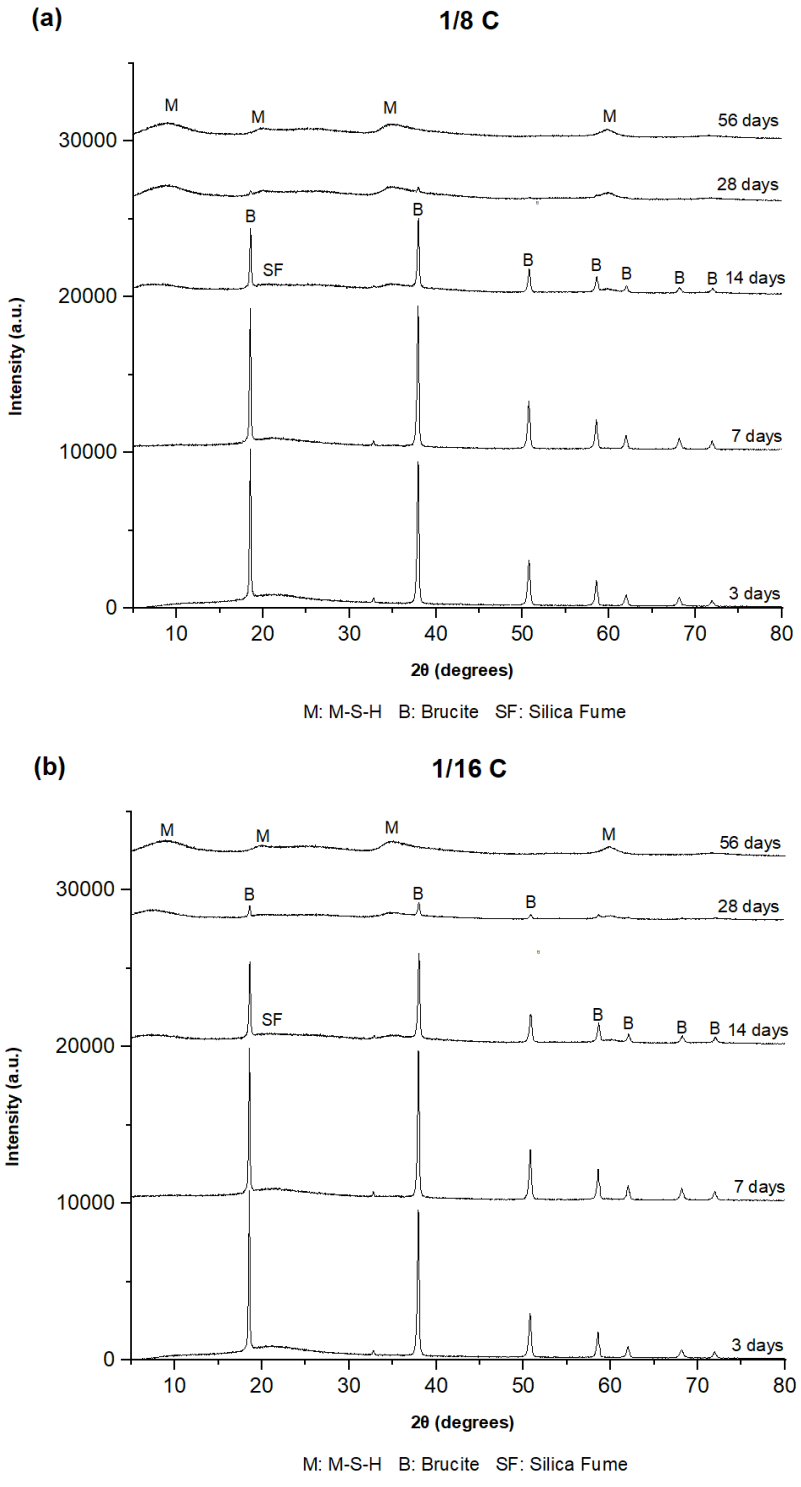

Figure 4. The XRD pattern of samples at different ages: (a) 1/8C, (b) 1/16C samples. Reflection peaks are labelled as: brucite (B), silica fume (SF), M-S-H gel (MSH).

5.3.1.4 Effect of initial pH and Na^+ ions (8.77pH-C, NaOH-C)

The XRD patterns for 8.77pH-C samples shown in Figure 5 (a) indicate that a large amount of brucite was still remained at 28 days, and the consumption is not completed at 56 days. Because this system was designed to have the same initial pH value to the $NaHCO_3$ system which indicated a significant acceleration in the M-S-H development, it can be said that the initial pH cannot solely be the cause of the acceleration and the presence of certain ions are necessary. However, the 8.77pH-C samples still shows faster brucite consumption rate than the system without carbonate [60], even with the addition of 0.003 g (0.0015 wt%) of sodium carbonates.

For NaOH-C samples, Figure 5 (b) reveals that a significant amount of the brucite remained in the system without reacting up until 56 days. This system differs from the 1C system by the lack of carbonate ions and introduction of extra hydroxyl ions. Therefore, the results imply that the acceleration in M-S-H hydration is not caused solely by the concentration of Na^+ ions of the initial solution and that the presence of carbonate ions is important.

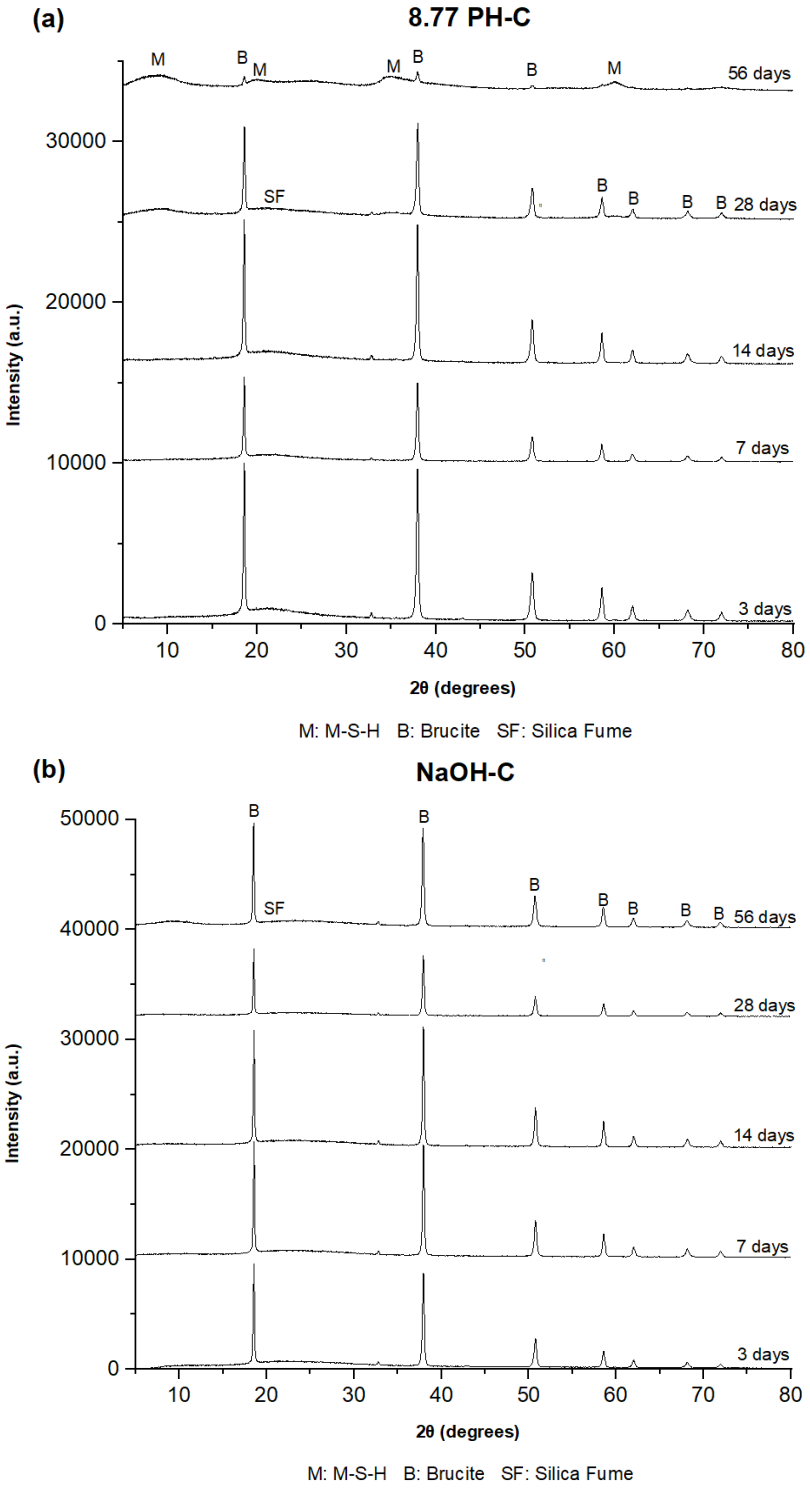

Figure 5. The XRD pattern of samples at different ages: (a) 8.77pH-C, (b) NaOH-C samples. Reflection peaks are labelled as: brucite (B), silica fume (SF), M-S-H gel (MSH).

5.3.2 Evolution of pH

The results of the pH measurement for the 1C, 1/2C, 1/4C, 1/8C, 1/16C, 8.77pH-C and NaOH-C samples are shown in Figure 6.

Most of the systems have a decreasing trend of pH value in the first 7 days, then the pH is increasing from 7 days to 14 days, followed by a gradual decrease after 14 days. This bimodal trend becomes milder when the concentration of the added Na_2CO_3 decreases and negligible for the 1/16C system in which the pH value decreases continuously. Differing from the bicarbonate system [60], all the carbonate samples are having starting pH around or higher than 10.5 (the pH of saturated brucite solution). The relatively high pH value encourages the dissolution of silica fume but hinders the dissolution of brucite [35], also the relatively large CO_3^{2-} concentration from the dissolved Na_2CO_3 can act as strong inhibitors of brucite dissolution [89]. These factors can be the possible reasons for the limited consumption of brucite at the initial stage, as suggested in the XRD patterns.

For 1C samples, the XRD data (Figure 1) suggests that the consumption of brucite mostly occurred between 7 and 14 days, which correspond to the increase in the pH of the system shown in Figure 6. The relatively high initial pH must have inhibited the dissolution of brucite at the early stage, as brucite can reach its saturation at the pH value of ~10.5 [14]. Since little brucite is reacting, the decrease in the pH value in the first 7 days is likely caused by the dissolution of silica. It is known that the dissolution of silica in a high pH environment results in formation of silicate ions with the consumption of OH^- ions and associated decrease in pH [35]. When the pH lowers to the sufficient level by 7 days, brucite appears to start reacting, which in return increases the pH of the system again. It is interesting to see the system maintains its pH > 10.5 while brucite is reacting. The presence of silicate and/or carbonate ions may be assisting this.

For the 1/2C samples, it is difficult to clearly interpret the pH evolution of this system. Although it follows the general bimodal trends, decrease of the pH value in the first 7 days followed by the increase up to 14 days, the XRD data of this system did not follow the general trends observed in the other systems. A significant amount of brucite remained in the system until 28 days as presented in the XRD data. A significant reaction of brucite between 28 and 56 days appeared to have resulted in a possible increase in pH during this period. It should be noted that the 1/2C samples are having similar CO_3^{2-}concentration (1.03 mol/L) to the 1H sample (1.14 mol/L) in our previous study, which indicated a significant acceleration in the development of M-S-H [60]. Since the 1/2C samples indicated only a minimal acceleration in the M-S-H development, the CO_3^{2-}concentration cannot solely be the main rate determining

condition of M-S-H formation. The 1C samples are containing approximately two times of Na^+ ions and associated high pH environment compared with the 1H samples.

With the decreasing of Na_2CO_3 concentration, the starting pH value and 56 days pH value become lower in the 1/4C, 1/8C and 1/16C systems. As previously mentioned, the bimodal trend of pH evolution becomes milder with the lower the concentration of the added Na_2CO_3.

The concentration of Na^+ ions in the 1/4C samples (1.03 mol/L) are similar to that in the 1H sample (1.14 mol/L) in our previous study [60] while the CO_3^{2-}concentration of 0.51 mol/L is approximately half of 1.14 mol/L in the 1H samples. Since the 1/4C samples indicated a similar level of acceleration in the brucite consumption to the 1/2H samples which have a CO_3^{2-} concentration of 0.57 mol/L [60], especially after the initial dormant period of 7 days, it appears that the concentration of CO_3^{2-} ions appears to control the acceleration of brucite reaction and M-S-H development, and having the Na^+ concentration in this range is important for the CO_3^{2-} ions to work.

The 8.77pH-C samples are having similar pH values (9.92 at 3 days, 9.91 at 7 days) to the 1H sample using $NaHCO_3$ (9.91 at 3 days, 9.96 at 7 days) in our previous study [60], but the consumption of brucite is much slower, which confirms that the dissolution of brucite and formation of M-S-H is not solely determined by the initial pH of the batch.

The NaOH-C samples are having much higher pH values at all testing dates, inhibiting the dissolution of brucite as suggested in the XRD patterns. Although the high pH environment should enhance the dissolution of silica component, resulting in the reduction of pH in the first 7 days, the level of pH appears to be still too high for the smooth reaction of brucite. As observed in the XRD data, a significant amount of brucite appears to be present in the system even after 56 days. The obtained results imply that the dissolution of brucite and formation of M-S-H cannot be accelerated solely by the presence Na^+ ions in the sample.

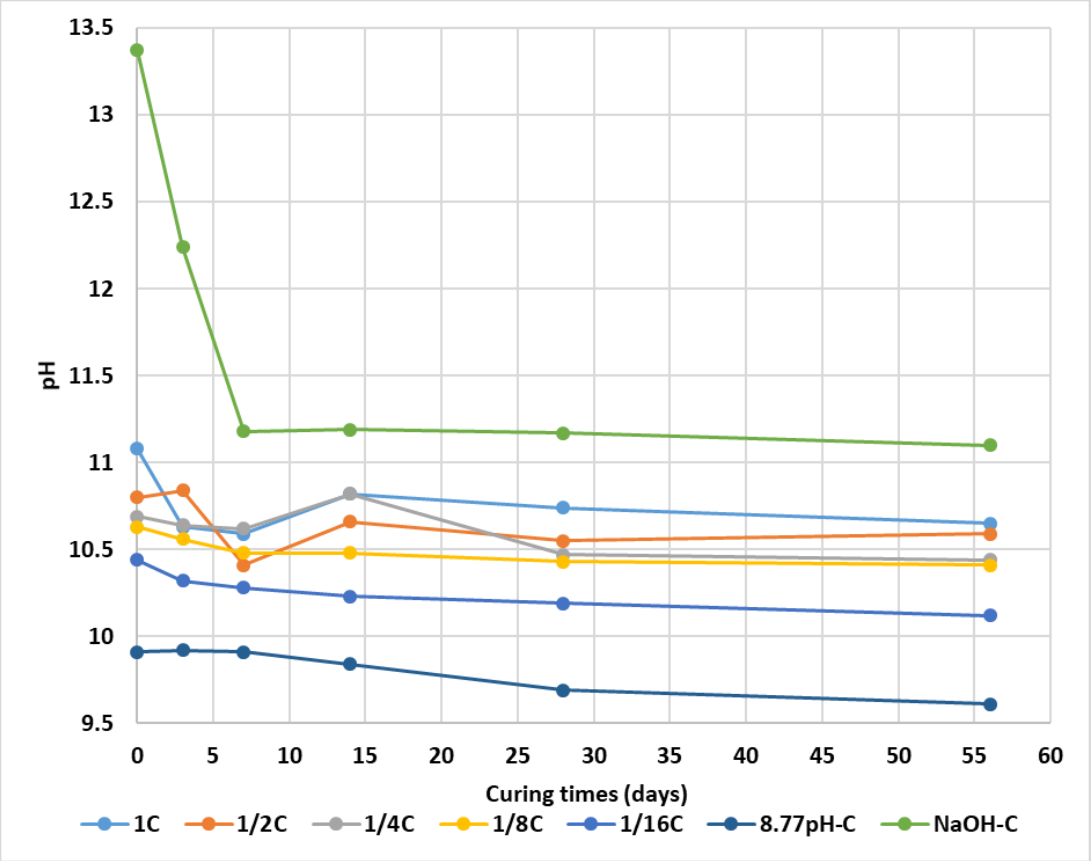

Figure 6. The pH measurements over time for cements with different starting solutions.

5.3.3 Quantification of phases

Thermal analysis was performed on the Na_2CO_3 samples to further investigate the phase development. The thermogravimetric (TG) curves and differential thermogravimetric (DTG) curves of 1C samples are shown in Figure 7. The weight loss step around 90°C corresponds to the loss of water bounded to M-S-H [21, 62]. The peaks are increasing from 3 to 28 days and then reduced after curing for 56 days. The similar trend also appears in our previous sodium bicarbonate samples [60]. The weight loss step around 370°C is mainly caused by the thermal decomposition of brucite [21], and it consistent with the XRD data that the brucite are maintained in the samples at 7 days and almost consumed after 14 days.

The broad peaks attributes to the loss of the coordination water of M-S-H at around 500 – 600 °C is not showing the increasing trend with time in the DTG curves [21], which may due to the overlapping with other dehydration or decarbonation steps. However, the peaks at around 730°C is showing the growth trend with time, which can be attributed to the dehydration of chemically bound water from talc ($Mg_3Si_4O_{10}(OH)_2$). Although natural talc tend to lose its water over 800°C, synthetic talc can lose their water at lower temperatures [90].

The TG and DTG curves for 1/2 C samples are presented in Figure 8. Unlike the 1C samples (Figure 7(b)), the DTG curves show increasing trend up to 56 days in the first weight loss step at the lower temperature (~70°C). This is probably due to the curing time is not long enough for this type of water bounded to M-S-H to be reduced, since the reactions were quite limited in this particular system until 28 days as suggested by the XRD analysis. The thermal decomposition step of brucite at around 380 °C shows relatively large amounts of brucite are remained in the samples up to 28 days and are almost consumed at 56 days, which is consistent with the XRD results.

In 14 and 28 days, the peaks at ~420°C may indicate the presence of hydromagnesite [91], implies the hydromagnesite was formed as the intermediates during the reaction, as this peak is not presenting at 56 days while the broad curve at 500 – 600 °C shows the formation M-S-H [21]. The peaks at ~800°C is not showing clear trend with curing time, and may refers to the limited formation of dolomite ($CaMg(CO_3)_2$) [92].

The TG and DTG curves for 1/4 C samples are presented in Figure 9. The first weight loss step at ~70 °C is showing the increasing trend until 28 days and then reduced at 56 days. The step indicating the brucite decomposition at ~370 °C [21] also consistent with the XRD data, which brucite are remained in the samples until 14 days and then almost consumed between 14 days and 28 days. The broad peaks in the 28 days and 56 days around 500 – 600 °C shows the development of M-S-H [21], and implies the M-S-H are almost fully developed at 28 days.

The 1/4 C samples are having similar Na^+ ions concentration and approximately half of CO_3^{2-} concentration compared to the 1H samples [60]. By making comparison of the DTG curves between them, the peaks for magnesite or hydromagnesite are not showing in the 1/4 C samples, probably due to the less CO_3^{2-} existing in the samples. However, the consumption of brucite and formation of M-S-H is slower in the 1/4 C samples, implies the addition of CO_3^{2-} aids the formation of magnesite or hydromagnesite and accelerates the reaction.

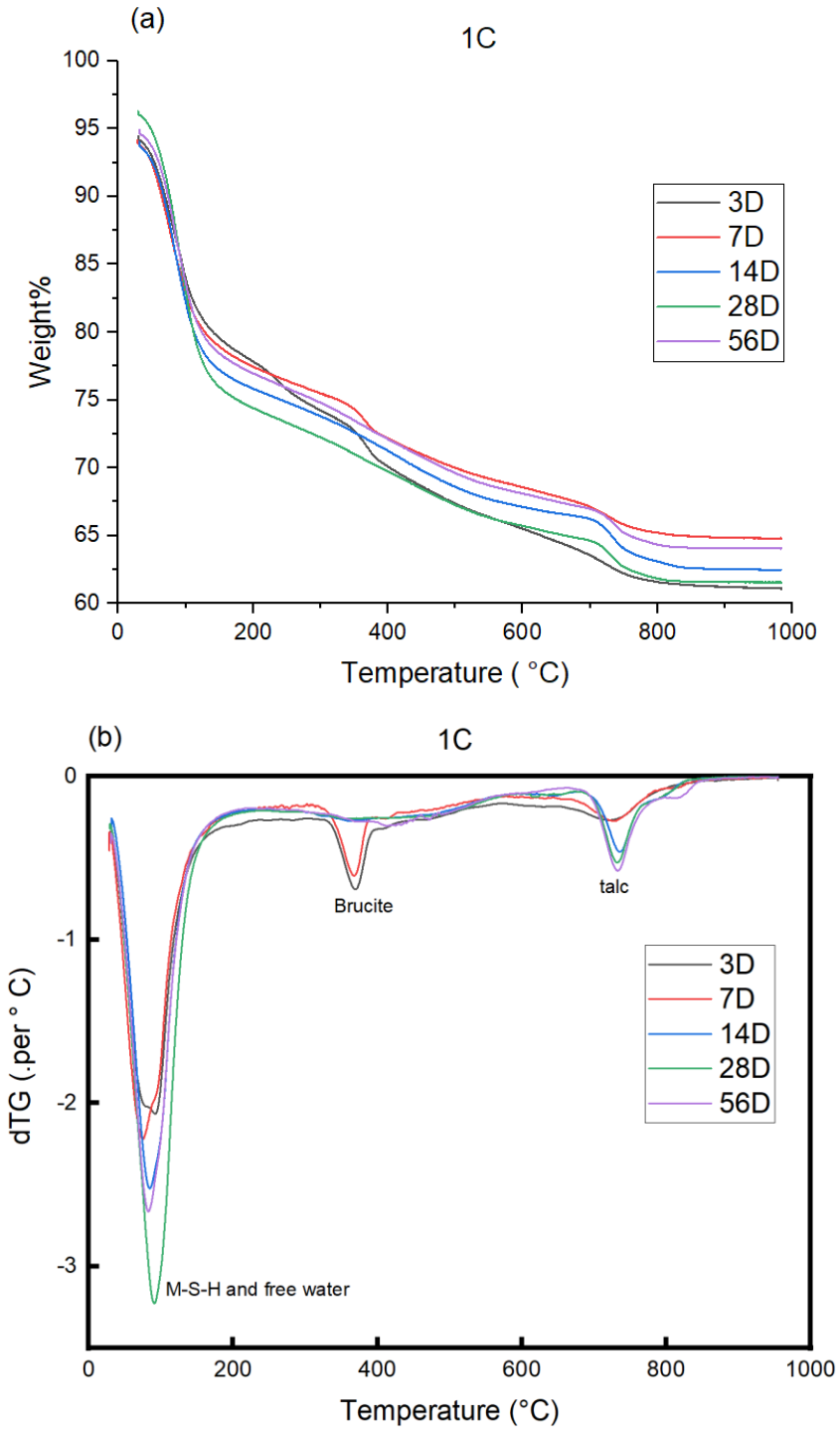

Figure 7. The thermal analysis of 1C samples: (a) TG curves; (b) DTG curves.

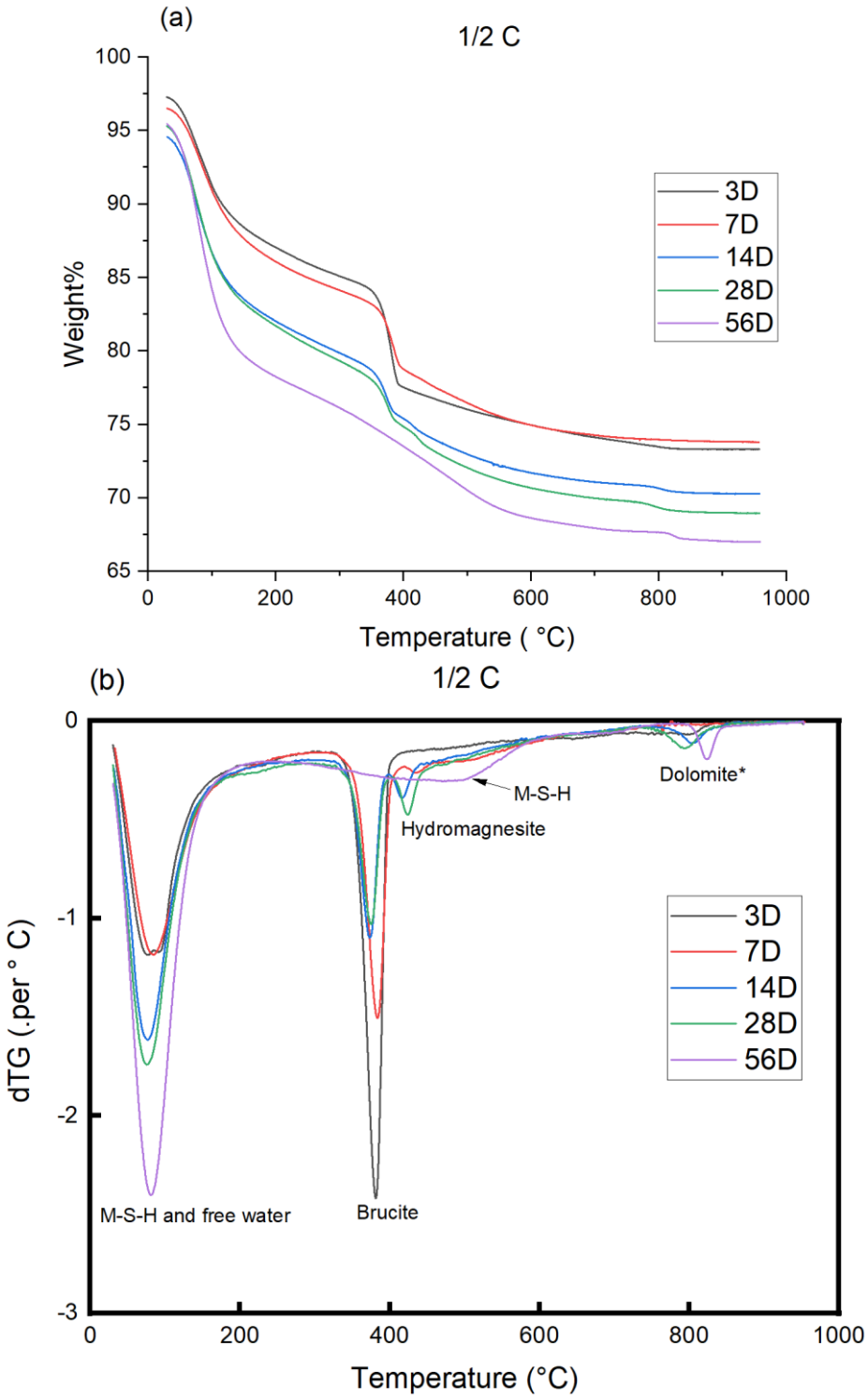

*Figure 8. The thermal analysis of 1/2 C samples: (a) TG curves; (b) DTG curves. (*indicate the possible phases)*

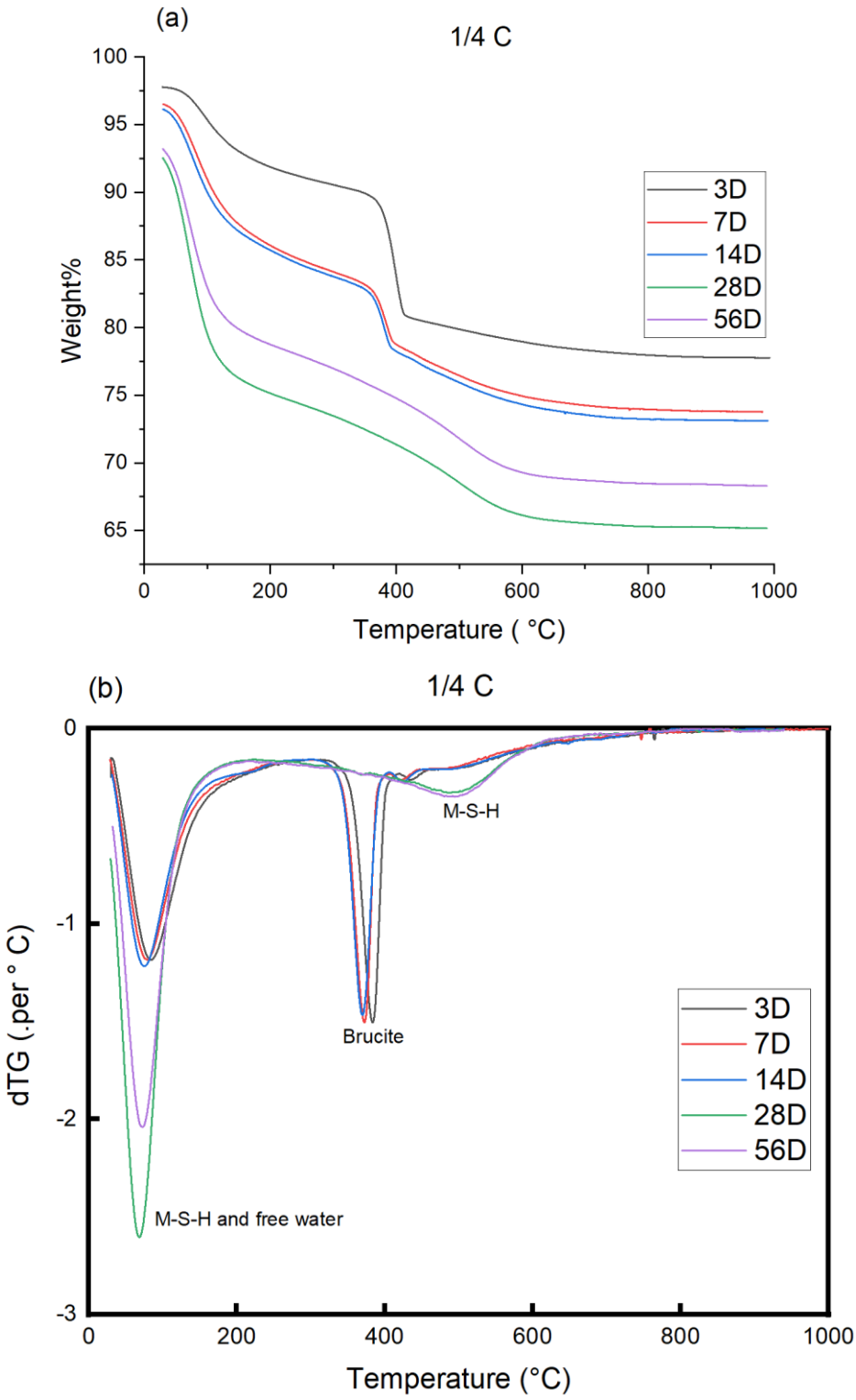

Figure 9. The thermal analysis of 1/2 C samples: (a) TG curves; (b) DTG curves.

5.3.4 Difference between Na_2CO_3 and $NaHCO_3$ systems

The obtained results suggest that the introduction of Na_2CO_3 has different effects on the reactions taking place in the $Mg(OH)_2$-SiO_2 system investigated, compared with the introduction of $NaHCO_3$. Formation of magnesite species was previously identified with the introduction of $NaHCO_3$ [60], which appeared to be advantageous to accelerate the consumption of $Mg(OH)_2$, while the formation of magnesite species was not observed when Na_2CO_3 was used in the present work.

Fundamental difference between Na_2CO_3 and $NaHCO_3$ was investigated in our previous study using PHREEQC calculation [93], focusing on the interaction between $Mg(OH)_2$ and Na_2CO_3 or $NaHCO_3$ in the aqueous system (summary of calculation is provided in Appendix). According to the calculations, as shown in Figure 10 (a), the formation of magnesite is difficult in the Na_2CO_3 system, and it is highly limited even at 80°C. Only a small amount of brucite (0.001 mol) can react in the Na_2CO_3 system, and any brucite introduced beyond this level remain in the system without reacting. On the other hand, a significant magnesite formation can occur in the $NaHCO_3$ system as shown in Figure 10 (b). The amount of magnesite increased with the amount of brucite introduction up to 0.01 mol. The results of calculation are consistent with the experimental results and confirm that Na_2CO_3 and $NaHCO_3$ interact with brucite differently in the aqueous environment.

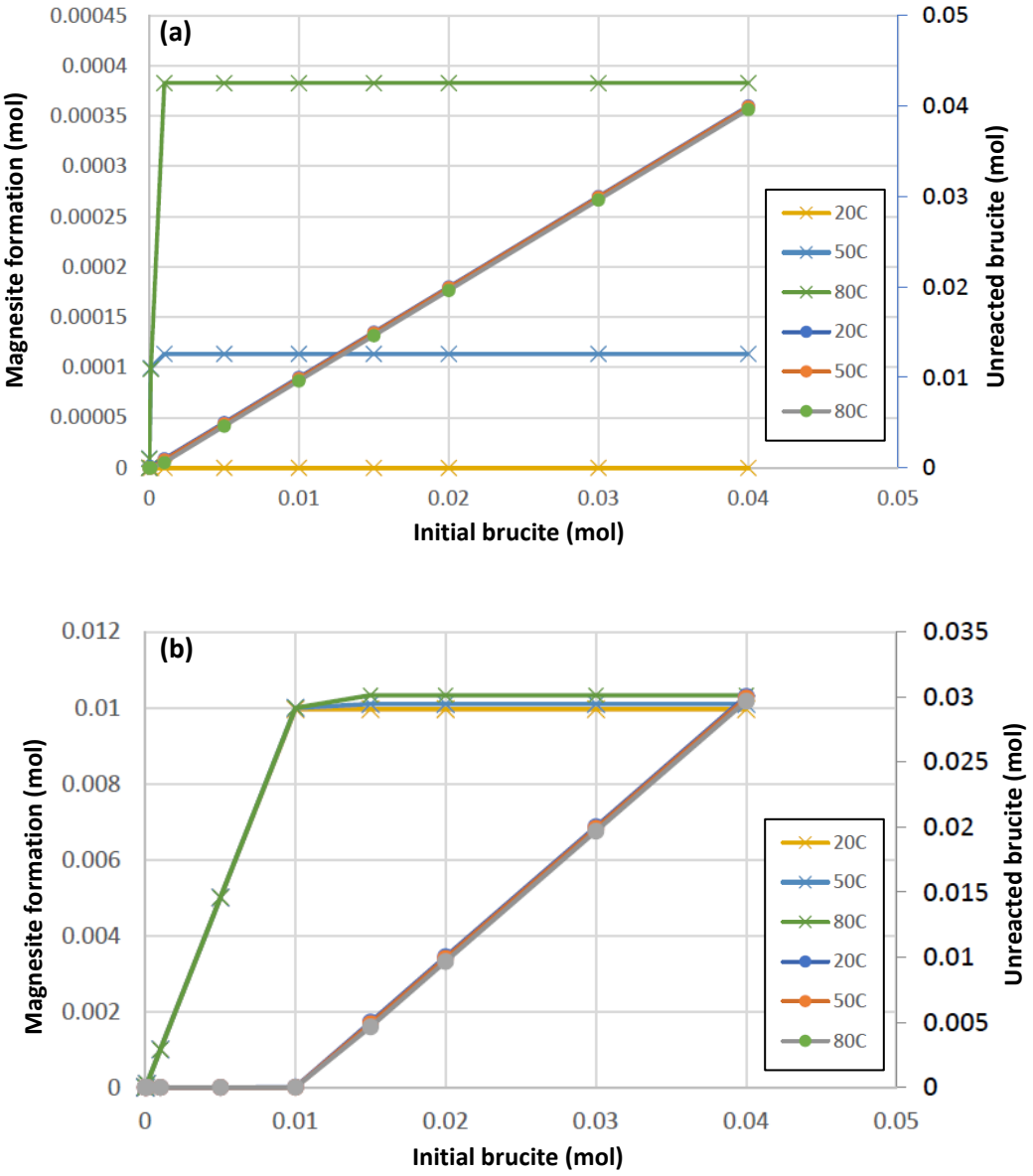

Figure 10. Behaviour of brucite in Na_2CO_3 and $NaHCO_3$ solutions calculated using PHREEQC [93]: magnesite formation and remaining brucite (a) in Na_2CO_3 solution, (b) in $NaHCO_3$ solution.

As shown in Figures 11 (a) and (b), the pH is about 11 in both systems, but their nature seems quite different. In the Na_2CO_3 system shown in Figure 11 (a), the reaction of brucite is negligible at all brucite introduction examined, suggesting that the pH of the system is controlled by Na_2CO_3, and brucite is remaining in the system without reacting (or dissolving). On the other hand, in the $NaHCO_3$ system shown in Figure 11 (b), while the pH is maintained high, the amount of brucite consumption increases with the amount of $NaHCO_3$ introduced, and all brucite is consumed at 0.04 mol of $NaHCO_3$. Thus, the high pH of the system is controlled by brucite in the $NaHCO_3$ system.

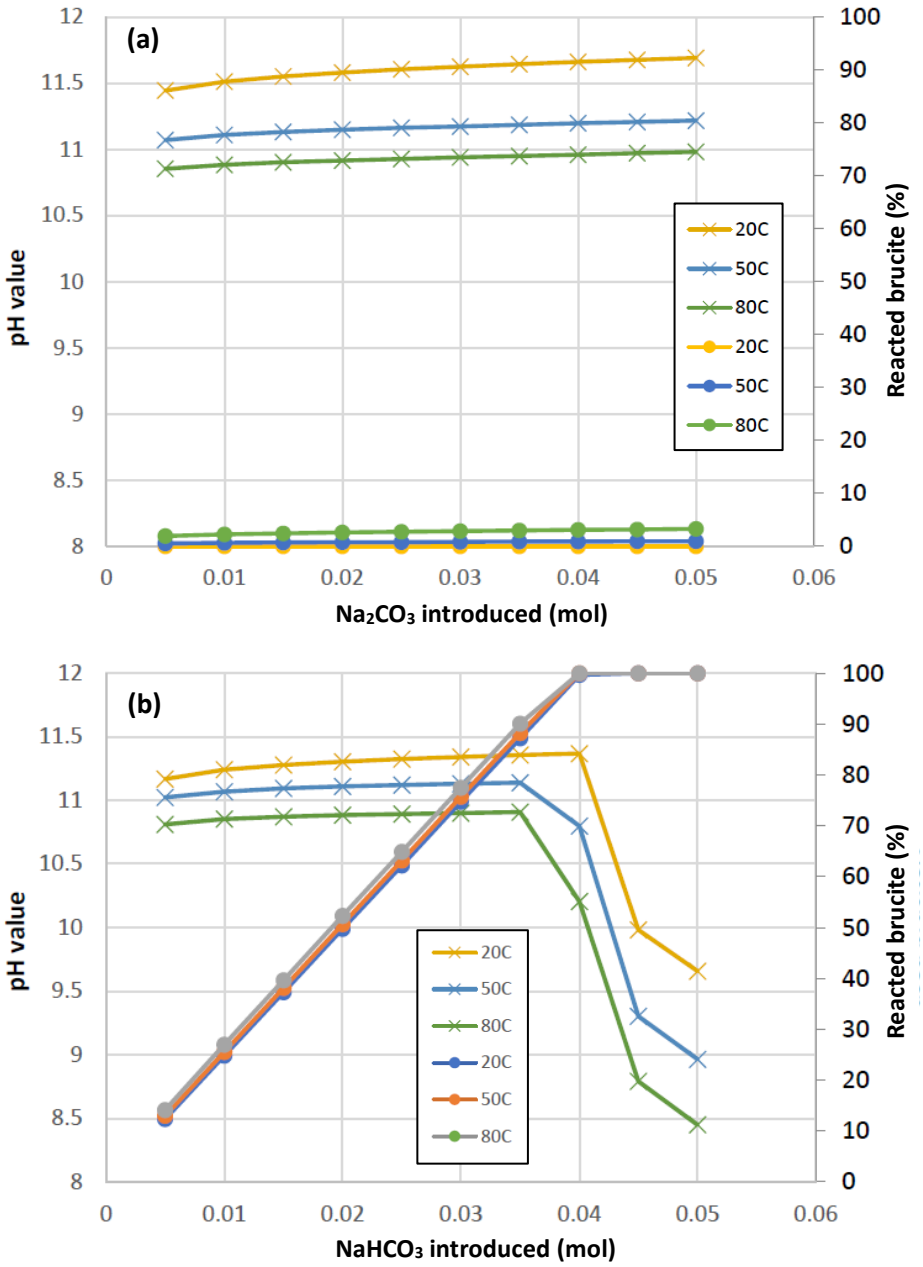

Figure 11. Effects of Na_2CO_3 and $NaHCO_3$ on pH of the system and brucite consumption, calculated using PHREEQC [93]: (a) in Na_2CO_3, (b) in $NaHCO_3$.

5.4 Conclusion

The formation of M-S-H cement with different amounts of Na_2CO_3 was investigated. The addition of sodium carbonate is able to accelerate the formation of M-S-H, with the extent of acceleration reaches the maximum at saturated concentration and generally decreases with the reducing concentration. Controlling the initial pH or the concentration of Na^+ ions of the cement batches does not solely improve the reaction speed. It appears that the concentration of carbonate ions is important, but the concentration of Na^+ ions (or pH of the system) has to be in the certain range for the carbonate ions to work effectively. The final products of the cement batches can change based on the concentration of sodium carbonate solution added, additional phases such as talc and dolomite may present in the final product. According to the PHREEQC calculation, the addition of Na_2CO_3 can limit the dissolution of the brucite, and therefore having a dormant period for the brucite reaction, resulting in a weaker acceleration effect compared to using $NaHCO_3$ as the additive.

Chapter 6. Formation of magnesium silicate hydrate by using substitutional magnesium and silicate materials

Abstract

In the purpose of making the M-S-H cement more eco-friendly and reduce the production cost, alternative raw materials are used for M-S-H formation and the reactions are studied in the present work. Mg dross from alloy industries are used as the alternative to $Mg(OH_2)$ (Mg source) and metakaolin are used as the alternative to silica fume (Si source) with/without the addition of sodium bicarbonate. The samples are analysed by X-ray diffraction (XRD), ex-situ pH measurements thermogravimetry (TG) and compressive strength test. The results indicate M-S-H was formed in the Mg dross samples prepared with silica fume, and the addition of sodium bicarbonate accelerated the reaction. The metakaolin samples prepared with brucite showed limited reaction without sodium bicarbonate, while the addition of sodium bicarbonate motivated the formation of hydrotalcite but the formation of M-S-H was not observed. Only limited development of compressive strength was shown in the Mg dross samples, and metakaolin samples did not develop any measurable compressive strength.

6.1 Introduction

The needs of reducing carbon footprint in the cement industries keep raising in recent years, driving to the study of alternative cement to substitute the existing high-CO_2 emission Portland cement [1]. Magnesia-based cements have been proposed as a possible alternative to Portland cement. This is because the production of raw materials, magnesia (MgO), for magnesia-based cements requires a relatively low temperature input (650°C) for its production, and thus, less energy is required in the manufacture process compared to the production of clinker phases in Portland cement at a significantly high temperature (1450°C) [94]. This lower temperature requirement for the magnesia-based cement production may enable the mitigation of total CO_2 emission. However, the standard production procedures of MgO from the decomposition of magnesite ($MgCO_3$) mineral still release CO_2 inevitably [33]. Searching for substitutional raw materials or methods to obtain MgO is desirable, as they can possibly be a more effective method to reduce the overall carbon footprint of magnesia-based cement production.

Magnesium silicate hydrate (M-S-H) cement is one of the promising magnesium based cements, and the main binding phase, M-S-H, is mostly formed by the reaction between magnesium compounds such as MgO or $Mg(OH)_2$ with soluble source of SiO_2 such as silica fume in the presence of water. As previously mentioned, the conventional production of MgO (or $Mg(OH)_2$) from $MgCO_3$ minerals through Reactions 1 and 2 still involves the release CO_2 from the raw materials.

$$MgCO_3 \rightarrow MgO + CO_2 \qquad (1)$$
$$MgO + H_2O \rightarrow Mg(OH)_2 \qquad (2)$$

The substitutional raw materials were investigated as alternative Mg and Si sources in the present work, for the purpose of making the M-S-H cement more environmental-friendly and easier to implement. The substitutional Mg source material examined in the present investigation is centrifuged Mg-rich dross produced as the by-product of magnesium alloy manufacturing. Using such by-products from other industries may potentially offer a sustainable solution to the M-S-H cement raw material acquisition and the reduction of waste through the effective use of resources.

The alternative Si source material studied in this work is metakaolin. Metakaolin is dehydroxylated aluminium silicate manufactured by calcining kaolinite clay at temperature between 600 °C and 900 °C, and is often used as pozzolanic supplementary cementitious material with Portland cement [95]. The cost of metakaolin is relatively high compared with cement, but can potentially be reduced by increase the production and application scale of metakaolin [95, 96].

Since silica fume is a by-product from silicon production [97, 98], replacing it with metakaolin may not offer a significant advantage in terms of direct carbon footprint. The main interest of studying metakaolin is to increase the viable Si source for M-S-H cement, as exclusively silica fume is currently used as Si source to produce M-S-H [15, 19]. Although it may cost more than cement, metakaolin is considered as environmental-friendly material due to the low temperature requirements and limited CO_2 emission [95]. It is also known that the addition of metakaolin to Portland cement can provide the cement with long-term strength, and enhances the properties of cement such as improve durability, reduce permeability and reduce setting time [95, 96]. It would be beneficial for the M-S-H cement if similar effects can be provided.

The aluminium content from metakaolin can be incorporated into the M-S-H system to form M-A-S-H [77]. The aluminium ions will be taken into the vacant sites in the M-S-H, so no magnesium ions replaced by aluminium ions occurs [77]. Therefore, the formation process M-A-S-H is similar to M-S-H, and its production usually follows the same reaction procedures [99].

The formation of M-S-H gel in the pastes prepared using Mg dross or metakaolin is studied in the present work. To make the studies comparable, the Mg dross and metakaolin was used to substitute the Mg or Si content to provide the same amount (moles) of Mg or Si ions in the samples as those investigated in previous studies, with the Mg/Si and water to binder ratios also maintained the same [60]. The effect of $NaHCO_3$ addition to accelerate the formation of M-S-H in the Mg dross and metakaolin samples was also studied.

6.2 Material and methods

6.2.1 Materials

Part of the raw materials used in this work are same as our previous work [60], including brucite from Sigma-Aldrich with purity ≥95%, microsilica 940-U from Elkem, sodium bicarbonate from Sigma-Aldrich with purity ≥99.0% and laboratory distilled water.

The dross used in this work is a centrifuged dross obtained from Luxfer (UK), produced as the by-product of magnesium alloys manufacture. The main composition of the dross is brucite, and its XRF data is shown in Table 1, presenting oxide composition with >1 wt% and loss on ignition (LOI). Due to the large value of LOI, suggesting a significant amount of moisture content, the dross was desiccated in a 35°C oven for 28 days before use. The XRD data of the Mg dross is presented in Figure 1, identifying the presence of brucite ($Mg(OH)_2$), sellaite (MgF_2), fluorite $Ca(F_2)$, aenigmatite ($Na_2Fe_5TiSi_6O_{20}$), quartz (SiO_2) and calcite ($CaCO_3$).

Table 1. Oxide composition of the Mg dross

Element	**MgO**	**CaO**	**ZrO_2**	**SiO_2**	**Al_2O_3**	**BaO**	**LOI**
Weight% (with LOI)	45.19	5.76	5.37	5.20	1.70	1.54	32.92
Weight% (without LOI)	67.37	8.58	8.01	7.75	2.53	2.30	n/a

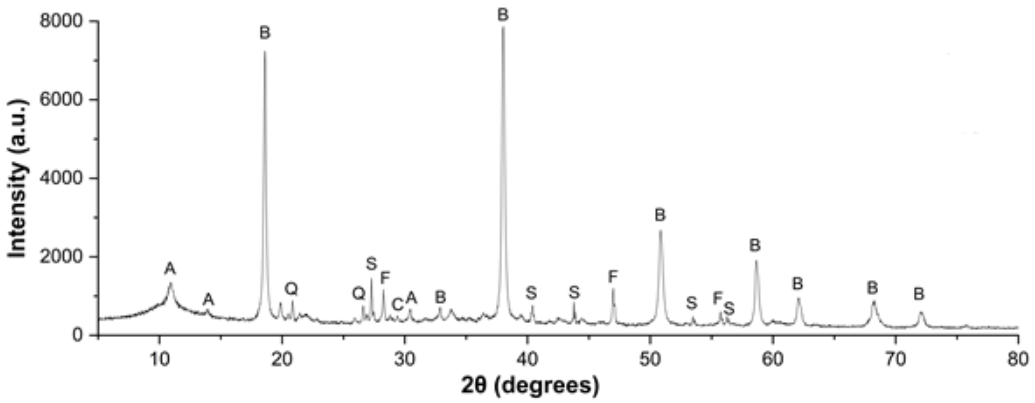

Figure 1. X-ray diffraction patterns for the dross products. Identified phases include B – Brucite, S – Sellaite, F – Fluorite, A – Aenigmatite, Q – Quartz, C – Calcite.

The metakaolin used in this experiment is Argical M1200 obtained from Imerys (UK). M1200 is flash calcined clay with relatively low crystallinity and high reactivity. The XRF data of M1200 is shown in Table 2, presenting oxide composition with >1 wt%. The XRD pattern of M1200 is presented in Figure 2, identifying the presence of quartz (SiO_2), anatase (TiO_2), mullite ($Al_6Si_2O_{13}$), calcite ($CaCO_3$) and pseudowollastonite ($Ca_3Si_3O_9$).

Table 2. Oxide composition of M1200 metakaolin

Element	**SiO_2**	**Al_2O_3**	**TiO_2**	**Fe_2O_3**	**K_2O**	**LOI**
Weight%	52.18	42.40	1.74	1.90	1.07	trace

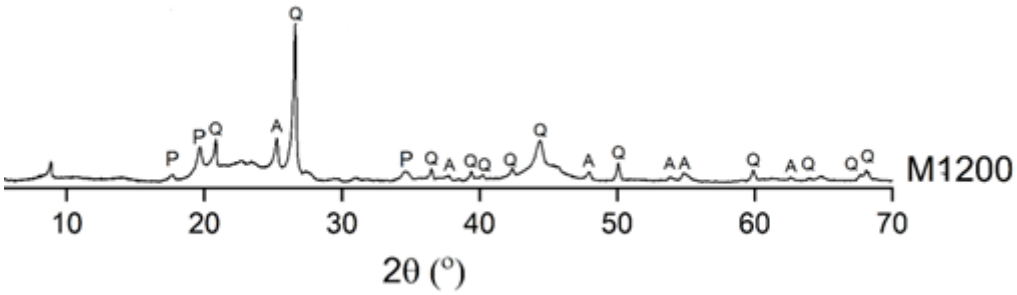

Figure 2. X-ray diffraction patterns for the raw MK products. Identified phases include, Q – quartz, A – anatase and P – pseudowollastonite [100].

6.2.2 Sample mix design

Cement paste was prepared by mixing Mg source and Si source with distilled water or concentrated $NaHCO_3$ solutions. The Mg source used was Mg dross or brucite and the Si source used was silica fume or M1200 metakaolin. The formulation of the pastes was based on that used in the previous study [60], but replacing $Mg(OH)_2$ with the dross, or replacing silica fume with metakaolin for the corresponding formulations. The Mg/Si ratio and amount of $NaHCO_3$ used were maintained the same to the previous study, providing saturated $NaHCO_3$ solution at 20 °C [60]. The quantity of the material used is listed in Table 3. The DW notation represents the distilled water was used to prepare the samples, and 1H notation represents saturated $NaHCO_3$ solution was used to prepare the samples.

Table 3. Composition design of the systems

		Solution		Solid	
Samples	**Sample ID**	**Water (mL)**	**$NaHCO_3$ (g)**	**Mg Source (g)**	**Si Source (g)**
Mg Dross	Dross-DW	200	0	Mg Dross 152	Silica fume 100
	Dross-1H	200	19.2	Mg Dross 152	Silica fume 100
Metakaolin	M1200-DW	200	0	$Mg(OH)_2$ 100	M1200 191.6
	M1200-1H	200	19.2	$Mg(OH)_2$ 100	M1200 191.6

6.2.3 Experimental procedure

The $NaHCO_3$ solution was prepared by dissolving the $NaHCO_3$ in the distilled water with magnetic stirrer for approximately 15 minutes at laboratory temperature (~20°C) until the solution becomes colourless. The $NaHCO_3$ solution was placed into a mixer (Heidolph RZR2020, 600rpm), and then the brucite or dross powder was added over approximately 5 minutes of mixing for each. The dried dross was ground using a pestle and mortar for approximately 10 minutes before being mixed with the solution. Silica fume or M1200 metakaolin was then slowly added into the mixer with approximately 20 % of total mass every minute (total of 5 minutes).

After mixing, the cement paste was poured into 20 mm × 20 mm × 20 mm cubic steel mould, which was manually shaken/vibrated for few times to remove the possible air bubbles and make sure the bottom part of the mould was fully filled. The filled mould was placed inside a plastic bag (not sealed) and then put into another humidified plastic bag (sealed with small amounts of water) to avoid the sample directly contacting with air and water but maintain high humidity.

The samples were then cured in a 35°C oven and taken out at 7, 14, 28 and 56 days. After performing compressive strength test, the samples were crushed into small pieces and washed in approximately 200 mL of acetone for 5 minutes. Then, the washed samples were separated from the acetone using filter paper and a Büchner funnel assisted with vacuum pump for approximately 5 minutes. The separated materials are immersed into approximately 200 mL of acetone again and kept for 48 hours in order to remove the free water. The samples were separated from acetone again by using filter paper and Büchner funnel for 15 minutes. The dried samples are stored in sealed centrifuge tubes with parafilm until further analysis.

6.2.4 Characterisation methods

6.2.4.1 X-ray diffraction

The X-ray diffraction (XRD) machine used was benchtop Bruker D2 PHASER apparatus armed with a Cu-Kα radiation source running at 30 kV and 10 mA. The divergence silt used was 1 mm, the upper and lower discriminators were 0.11 and 0.25 V respectively. The scanning angle range was from 5° to 80° 2θ with an increment of 0.02°. The sample was rotating at 15 rpm during scanning to avoid uneven distribution and orientation. The samples are crushed and ground into powders before the measurement. Due to the availability of the equipment, the XRD measurements for Mg dross samples and M1200 samples were carried out on different Bruker D2 PHASER apparatus but with same settings.

6.2.4.2 Thermogravimetric analyses

Thermogravimetric analyses (TGA) was carried out by using PerkinElmer TGA 4000. Approximately 40 mg of samples were used for testing each time. The sample was heated from 30°C to 990°C at a rate of 10 °C/min under a nitrogen flow of 40 mL/min. Ten minutes of isothermal hold was used at both the start and end of the heating programme.

6.2.4.3 pH measurement

The apparatus used for the pH measurements was a Mettler Toledo pH/Cond bench meter SE S470-K equipped with an expert proISM probe (error = ±0.01). The probe was calibrated each day before use by immersing into standard buffer solutions with known pH values. Two methods are used for measuring the pH of the samples at different reaction stages. The pH of the sample at 0 days (when initially prepared) was examined right after the batch was mixed properly; a small portion of the batch was separated and then the testing probe was immersed directly into the paste to take the readings. For the cured samples, an ex-situ leaching method [51] was used for the pH measurement. For these tests, 1 g of powder sample was added into 80 mL of distilled water and stirred with a magnetic stirrer, and then the testing probe was inserted into the solution. The pH reading was recorded after > 15 minutes of stirring when the pH reading of the solution stabilised. The amount of cement added was decided by a preliminary experiment, in which 0.2 g, 0.6 g, and 1.0 g of cement sample was added into 80 mL of distilled water separately. These preliminary tests showed that the pH readings for > 0.6g addition are the same, and signifies that the solution is already saturated. However, using this method to measure the pH of the samples in the project assumes the pore solution of the cement is in over saturated state.

6.2.4.4 Compressive strength test

The mechanical test frame used to measure compression used was the Zwick Roell 50 kN load cell and calibrated each day before use. The cross-section area of the cubes was measured before each test. Three readings of width and length of the cubes are taken by vernier calliper, and the average values were used to calculate the cross-section area. The compression head was approaching the base at 0.2mm/minute during the measurement and stopped when there is a sudden decrease in compression force. The maximum compression force applied during compression was then recorded. These measurements were carried out in triplicates and the average value calculated.

6.3 Results and discussion

6.3.1 Phase formation and consumption of $Mg(OH)_2$

6.3.1.1 Mg dross samples

he XRD patterns of the Dross samples prepared with distilled water are presented in Figures 3. According to the literature, the broad humps at 20-30°, 35-39° and 58-62° 2θ can be attributed to M-S-H [21]. The hump at 10-13° often observed for M-S-H [19] was not detected in this series. The broad hump at 18–25° 2θ is attributed to unreacted silica fume [26], and the sharp reflection peaks at 18.6°, 38.0°, 50.8°, and 58.6° 2θ are for brucite [21]. Some small peaks may suggest the presence of aenigmatite (A, $Na_2Fe_5TiSi_6O_{20}$) [101], calcite (C, $CaCO_3$) [102], sellaite (S, MgF_2) (Powder diffraction file (PDF) 00-041-1443) and fluorite (F, CaF_2) (PDF 00-035-0816) as labelled on the axis.

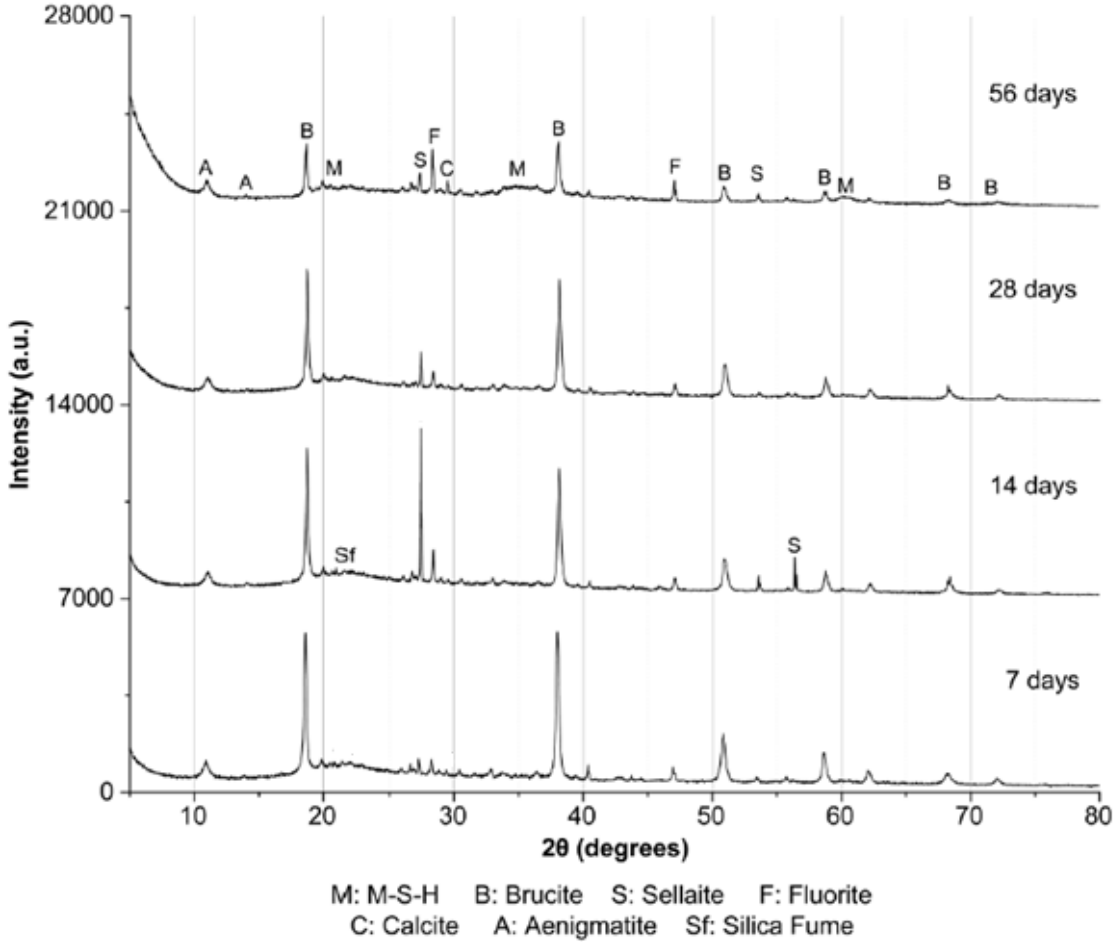

Figure 3. XRD patterns for the Dross-DW samples at 7, 14, 28 and 56 days of curing.

As shown in Figure 4, the Dross samples prepared with $NaHCO_3$ solution indicated the presence of similar phases with possible additions of hydromagnesite (H, $Mg_5(CO_3)_4(OH)_2{\cdot}4H_2O$) [52].

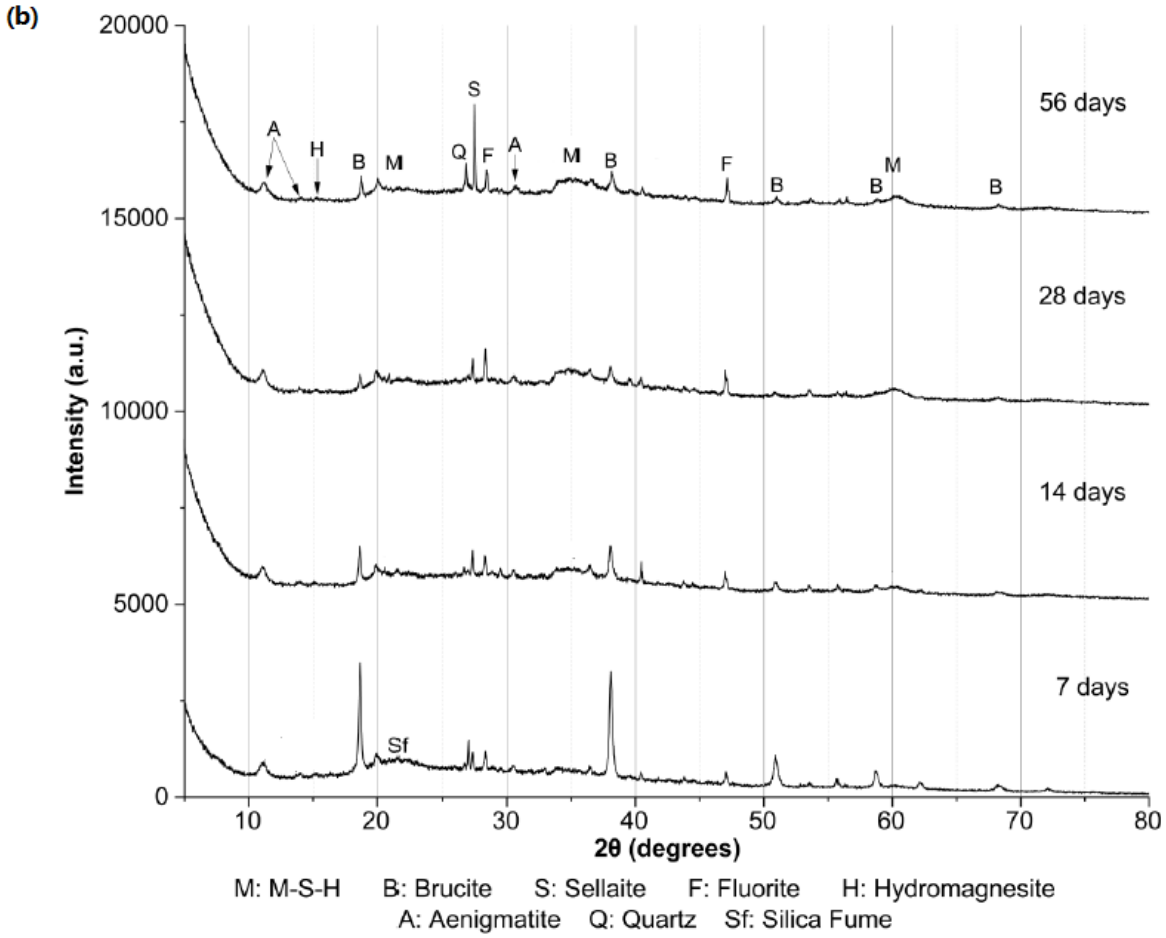

Figure 4. XRD patterns for the Dross-1H samples at 7, 14, 28 and 56 days of curing.

The XRD patterns of both Dross-DW and Dross-1H samples reveal the consumption of brucite and formation of M-S-H with time. However, the peaks for brucite are decreasing slowly in intensity up to 56 days in distilled water samples, while in 1H samples significantly decrease between 7-14 days and remain constant after 14 days. This acceleration effect of brucite consumption by the addition of $NaHCO_3$ follows the results from our previous studies using reagent grade $Mg(OH)_2$ [60], although the reaction seems slightly slower in the Mg dross samples [60].

The possible peaks for hydromagnesite in the Dross-1H samples become less visible at 56 days, which coincides with the observation previously made in the reagent grade $Mg(OH)_2$ 1H system in which hydromagnesite was formed as intermediates and then consumed during the M-S-H formation [41].

Aenigmatite, calcite, quartz, sellaite and fluorite, originally presented in the Mg-Dross used as the starting material, still indicated their reflection peaks in the products as shown in Figures 3 and 4. The peaks for aenigmatite remain constant in both pastes from 7 to 56 days, implying that aenigmatite is rather inert and did not participate the reaction. The reflection peaks for calcite and quartz became significant at 56 days of curing. The increase in the calcite peak intensity at 56 days in the Dross-DW sample is likely due to the carbonation of the system. The increase in the peak intensity of quartz in the Dross-1H sample is difficult to explain, but potential reasons are the orientation of the crystal and the inhomogeneous nature of the Mg-Dross.

The peak intensity for sellaite keep changing in both samples, and thus, it is difficult to gain a clear trend. In the Dross-DW samples, the peak intensity reaches the maximum at 14 days and then decreases, while in Dross-1H samples the peak intensity almost stays constant in the first 28 days and then increase at 56 days. A possible explanation to this observation is the formation of magnesium hydroxide fluorides $MgF_{2-x}(OH)_x$. Because sellaite (MgF_2) shares a similar main reflection peak position with $MgF_{2-x}(OH)_x$ at ~27.4° 2θ [103], the XRD patterns are likely showing the presence of both phases.

In the Dross-DW system, when $Mg(OH)_2$ slowly starts to react, a part of it may react with sellaite in the system to form $MgF_{2-x}(OH)_x$. However, these magnesium hydroxide fluorides were formed as intermediates, and eventually Mg^{2+} ions are used to from M-S-H, leaving sellaite behind or release F^- ions to form fluorite. In the 1H samples, the XRD pattern suggests that the reaction of $Mg(OH)_2$ results in the formation of hydromagnesite as an intermediate, and thus, the formation of magnesium hydroxide fluorides is not readily available. Only when hydromagnesite starts reacting, the formation of magnesium hydroxide fluorides can become observable, and that is why the formation is later than the Dross-DW system.

6.3.1.2 Metakaolin M1200 samples

The XRD pattern of the Metakaolin samples are presented in Figures 5 and 6. The peaks for M-S-H and brucite are similar to the Mg-dross system, where the broad humps at 20-30°, 35-39° and 58-62° 2θ should attributed to M-S-H [21] and the sharp peaks at 18.6°, 38.0°, 50.8°, and 58.6° 2θ are for brucite [21]. The peaks for anatase (PDF 01-071-1166), pseudowollastonite (PDF 04-011-3072) and quartz (PDF 01-078-1252) are pre-exist in the M1200 metakaolin as presented in Figure 2.

As shown in Figure 5, in the M1200-DW samples, all the peaks remain constant during the period of 56 days, implying that the brucite did not react with the metakaolin within 56 days. In the M1200-1H samples, as seen in Figure 6, the peaks for brucite gradually decrease with time but still persist at 56 days. The peaks observed in the M1200-1H systems at ~11°, ~23°, ~35°, ~39°, ~47° and ~60 °2θ are characteristic for hydrotalcite [104]. The hydrotalcite peaks keep increasing up to 56 days, while the other pre-existing M1200 peaks indicate no change. The humps for M-S-H cannot be clearly observed in both M1200-DW and M1200-1H systems, implying the formation of M-S-H is limited in these samples.

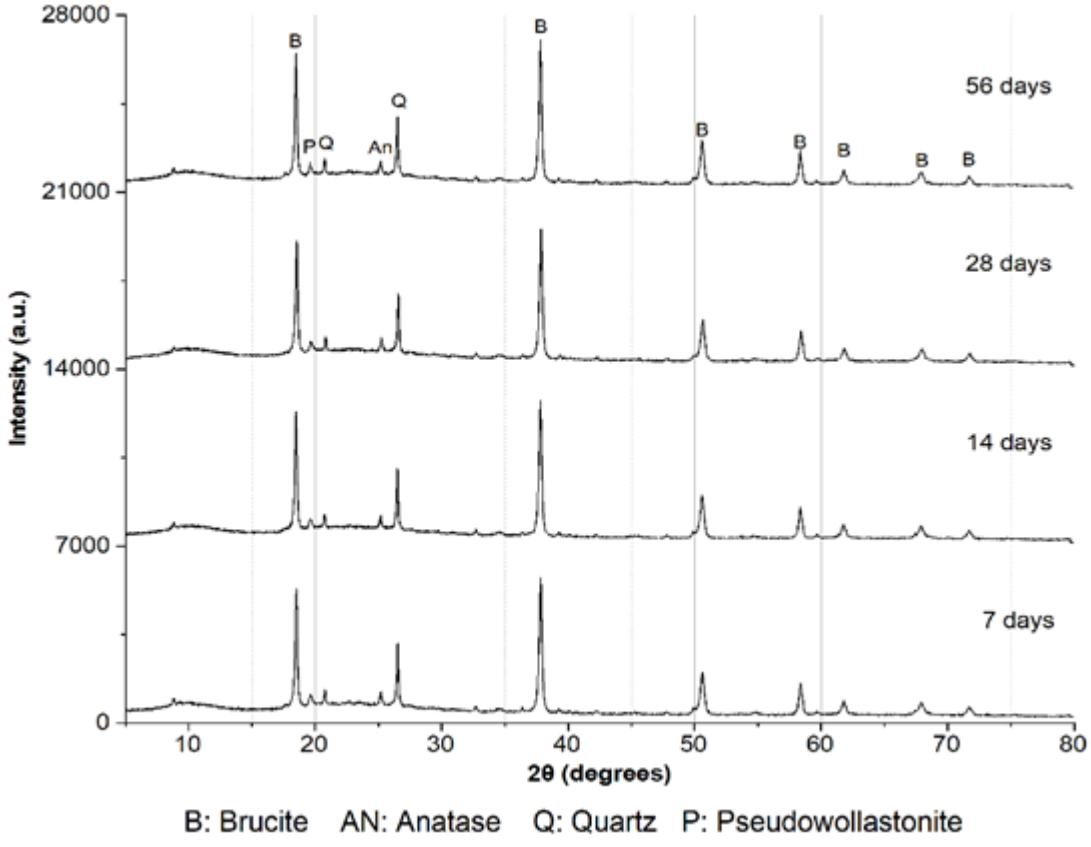

Figure 5. XRD patterns for the M1200-DW samples at 7, 14, 28 and 56 days of curing.

The acceleration effect of $NaHCO_3$ appears to remain effective to a limited extent, and $NaHCO_3$ may become the initiator for the reactions in the metakaolin system. Metakaolin can be used as a precursor for alkali-activated materials (or geopolymer cement) by activated by alkaline solution [105]. However, the consumption of brucite is slower compared to the samples prepared in the previous study using silica fume without metakaolin substitution [60]. The peaks for hydromagnesite and the formation of M-S-H phases were not observed in the M1200-1H samples, but relatively large amount of hydrotalcite was formed, suggesting that the formation of hydrotalcite is preferred to the formation of M-S-H in this system. These results may be beneficial to the cement since the formation of hydrotalcite can reduce the porosity of the system and enhance its mechanical performance [77, 106], but the system needs to be investigated further to enable the formation of M-S-H binder phase during the reaction.

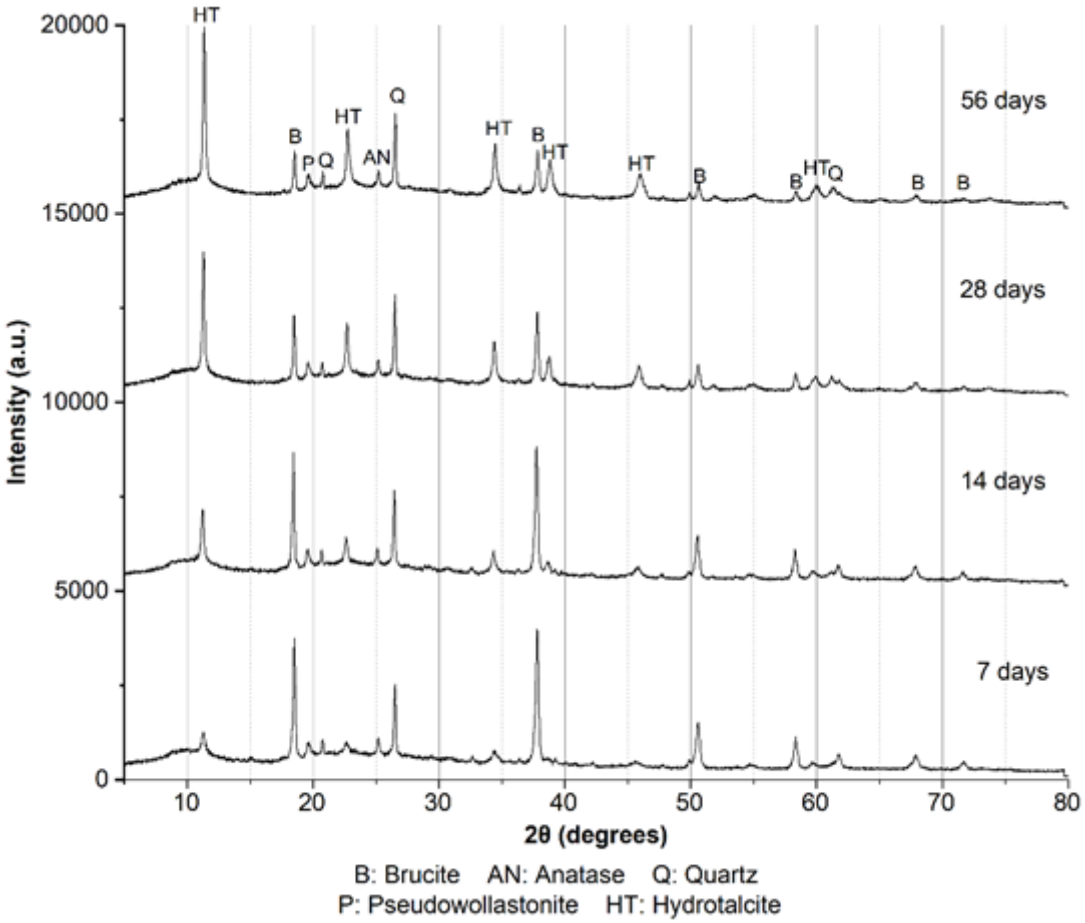

Figure 6. XRD patterns for the M1200-1H samples at 7, 14, 28 and 56 days of curing.

6.3.2 Strength development

The compressive strength data for Mg-dross and metakaolin samples at each curing period are presented in Table 4. The term N/A in the table shows the lack of reliable data, indicating that the samples were not strong enough to be tested by the machine to obtain an effective value.

Table 4. The compressive strength test results for Mg-Dross and Metakaolin samples

	Compressive strength (Mpa)			
Sample ID	**7 days**	**14 days**	**28 days**	**56 days**
Dross-DW	N/A	N/A	N/A	4.60 ± 0.23
Dross-1H	N/A	2.92 ± 0.48	2.93 ± 0.14	2.95 ± 0.07
M1200-DW	N/A	N/A	N/A	N/A
M1200-1H	N/A	N/A	N/A	N/A

The Dross-1H samples cured for 14, 28 and 56 days are having similar compressive strength around 2.93 MPa, implying that the cement was almost fully reacted by 14 days, which is consistent with the XRD data. The Dross-DW samples developed their strength slowly and only showed strength of 4.6 Mpa at 56 days. This result concurrents with the XRD data, where the M-S-H is mainly developed between 28 days and 56 days in the Dross-DW samples. Bernard et al. [44] recently investigated similar M-S-H systems, but prepared from MgO and silica fume (mixture of low grade 96% purity and high grade 98%) with addition of Na_2CO_3 and reported a similar trend in the strength development. The majority of strength development was achieved in the first two weeks, and it was faster with the systems with higher carbonate contents.

It should be noted, although the strength development is slower than the Dross-1H samples, it reached a higher value in strength at 56 days. The presence of $NaHCO_3$ in the system may have negatively interacted with the minor constituents of Mg-dross, resulted in reduction of strength. Further investigation is required to elucidate this aspect.

The M1200 samples did not show measurable strength both in the distilled water samples and $NaHCO_3$ samples. As suggested by the XRD data, the M1200-DW samples generally had little reactions, and thus, the obtained data appears to be reasonable, but this is a quite contrast from the literature data for a similar system.

According to the work by Bernard et al. [44] previously mentioned, their M-S-H cement prepared using MgO and metakaolin with addition of Na_2CO_3 developed a strength of > 20 MPa in 28 days. Their formulation is summarised in Table 5, in comparison to the present work. Since MgO readily forms $Mg(OH)_2$ when it is mixed with water, the difference in the Mg source is not expected to cause such a difference. One of the distinct differences between the two studies is the type and amount of the additive. The present study introduced $NaHCO_3$ (96 g/L = 1.14 mol/L) while their study used Na_2CO_3 (17 g/L = 0.162 mol/L), which leads to 3.5 times of Na^+ ions and 7 times of CO_3^{2-} ions in the present system. The composition of Mg relative to Si and Al in their system is also significantly higher than the present study, and possibly be the key factor of the formation of M-S-H gel.

Table 5. Comparison of formulation between present work and that by Bernard et al [44]

	Mg source	Si source	Additive	Sol./Binder	Mg/Si/Al
Present work	$Mg(OH)_2$	Metakaolin	$NaHCO_3$ (96 g/L)	0.75	17/17/16
Bernard et al. [44]	MgO	Metakaolin	Na_2CO_3 (17 g/L)	1.00	35/23/23

While the XRD results showed the formation of hydrotalcite similar to the work reported by Bernard et al., there are no M-S-H phases identified in the present work. The strength data of the M1200-1H samples implies that the hydrotalcite itself may not be able to provide enough strength to the cement and the formation of M-S-H is essential.

The strength of the samples is not high enough for most of the civil applications. The w/s ratio used for the dross samples was 0.8 and for metakaolin samples are 0.69, and these relatively high w/s ratios may be one of the possible reasons for these low strength, since high water content will results higher porosity in the cement [107, 108]. The amount of additive may also have a significant impact on the strength development, as a reasonable strength development has been reported with much smaller amount of Na_2CO_3 introduction despite larger amount of water used in their system. The present study also implies the same trend, as the dross samples eventually developed higher strength when $NaHCO_3$ was not introduced.

6.3.3 Evolution of pH

The pH values of the samples are presented in Figure 7. The initial pH of the samples with $NaHCO_3$ addition are closer to the pH value of saturated $NaHCO_3$ solution (pH 8.8) [60] while that of distilled water shows a wider range from 7.2 to 8.9. The pH values of the dross samples are generally higher than the metakaolin samples, likely due to the presence of minor components in the dross such as calcium oxide (as presented in Table 1).

Compared to the samples prepared from $Mg(OH)_2$ and silica fume in our previous study [60], the pH values are slightly lower for the samples examined in the present study. This lower pH value implies slower dissolution of brucite, so that the OH^- ions concentration in the solution was less, therefore, leading to slower formation of M-S-H. This feature is particularly strong in the M1200-DW sample, which indicated little reaction of the system.

In the pastes with $NaHCO_3$ addition, the pH initially rises up to 7 days, correlating to the release of OH^- from $Mg(OH)_2$ dissolution. The formation of surface complexes between brucite and HCO_3^- which accelerates the brucite dissolution increases the amount of Mg^{2+} and OH^- in solution and therefore, contributes to a rapid rise in pH [89]. The formation of hydromagnesite in the dross samples which releases OH^- may also contribute to this pH rise [109]. The high pH then encourages SiO_2 dissolution and OH^- consumption, and consequently the pH can be seen to reduce at 14 days as M-S-H forms. The rate of brucite dissolution is greater than that of OH^- consumption in the first 7 days.

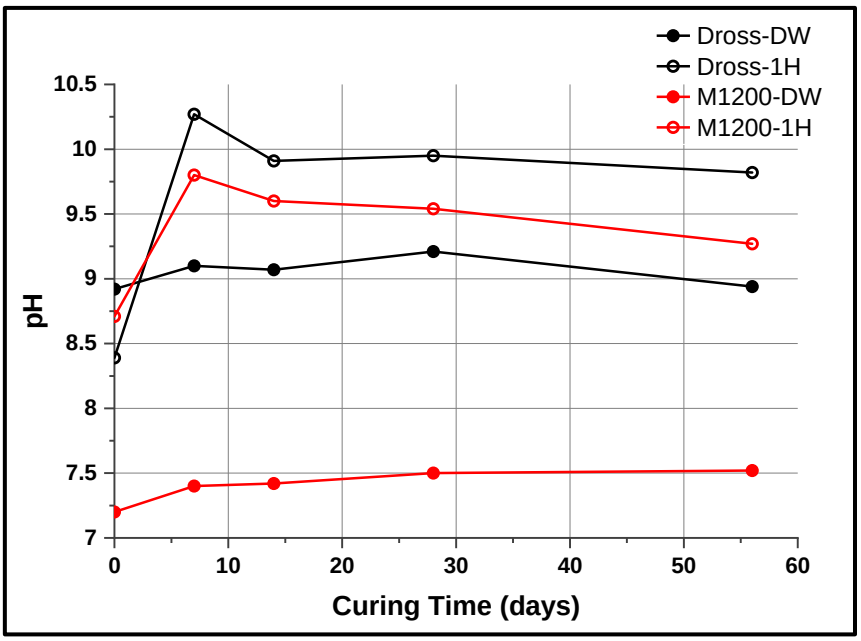

Figure 7. The pH measurements of the samples over 56 days.

The pH evolution of the Dross-DW samples is having a slightly different trend. The pH values are fluctuating around 9 with minimal changes, suggesting a limited dissolution of brucite. Because the pH did not increase sufficiently, most likely the dissolution of silica fume was not encouraged either, resulting in the overall slow reaction of the system and M-S-H formation.

In the M1200-DW samples, the pH value stays in the near-neutral region for 56 days, being concurrent with the XRD data showing that little reaction was occurred. The relatively low starting pH value is not able to activate metakaolin [110]. Although the pH value of 7-7.5 should encourage the dissolution of brucite, according to XRD the dissolution of brucite is limited, the reason behind this phenomenon remains unclear and require further investigation.

6.3.4 Phase evolution

To further understand the effects of $NaHCO_3$ on the evolution of phases, thermal analysis was performed both for dross and metakaolin samples. The thermogravimetric (TG) curves and differential thermogravimetric (DTG) curves for the Dross-H1 samples are presented in Figure 8. The weight lost step around 80-250 °C is mainly due to the loss of water bounded to M-S-H [21, 62]. It initially increases up to 28 days, then decreases by 56 days of curing. The similar trend was observed in our previous study on the M-S-H cement prepared from brucite and silica fume [60]. The decomposition of brucite resulted in the weight loss step around 320 – 480 °C, corresponding to the amount of brucite remained in the system [21].

The broad weight loss step around 500 – 600 °C attributes to the loss of the coordination water of M-S-H, which can be used as the indication of M-S-H formation [21]. The DTG curves reveal the formation of M-S-H at 14 days, with a significant decrease in the brucite peak at 400 °C and growth of the M-S-H peaks at 100 °C. This is consistent with the XRD results which shows that most of the brucite consumption and M-S-H formation were occurred between 7 and 14 days.

It should be noted that the gradual increase in the weight loss at 500 – 600 °C does not match with the weight loss at around 100 °C which, as previously mentioned, increased up to 28 days and then reduced at 56 days. As the effects of free water is expected minimum, the majority of the water loss at ~100°C should be from M-S-H. These results suggest that the nature of M-S-H may change with time: a larger amount of water is bounded to the young M-S-H, and in the later stage, either the bound water is released from the M-S-H or the young M-S-H is replaced by the new M-S-H with less bound water.

The 7 day DTG curve is having a small weight loss peak at around 440 °C, which may attribute to the dehydroxylation and decarbonation of hydromagnesite [91]. The peaks for the hydromagnesite only appears in the 7 days samples, consistent with the XRD data which suggests that hydromagnesite is formed as an intermediate. The peaks around 480 °C may attributes to the magnesite [54], which is not presented in the XRD data most likely due to its small quantities.

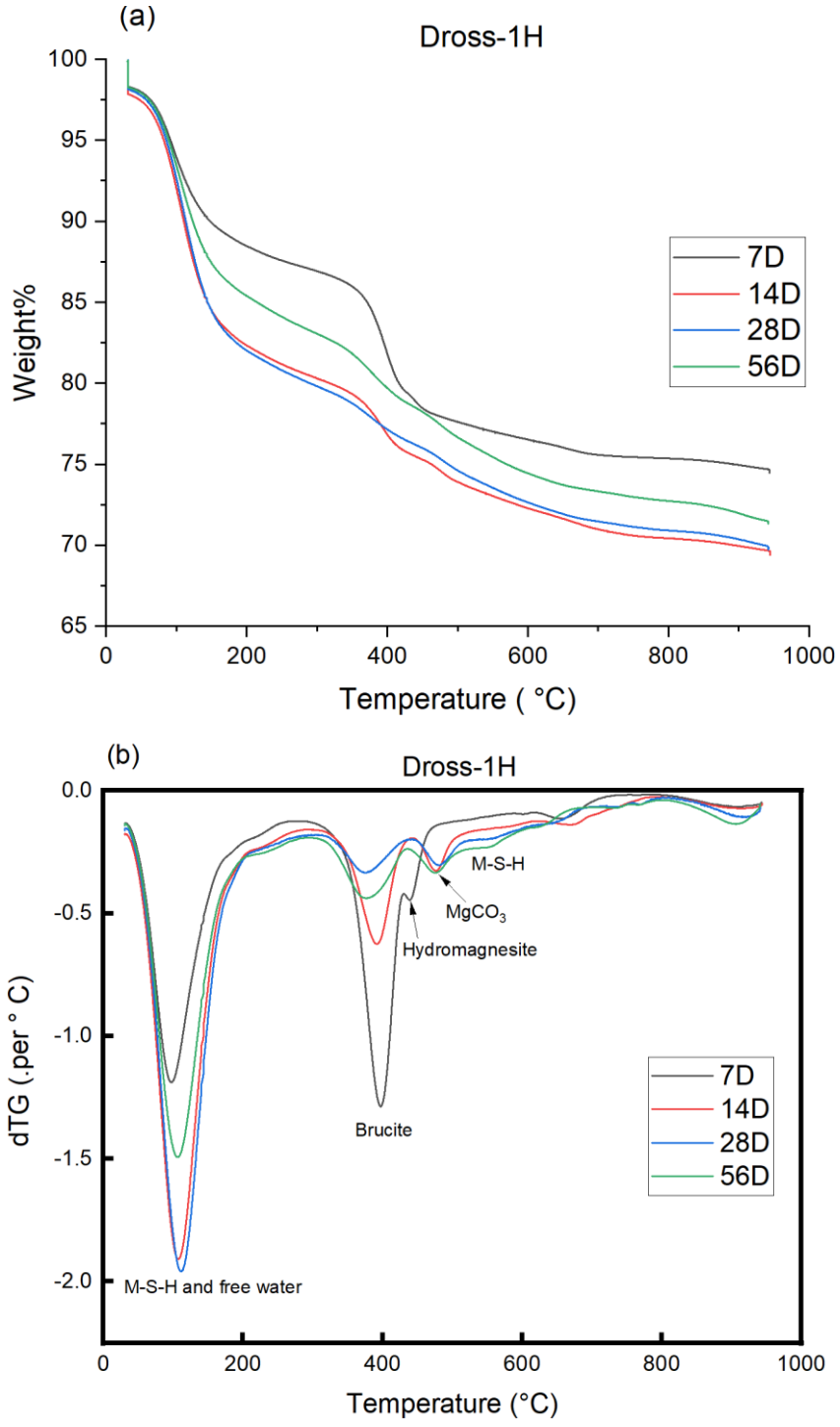

Figure 8. The thermal analysis of Dross-1H samples: (a) TG curves; (b) DTG curves

The TG and DTG curves for the M1200-H1 samples are presented in Figure 9. The DTG curves show a weight loss event increasing with time at 50°C. Since metakaolin would not indicate a weight loss in the TG, being a calcined product, this is related to a reaction product, especially it increases with time. However, the peak position in the DTG is significantly lower compared to that usually attributed to the release of the water bounded to M-S-H [21, 62]. The weight loss peaks at 150 - 200 °C corresponds to the dehydration of the hydrotalcite [111]. The peaks from 300 – 500 °C are the overlapped peaks for the dehydroxylation of brucite and the hydrotalcite decomposition [21, 111], which makes it difficult to quantify these phases in the samples. Small weight loss peaks are observed at 590 °C in the DTG curves. Although the coordination water of M-S-H could be lost at high temperature, it is usually observed as a broad weight loss event in DTG ranging 500 – 600 °C [21]. Therefore, it is difficult to assert this small weight loss as an indication of M-S-H formation although it may have formed in a small quantity. Instead, this small weight loss peak may attribute to $MgCO_3$ formed from the dehydration of hydromagnesite [112].

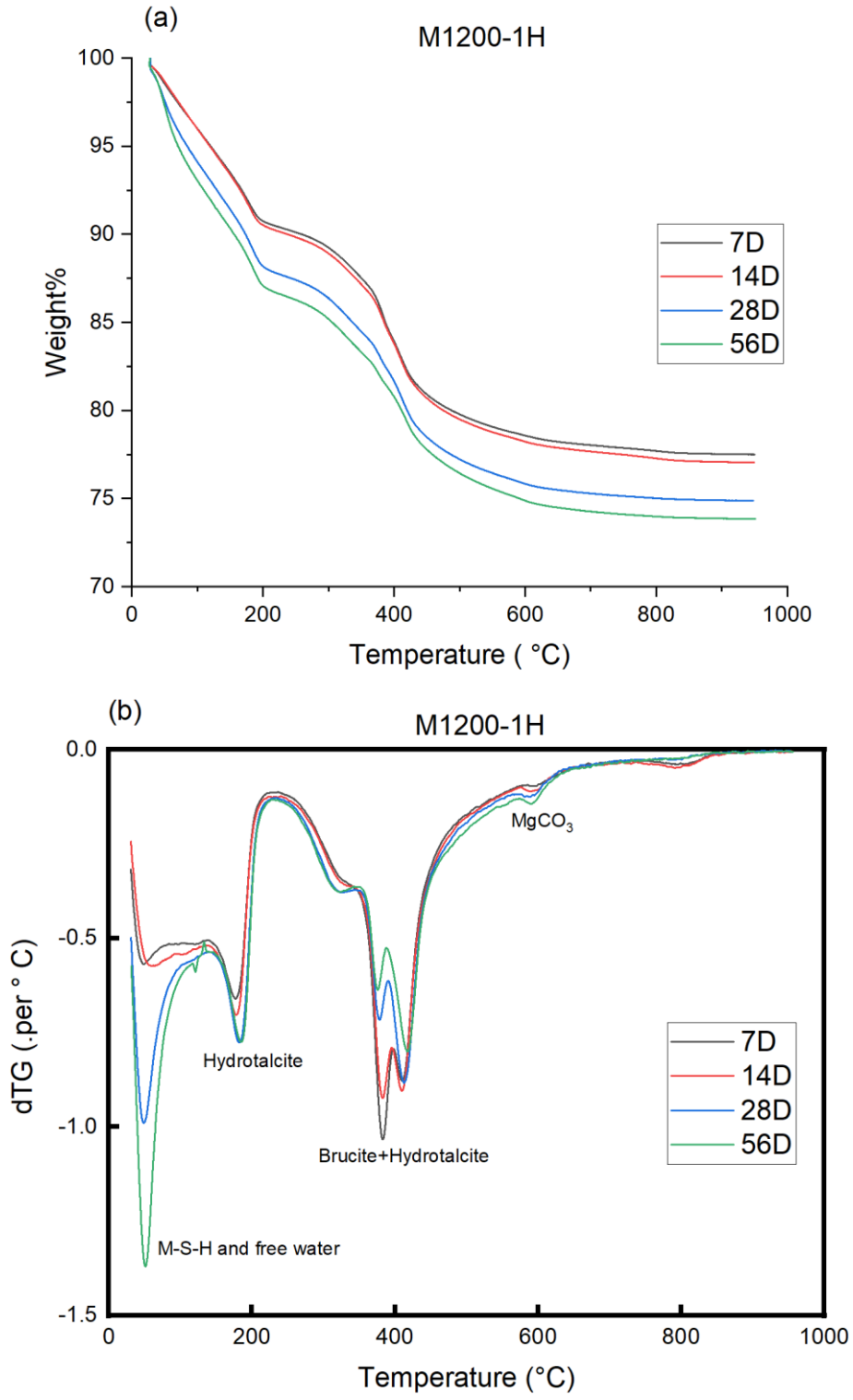

Figure 9. The thermal analysis of M1200-1H samples: (a) TG curves; (b) DTG curves.

6.4 Conclusion

The formation of M-S-H cement using Mg dross and metakaolin, and the effect of $NaHCO_3$ on their hydration behaviour were studied in this paper. M-S-H was formed with the Mg dross and the reaction was accelerated with the addition of $NaHCO_3$. The XRD data are showing serval different phases in the final products mostly impurities originally presented in the dross, implying the formation of M-S-H was not hindered by the impurities in the raw material. The compressive strength of the Mg dross samples without $NaHCO_3$ addition reached 4.6 Mpa at 56 days while the samples with the addition of $NaHCO_3$ reached 2.92 Mpa at 14 days. These results suggest that the addition of $NaHCO_3$ can accelerate the reaction but may reduce the overall compressive strength. Therefore, it is important to optimise the amount of $NaHCO_3$.

The samples using the metakaolin as the raw materials did not show evidence of M-S-H formation. The sample without $NaHCO_3$ addition have limit reaction occurred during 56 days while the samples with $NaHCO_3$ addition illustrate the formation of hydrotalcite instead of M-S-H. Both metakaolin samples were not showing sufficient compressive strength, suggesting that the metakaolin itself is not able to provide enough strength to the products. However, the results indicate the addition of the $NaHCO_3$ to the batches is capable to produce the alkali condition for metakaolin activation.

Chapter 7. Introduction of sodium hexametaphosphate to the M-S-H system with the addition of sodium bicarbonate

Abstract

The acceleration of the M-S-H formation has been successfully achieved in our previous study by the use of $NaHCO_3$ [60]. However, the strength of the M-S-H cement has been restricted by its relatively high water content. The effect of sodium hexametaphosphate (NaHMP), to the M-S-H system is studied in the present work. NaHMP has been used as an inorganic deflocculant as a means to reduce water demand in similar M-S-H systems [24, 26, 46], but not together with sodium bicarbonate ($NaHCO_3$). Samples are examined using mini slump test, X-ray diffraction (XRD), ex-situ pH measurements, thermogravimetry (TG) and compressive strength test. The results show that NaHMP was able to work with $NaHCO_3$, allowing to reduce the water demand and accelerate the M-S-H formation simultaneously. The introduction of NaHMP and the associated change in the w/s ratio did not affect the pH value of the system. However, the effect of NaHMP on the workability may be reduced by $NaHCO_3$, and the addition of NaHMP can reduce the acceleration effect of the M-S-H formation.

7.1 Introduction

The practical application of M-S-H cement is currently constrained by its slow setting time and low strength development. It may take few months for the M-S-H cement to achieve the desired strength [22]. As demonstrated in our previous study [60], the formation of the M-S-H binder can be accelerated by the addition of sodium bicarbonate ($NaHCO_3$) to the batch. To further improve the mechanical performance of M-S-H cement, the present study investigates the introduction of sodium hexametaphosphate ($(NaPO_3)_6$, NaHMP) as a superplasticiser, in an attempt to reduce the water content of the system.

The formation of M-S-H cement in the MgO-silica fume system has been known to demand a relatively high volume of water with relatively poor workability [47, 48, 113]. For such a system with fine particles to form a paste with a sufficient fluidity, a significant amount of water is necessary. This high water level usually causes a high porosity in the cement and consequently results in the low density and strength of the cement products.

The water requirements can be reduced by introducing superplasticizers to the system. The superplasticizers can assist uniform dispersion of the fine particles and increase the fluidity of the cement [48]. However they may also retard the setting time of the cement when introduced too much [114]. Zhang et al. [47] used sodium hexametaphosphate ($(NaPO_3)_6$, NaHMP) as the superplasticizers in the 40 wt.% MgO - 60 wt.% silica fume system and reported that the optimum amount of NaHMP is 1 wt.%, which enables the formation of paste at 0.4 water to solid (w/s) ratio. Walling et al. [24] reported that 1 wt.% of NaHMP is the optimum amount also for the 1 $Mg(OH)_2$: 1 SiO_2 system. Although the beneficial effects of superplasticizer, NaHMP, on the MgO/silica fume system and $Mg(OH)_2$ /silica fume system are known, the effects of using NaHMP together with $NaHCO_3$ on the chemistry and hydration reactions of the M-S-H cement remain unclear.

The present work investigates the effects of NaHMP for the formation of M-S-H cement with the addition of $NaHCO_3$ solutions at various levels of water to solid (w/s) ratio. The strength development in the M-S-H samples were also studied, to examine their feasibility for practical applications.

7.2 Materials and Methods

7.2.1 Materials

Majority of the raw materials used in this work are same as our previous work [60], including brucite from Sigma-Aldrich with purity ≥95%, microsilica 940-U from Elkem, sodium carbonate from Sigma-Aldrich with purity ≥99.5% and laboratory distilled water. The sodium hexametaphosphate used is from Sigma-Aldrich with purity of 96%.

7.2.2 Sample mix design

M-S-H cement pastes were prepared by mixing brucite and silica fume with $NaHCO_3$ and/or NaHMP solutions, and the sample information is listed in Table 1. The lowest w/s ratio is determined by a preliminary mixing test, which measured the minimum water demand from making a paste.

The Mg/Si ratio for all the samples are kept the same to the previous study [60]; The mass of sodium bicarbonate is determined by its solubility in water at 20°C, which is 9.6 g/l00ml [61]. The 1H notation represents the mass of $NaHCO_3$, being equal to its solubility (saturated water

solution); The decimal number at the end of the notation represents the w/s ratio; The P-notation represents the addition of NaHMP. The amount of NaHMP used is 1 wt.% of the solid materials, which is the optimum quantity according to the literature [24, 47]. Each set of the samples with different w/s ratio were prepared in cubic mould for compressive strength testing.

Table 1. Composition design of the samples with NaHMP.

	Solution			Solid	
Sample ID	**Water (mL)**	**$NaHCO_3$ (g)**	**NaHMP (g)**	**$Mg(OH)_2$ (g)**	**Silica fume (g)**
1H-1	400	38.4	0	200	200
1H-0.75	300	28.8	0	200	200
P-1H-0.75	300	28.8	4	200	200
P-1H-0.625	250	24.0	4	200	200
P-1H-0.5	200	19.2	4	200	200

7.2.3 Sample preparation

For all samples, the solution was prepared first by dissolving the $NaHCO_3$ (plus NaHMP in P-samples) in the distilled water with magnetic stirrer for approximately 15 minutes at laboratory temperature (~20°C) until the solution becomes colourless. The $NaHCO_3$ solution was placed into a mixer (Heidolph RZR2020, 400rpm), and then all the brucite powder was added over approximately 5 minutes of mixing. Silica fume was then slowly added into the mixer with approximately 20 % of total mass every minute (total of 5 minutes) for homogeneous mixing and minimise dust loss.

After mixing, the cement paste was placed into 20 mm × 20 mm × 20 mm cubic steel moulds, which were manually shaken/vibrated to remove the possible air bubbles and make sure the bottom part of the mould was fully filled. The filled mould was placed inside a plastic bag (not sealed) and then put into another humidified plastic bag (sealed with small amounts of water) to avoid the sample directly contacting with air and water but maintain high humidity.

The samples were then cured in a 35°C oven and taken out at 3, 7, 14, 28, 56, and 112 days. After performing compressive strength test, the cubes were crushed into small pieces and immersed in approximately 200 mL of acetone for 5 minutes to wash. Then, the washed samples were separated from the acetone by using filter paper and a Büchner funnel assisted with vacuum pump for approximately 5 minutes. The separated materials are immersed into

approximately 200 mL of acetone again and kept for 48 hours in order to remove the free water. The samples were separated from acetone again by using filter paper and Büchner funnel for 15 minutes. The dried samples are stored in sealed centrifuge tubes with parafilm until further analysis.

7.2.4 Characterisation methods

7.2.4.1 Mini slump test

The relative fluidity of the paste is tested by the mini slump test, using a downscaled Abrams cone with geometry of 19 mm top diameter, 38 mm bottom diameter and 57 mm height. The freshly mixed paste is full-filled into a cone and then placed on a board with grids. The cone was then lift up and the average diameter of the paste is measured after free flow. One example of the mini slump test is presented in Figure 1.

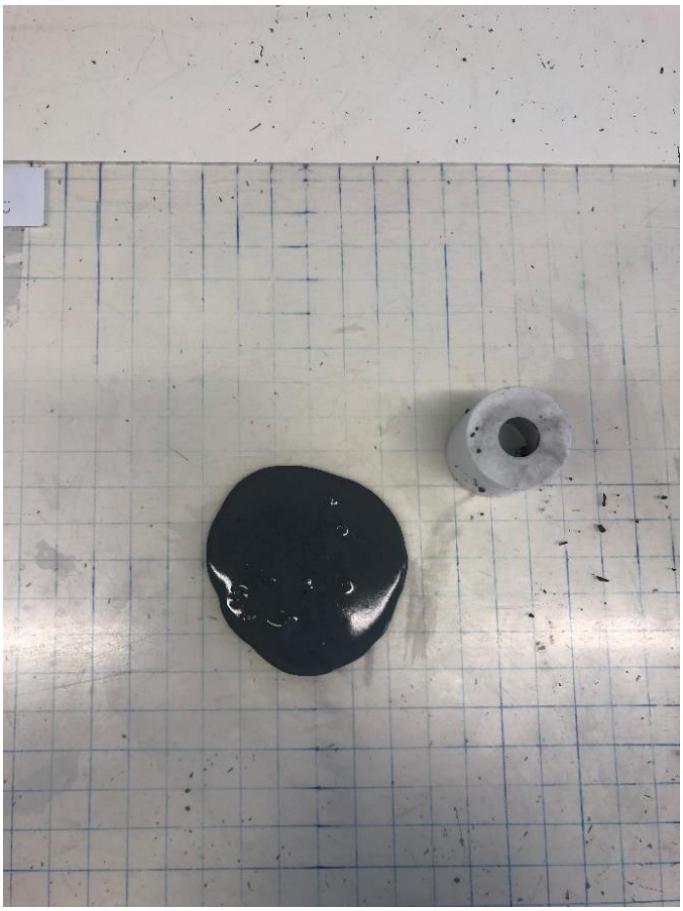

Figure 1. Picture of the example mini slump test after taking the measurements, with the white cone place beside (20mm grid).

7.2.4.2 X-ray diffraction

The X-ray diffraction (XRD) was used for the phase analysis. The machine used was benchtop Bruker D2 PHASER apparatus armed with a Cu-Kα radiation source running at 30 kV and 10 mA. The divergence silt used was 1 mm, the upper and lower discriminators were 0.11 and 0.25 V respectively. The scanning angle range was from 5° to 80° 2θ with an increment of 0.02°. The sample was rotating at 15 rpm during scanning to avoid uneven distribution of microstructure. The samples are crushed and ground into powders before placed on the sample holder for measurement.

7.2.4.3 Thermogravimetric analyses

Thermogravimetric analyses (TGA) were also used for the phase analysis. The tests were carried out by using PerkinElmer TGA 4000. Approximately 40 mg of samples were used for testing each time. The sample was heated from 30°C to 990°C at a rate of 10 °C/min under a nitrogen flow of 40 mL/min. Ten minutes of isothermal hold was used at both the start and end of the heating programme.

7.2.4.4 pH measurement

The apparatus used for pH measurements was a Mettler Toledo pH/Cond bench meter SE S470-K equipped with an expert proISM probe (error = ±0.01). The probe was calibrated each time before use by immersing into standard buffer solutions with known pH values. The pH of the samples at 0 day (initially prepared batch) was measured right after the batch was mixed properly; a small portion of the batch was separated, and then the testing probe was inserted directly into the paste to take the readings. For the cured samples, ex-situ leaching method [51] was used for the pH measurement. For each measurement, 1 g of powdered sample was added into 80 mL of distilled water and then stirred with a magnetic stirrer, before the testing probe was immersed into the solution. The pH reading was recorded after > 15 minutes of stirring when the pH reading of the solution stabilised. For the ex-situ tests, preliminary tests were performed to determine the suitable amount of cement to be added, in which 0.2 g, 0.6 g, or 1.0 g of a cured cement sample was added after powdered into 80 mL of distilled water These preliminary tests showed that the pH readings for > 0.6g addition are the same, implying that the solution is already saturated. It should be noted that this method to measure the pH of the samples assumes the pore solution of the cement is in over saturated state.

7.2.4.5 Compressive strength test

The electromechanical test frame used to measure compression used was the Zwick Roell 50 kN load cell and calibrated each day before use. The cross-section area of the cubes was measured before each test. Three readings of width and length of the cubes were taken by vernier calliper respectively and the averages are used to calculate the cross-section area. The compression head was approaching the base at 0.2mm/minute and stopped when there is a sudden decrease in compression force. The maximum compression force applied during compression was then recorded. These experiments were carried out in triplicates and the average value calculated. An example of the compressive strength test is presented in Figure 2.

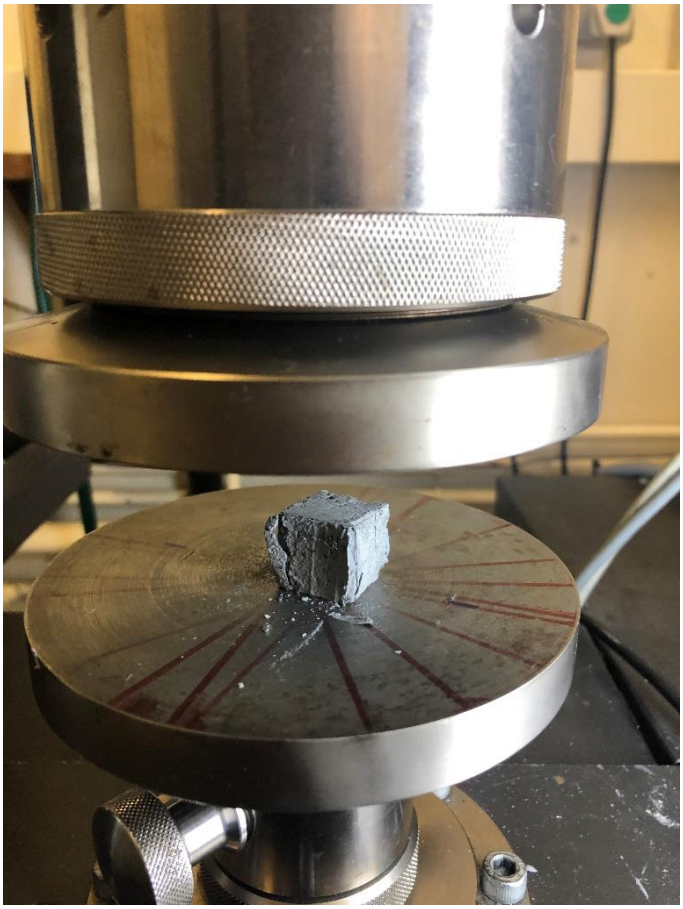

Figure 2. The compression heads and the tested cubes for compressive strength test.

7.3 Results and discussion

7.3.1 Mini slump

The average diameter of the sample pastes after free flow are measured, and the calculated paste areas are presented in Figure 3. The area of 11.3 cm^2 indicates no slump, which is the initial area of the cone. Although the minimum value of the w/s ratio reported in the open literature is 1 [24], the 1H samples without NaHMP was able to form a paste with 0.75 w/s ratio. In addition, the area of the slump recorded at 1.0 w/s ratio is larger than that of a similar system reported in the literature [24]. These results imply that, when NaHMP is not added, $NaHCO_3$ may act as a mild plasticizer at its saturation concentration and reduce the water demand of the paste. For the 1H series without NaHMP, the fluidity is overall quite limited, and little fluidity is observed for the 0.75 w/s ratio. Thus, it appears to be difficult to reduce the water content of the system from 1 w/s ratio.

On the other hand, the introduction of NaHMP improved the fluidity of the P-1H series significantly, even at the lower w/s ratios than 1H series. However, the 1H samples with NaHMP (P-1H) was able to form a paste with the minimum w/s ratio of only 0.5 instead of 0.4 reported in the literature [24]. The slump area at 0.75 w/s ratio is also smaller than that reported in the literature [24]. The comparison with the literature suggests that, when NaHMP is introduced into the samples, $NaHCO_3$ may reduce the effect of NaHMP as the superplasticizer and slightly increase the water demand of the cement.

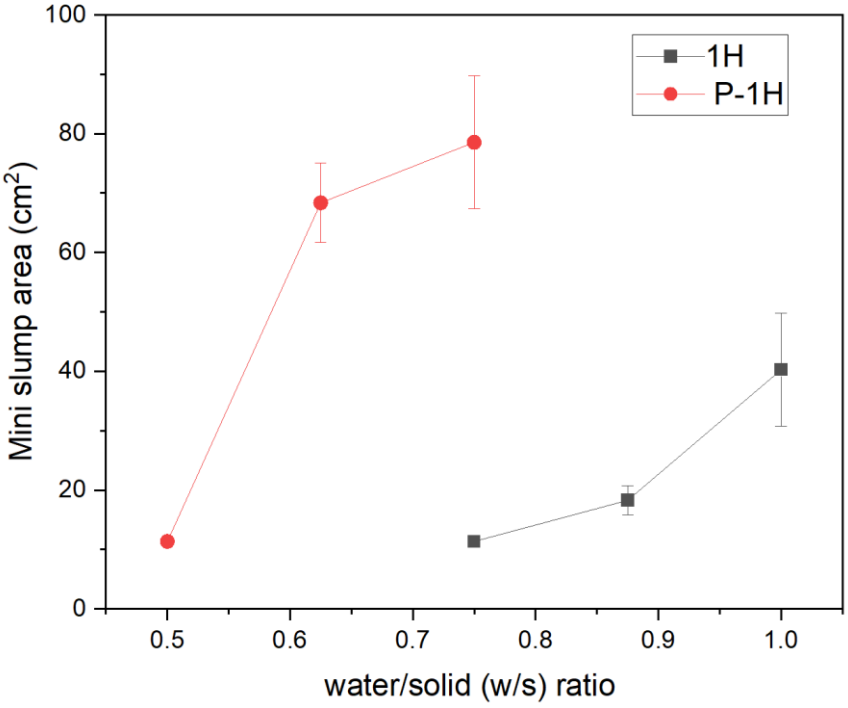

Figure 3. Mini-slump values for the samples as a function of water/solid ratio.

7.3.2 Phase formation and consumption of $Mg(OH)_2$

The XRD patterns of 1H and P-1H samples are presented in Figure 4. According to the literature, the broad humps at 10-13°, 20-30°, 35-39°, and 58-62° 2θ can be attributed to M-S-H [21]; The broad hump at 18–25° 2θ is attributed to unreacted silica fume [26]; The sharp peaks at 18.6°, 38.0°, 50.8°, and 58.6° 2θ are for brucite[21]; Small reflection peaks at ~15° 2θ attributed to the presence of hydromagnesite, $Mg_5(CO_3)_4(OH)_2{\cdot}4H_2O$ [52].

The X-ray patterns reveal the gradual formation of M-S-H and consumption of brucite in all the samples. The data in Figure 4 shows the small amount of brucite still remain in the samples after 14 days when w/s ratio is 1, while the brucite is completely consumed before 14 days when w/s is 0.75. This is interesting because the 1H-0.75 sample contains less $NaHCO_3$. In our previous studies, the acceleration of brucite consumption was generally reduced with the amount of $NaHCO_3$ in the system. A possible explanation is the formation of M-S-H being accelerated more in the 1H-0.75 system. Our previous study in reaction kinetics suggested that the rate of brucite consumption is controlled by the precipitation of M-S-H which may have been encouraged in the 1H-0.75 system.

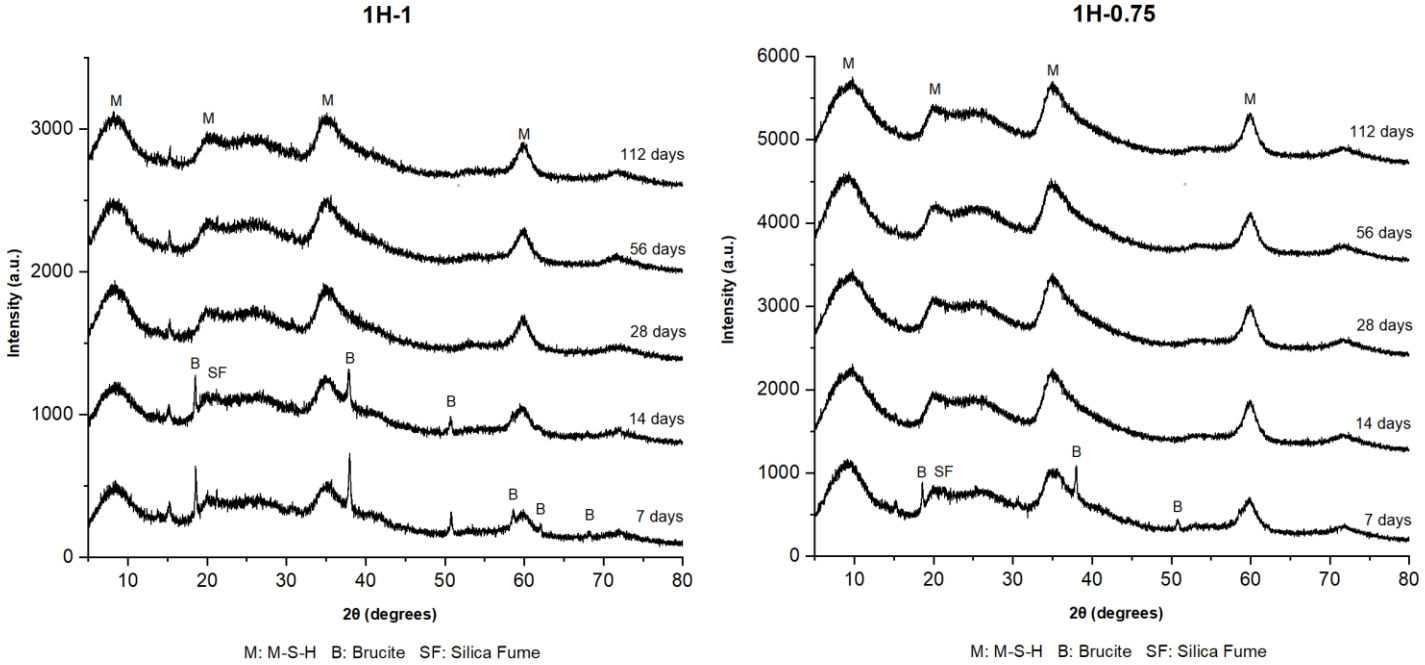

Figure 4. The XRD patterns for the 1H-1(left) samples and 1H-0.75 samples (right).

The same trend appears in P-1H samples as shown in Figure 5: the brucite was mostly consumed by 28 days in the w/s ratio of 0.75, by 14 days in the w/s ratio of 0.625, and less than 14 days when w/s ratio is 0.5. These results imply the reduction of water ratio can accelerate the M-S-H formation reaction, as previously discussed, which may due to higher local concentration of ions.

It is important to note that the introduction of NaHMP did not encourage additional crystalline phases to form as presented in XRD patterns, but may delayed the reaction in the system. The P-1H-0.75 samples are showing the slower consumption of brucite and formation of M-S-H compared to the 1H-0.75 samples (without introduction of NaHMP). This must be the common retardation effect of the superplasticizers, which is also be observed when $NaHCO_3$ is not added [24].

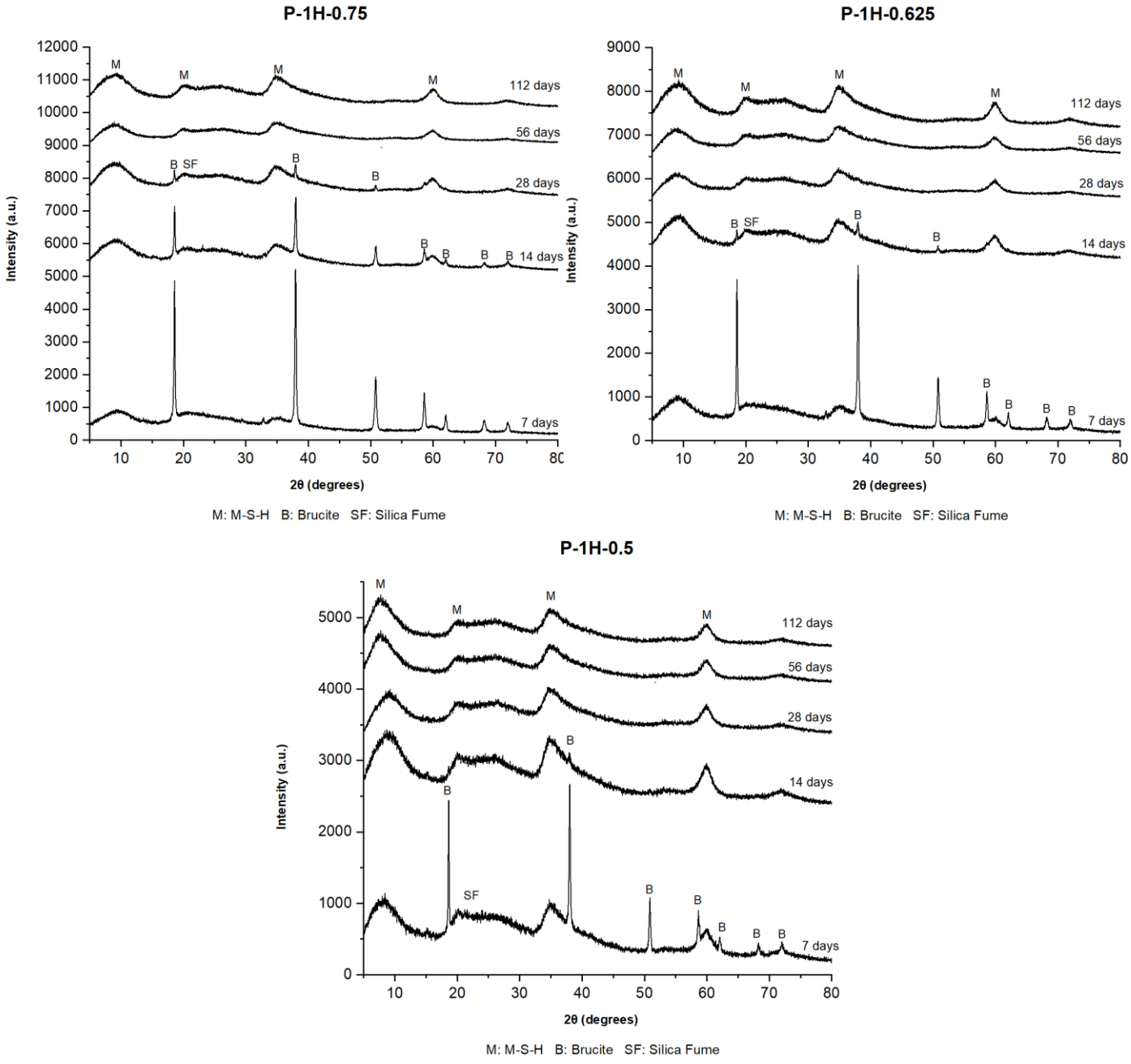

Figure 5. The XRD patterns for the P-1H-0.75 (top left) samples, P-1H-0.625 (top right) samples and P-1H-0.5 samples (bottom).

7.3.3 Variation of pH

The pH measurement results of the 1H and P-1H samples are presented in Figure 6. All the samples are having similar pH values most of the time from 0 days to 112 days. These results indicate the changing of the w/s ratio and the addition of NaHMP do not affect the pH of the system too much. The P-1H-0.75 sample is showing a slightly low pH value at 7 days of curing. Since this system indicated the most significant brucite consumption in the XRD data, it may be linked to the formation of M-S-H

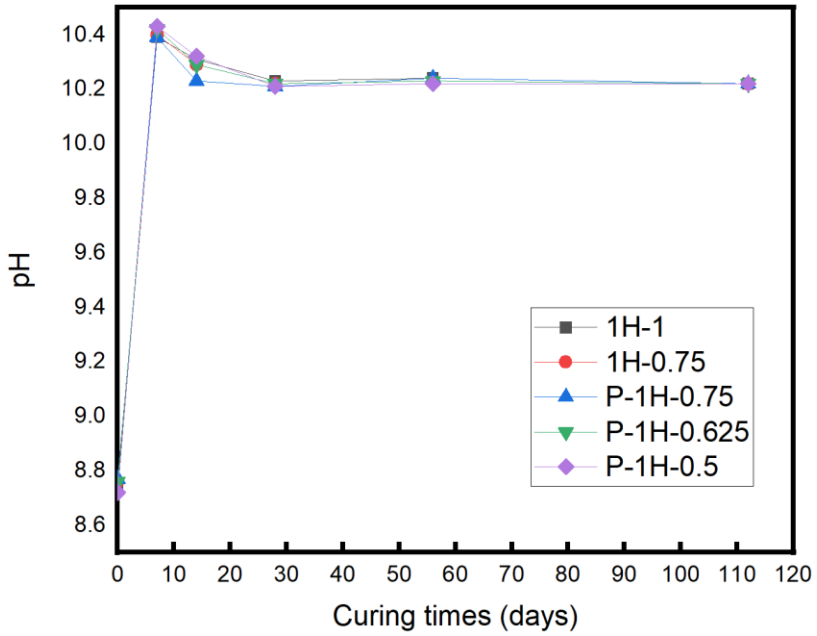

Figure 6. The pH measurements over time for 1H and P-1H cements with different w/s ratio.

7.3.4 Compressive strength

The compressive strength data obtained for 1H samples (w/s ratio of 1 and 0.75) and P-1H samples (w/s ratio of 0.75, 0.625 and 0.5) are shown in Figure 7. Three cube specimens were tested for each formulation, and the average strength values were then calculated. The lower water contents of the system allow the average strength of the samples to increase at each curing age. This is expected as the strength of the cement can be improved by the reduction in porosity enabled by water reduction [107, 108]. As previously discussed, the less w/s ratio may also encourage the formation M-S-H, which may be additionally aiding the strength development. The strength development is generally slow when w/s ratio is ≥ 0.625. The strength of each system almost stays constant in the first 56 days and increased slightly from 56 days to 112 days. Only the P-1H-0.75 shows the continuous increase in strength from 7 days to 56 days.

The overall strength of the materials tested in the present study is relatively low compared to similar systems found in other works. This may be due to the addition of $NaHCO_3$ (as reported in previous chapter) or the using of $Mg(OH)_2$ as the starting material. Sonat et al. used 1 % of sodium hexametaphosphate as superplasticizer, and prepared the M-S-H sample from 50 wt.% magnesia (MgO) and 50 wt.% silica fume at W/S ratio of 0.55 , obtaining the maximum strength of 47 MPa at 56 days [115]. Zhang et al. prepared the M-S-H sample using 40 wt.% magnesia and 60 wt.% silica fume with 1% of sodium hexametaphosphate as superplasticizer, and the compressive strength of samples with W/S ratio of 0.4 and 0.5 both exceeded 60 MPa at 28 days [47]. Tran et al. reduced the water demand of the M-S-H sample further by replacing 40 % of the 40 wt.% magnesia and 60 wt.% silica blend with crushed quartz filler, leaching W/S ratio of 0.21, and produced the cement sample with 87.3 MPa compress strength at 28 days [113].

Nonetheless, the compressive strength achieved is sufficient for specific applications such as in nuclear waste encapsulation. The compressive strength of all the samples with w/s ratio lower than 1 exceeds 5 MPa at 7 days, which is the requirement for the intermediate radioactive wastes (ILW) encapsulation [116].

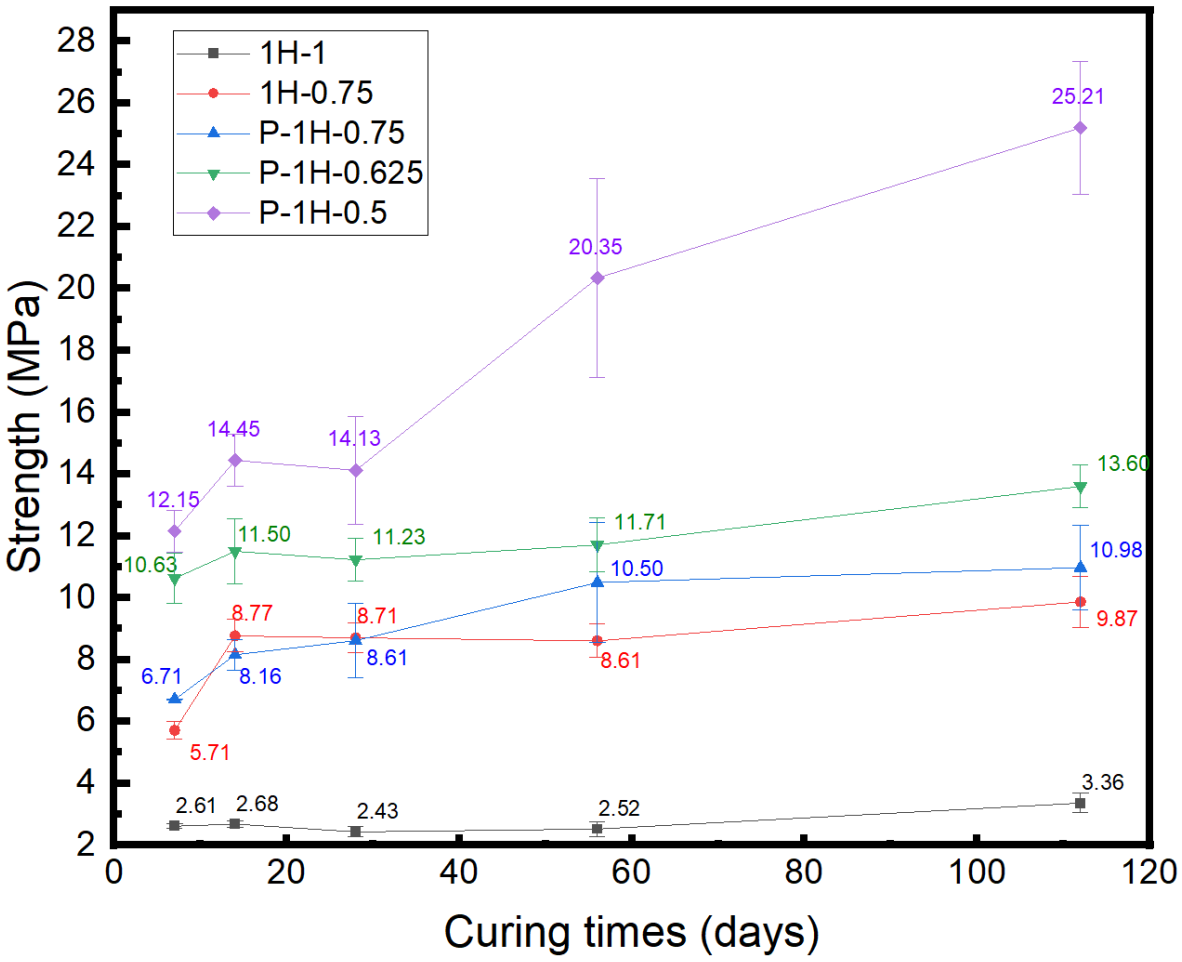

Figure 7. The compressive strength test of 1H and P-1H samples with different w/s ratio with standard deviation.

7.3.5 Quantification of phases

The thermogravimetric (TG) and differential thermogravimetric (DTG) curves for the samples are shown in Figures 8, 9, 10, 11 and 12. According to the literature, The weight loss step around 80-250 °C is mainly due to the loss of water physically bounded to M-S-H [21, 62]. The decomposition of brucite resulted in the weight loss step around 320 – 480 °C, corresponding to the amount of brucite remained in the system [21]. The broad weight loss step around 500 – 600 °C attributes to the loss of the chemically coordination water of M-S-H, which can be used as the indication of M-S-H formation [21]. The small peaks occurring around 500°C may indicate the presence of magnesium carbonate species such as hydromagnesite, $Mg_5(CO_3)_4(OH)_2{\cdot}4H_2O$ [55]. These are consistent with the data presented in the previous chapters.

The physically bonded water identified with the weight loss step around 80-250 °C is initially increases up to 28 days, then start decreasing by 56 days of curing in the samples without NaHMP. For the P-1H samples, the weight loss in this region keeps increasing until 56 days. This may be related to the retarding effect of NaHMP, delaying this evolution of M-S-H usually observed.

The regions in the DTG curves corresponding to brucite decomposition indicate that the consumption of brucite is generally faster in the system without NaHMP, consistent with the XRD data. However, once reaction starts, all brucite appears to be consumed by 28 days in the presence of NaHMP while a small amount of brucite persists to remain in the system even up to 112 days without NaHMP.

Relatively large peaks of hydromagnesite appears in the 1H-1 samples and 1H-0.75 at only 7 days, implying that the formation of hydromagnesite is preferred with higher water content level.

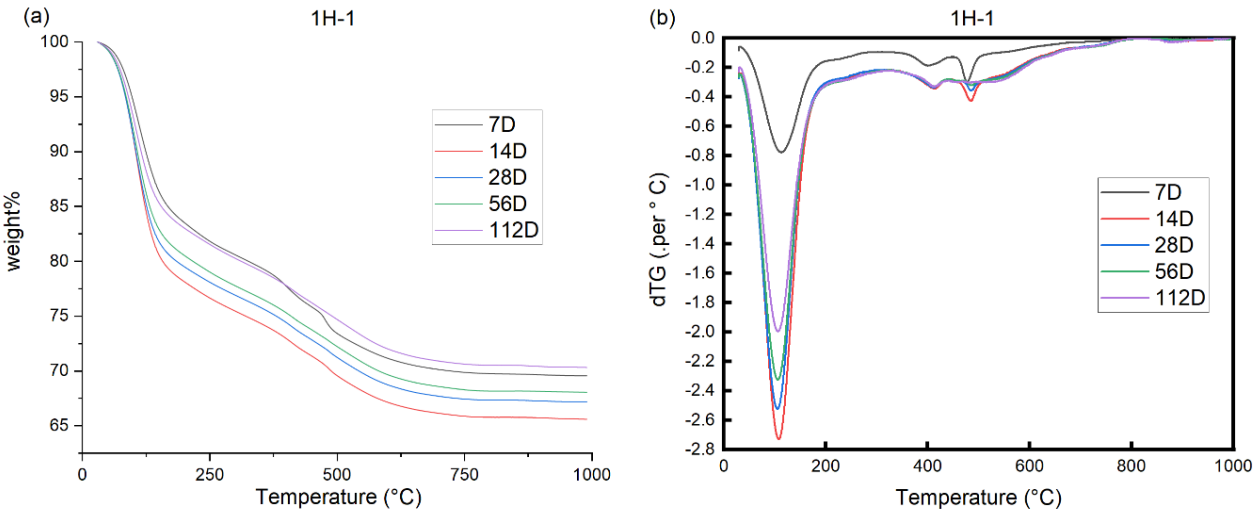

Figure 8. The thermal analysis of 1H-1 samples: (a) TG curves; (b) DTG curves.

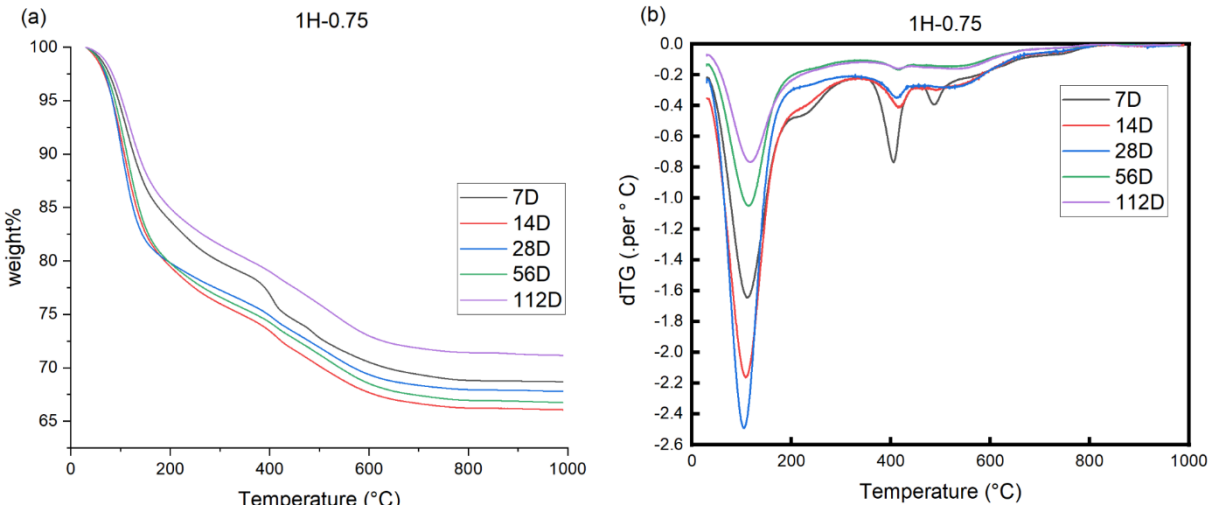

Figure 9. The thermal analysis of 1H-0.75 samples: (a) TG curves; (b) DTG curves.

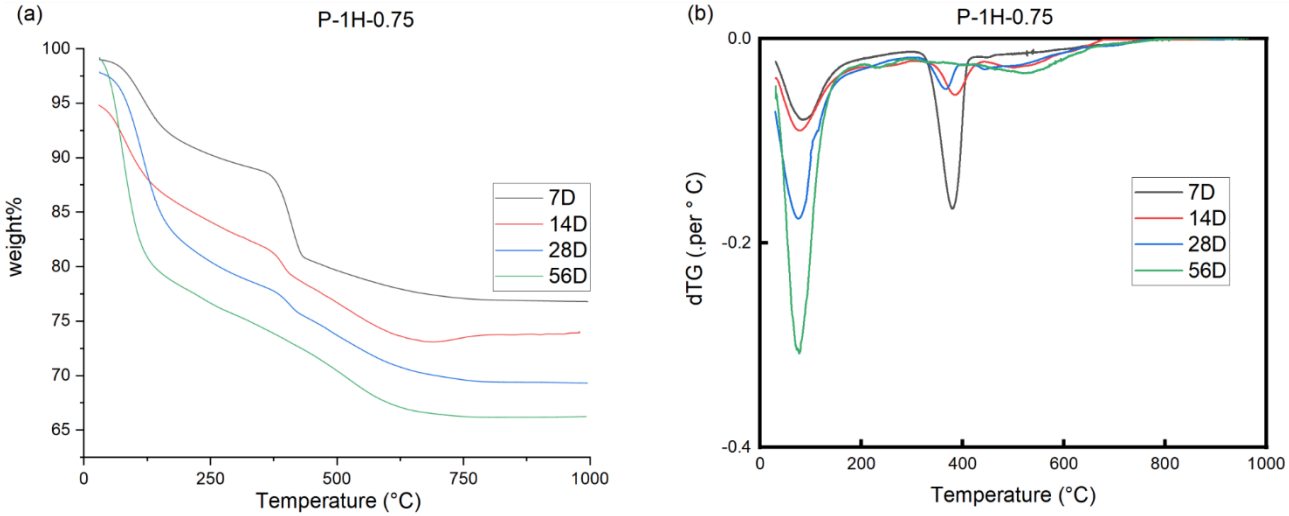

Figure 10. The thermal analysis of P-1H-0.75 samples: (a) TG curves; (b) DTG curves.

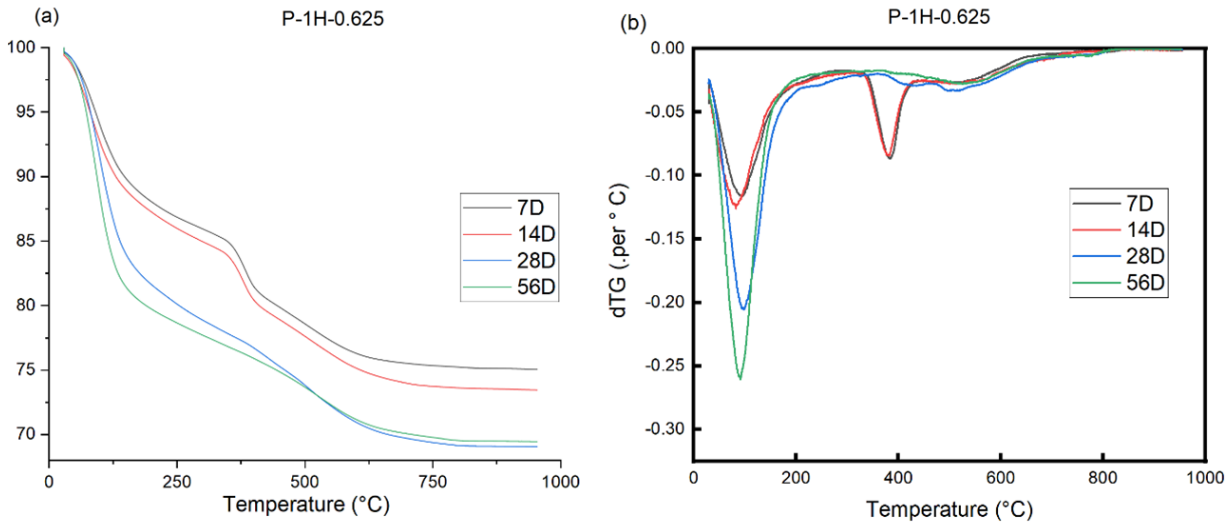

Figure 11. The thermal analysis of P-1H-0.625 samples: (a) TG curves; (b) DTG curves.

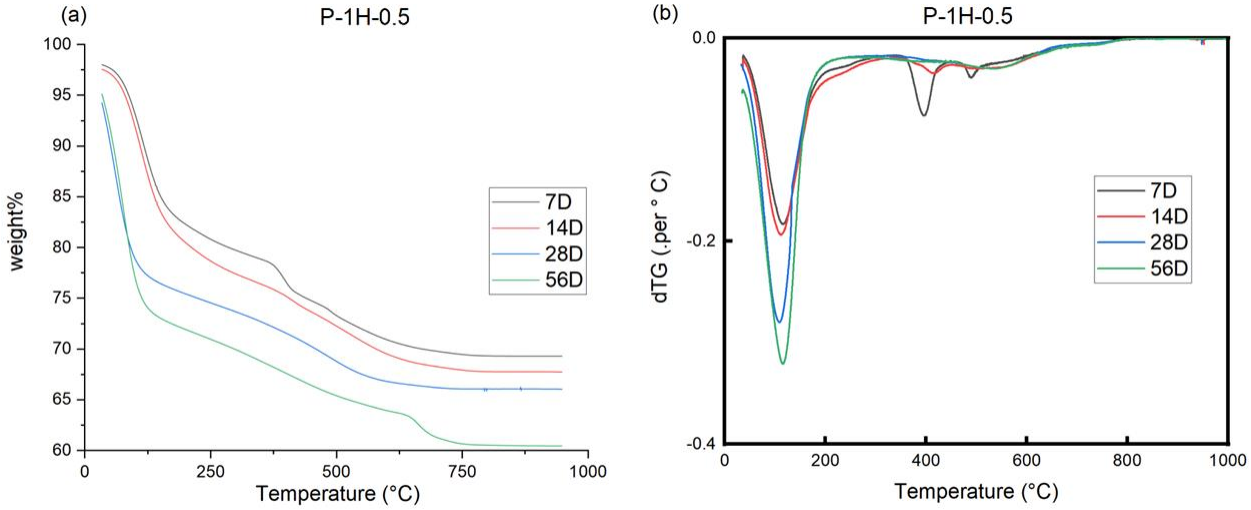

Figure 12. The thermal analysis of P-1H-0.5 samples: (a) TG curves; (b) DTG curves.

7.4 Conclusion

The formation of M-S-H with $NaHCO_3$ and NaHMP at various w/s ratio are studied in this present work. The results show the addition of NaHMP can retard the reaction, indicated by slower consumption of brucite and slower formation of M-S-H gel. However, the addition of NaHMP can increase the fluidity of the system and allows to reduce the requirement of w/s ratio for the 1 $Mg(OH)_2$: 1 silica fume system down to 0.5. The lowest w/s ratio of 0.5 achieved in the present work is slightly high compared to the literature [24], which may due to the effect of NaHMP is hindered by the presence of $NaHCO_3$. The results also suggest that the lowered w/s ratio can accelerate the reaction and improve the compressive strength of the cement. The highest compressive strength obtained is 25.21 MPa when w/s ratio is 0.5. It was also confirmed that the addition of NaHMP and varying the w/s ratio is not affecting pH of the system, which is useful for the applications sensitive to the pH environment.

Chapter 8. Conclusion and future work

8.1 Conclusion

The research on M-S-H gel has been carried out with the purpose of developing new environment friendly cementitious material, focused improving the behaviour of the M-S-H cement for practical applications. This thesis work shows a comprehensive analysis of the formation of M-S-H cement, that have been accelerated by using alkali carbonates. The findings filled some research gaps of the M-S-H cement and provide few perspectives for future study of the M-S-H binder system.

To solve the slow formation, one of the most significant limitations of the M-S-H cement, preliminary test of $NaHCO_3$ addition was conducted in chapter 3. The $NaHCO_3$ addition is proposed based on the assumption of the pH influence on the dissolution of the raw materials for M-S-H formation. The silica and $Mg(OH)_2$ is showing opposing solubility due to their acidic and basic nature, and the addition of $NaHCO_3$ can help the system reach an pH value, where both silica and $Mg(OH)_2$ is having relatively high solubility to aid the reaction. The comparison between samples with or without $NaHCO_3$ addition shows that it takes at least 56 days to consume all the brucite without the additives, while only 7 days are required to consume almost all the brucite when $NaHCO_3$ is added. The addition of $NaHCO_3$ raised the pH of the system to ~10.2 appears to be beneficial for the reaction. Although the addition of $NaHCO_3$ causes extra phases formed in the system, it offers a prospective research direction for M-S-H cement formation.

To further investigate the acceleration effect of $NaHCO_3$, chapter 4 examined the formation of M-S-H with the addition of various $NaHCO_3$ concentrations, along with the estimation of the reaction mechanisms and kinetics of the reactions. The $NaHCO_3$ are added into samples with different concentration (lower than solubility limit), and the investigation shows that the acceleration is promoted by higher $NaHCO_3$ concentration, but lower concentration can still provide a significant acceleration effect. However, it was also revealed that the amount of $Mg(OH)_2$ remained in the system after 112 days of reaction is increased with the $NaHCO_3$ concentration. The basic principle of the acceleration is proposed to be the formation of hydromagnesite as an intermediate product, which increase the Mg^{2+} ions concentration and aid the dissolution of silica fume. The reaction kinetics of the M-S-H formation are identified as nucleation-controlled based on the thermogravimetric analysis.

As the formation of hydromagnesite may be the key factor of the acceleration effect, it is reasonable to examine other alkali carbonate as the additives in the M-S-H cement system. Chapter 5 used Na_2CO_3 as the additive, and the formation of M-S-H is investigated with different concentrations of Na_2CO_3, along with the study for the influence of Na^+ ions and pH value of the system. The samples with Na_2CO_3 showed different reaction mechanism compared to the samples with $NaHCO_3$, which the consumption of brucite was highly limited in the first 7 days and then almost all being consumed in a relatively short period. The acceleration effect of Na_2CO_3 also increased with its concentration (up to saturation), and the samples with saturated Na_2CO_3 solution shows almost fully development of M-S-H gel at 14 days, which is slower than the $NaHCO_3$ samples mostly because of the initial dormant period of 7 days. PHREEQC calculation suggested that the reason for this slower acceleration may due the dissolution of $Mg(OH)_2$ is hindered by Na_2CO_3. The study also indicated the controlling the initial pH does not solely improve the reaction speed. The results suggest that the concentration of CO_3^{2-} ions is the key factor of acceleration but the concentration of Na^+ ions need to stay within a certain range. The final phases in the products can change, based on the concentration of the carbonates, where additional phases such as talc or dolomite might present in the products.

Chapter 6 used Mg dross from alloy industries and metakaolin as the alternative materials for brucite and silica fume respectively, in the purpose of producing M-S-H cement more sustainably. Since the previous chapters shows that $NaHCO_3$ is a better additive compared to Na_2CO_3, samples with or without the addition of $NaHCO_3$ were prepared for comparison. The results indicated the successful formation of M-S-H gel in the Mg dross samples but the compressive strength of the products is relatively low. The acceleration of $NaHCO_3$ remain effective for the Mg dross samples during the reaction, however the compressive strength is reduced with the addition of $NaHCO_3$. There is no evidence showing the formation of M-S-H in the metakaolin samples, and hydrotalcite was formed instead in the samples with $NaHCO_3$. Almost no reaction occurred when $NaHCO_3$ is not used. The formation of hydrotalcite indicates $NaHCO_3$ is capable to provide alkali condition for metakaolin activation. Both metakaolin samples were not showing any compressive strength, suggests that the hydrotalcite itself is not able to provide enough strength to the products.

Chapter 7 attempts to address the strength limitation of M-S-H cement. The strength of the M-S-H cement is low compared to the Portland cement, and reducing the water content is one of the promising methods to improve the performance of M-S-H cement. The effect of superplasticizers together with the addition of $NaHCO_3$ was investigated in this chapter. M-S-H samples with $NaHCO_3$ are prepared in different w/s ratio with or without the addition of NaHMP. The amount of NaHMP used is based on the optimum quantity from literature [47].

The results suggest that the addition of NaHMP will retard the formation of M-S-H but has little effects on the pH values of the system. NaHMP can effectively reduce the minimum amount of water required for making paste from 0.75 to 0.5 w/s ratio. The addition of $NaHCO_3$ may hinder the effect of NaHMP, making the lowest w/s ratio slightly higher compared to the literature values [24]. The results also suggest that the lower w/s ratio can accelerate the formation of M-S-H, which may be contributing to the improvement of the compressive strength of the product. The highest compressive strength obtained is 25.21 MPa when w/s ratio is 0.5.

8.2 Future work

There are still lots of issues need to be resolved before the M-S-H cement to be used for most applications. Possible experiments could be carried out to enhance the understanding of the M-S-H cement:

- The time interval between the measurements may be too long for most of the samples, it will be helpful to investigate the reaction within shorter period to find when exactly most of the hydration occur. By doing so, Isothermal Conduction Calorimeter (ICC) can be used during the hydration period and provide some initial studies of the reaction kinetics, which may be helpful to understand the formation mechanism of M-S-H cement.

- The pore solution of the cement can be investigated to directly obtain information of the dissolution process of the raw materials. The pore solution of the solution can be obtained by using vacuum or high-pressure extraction, by measuring the concentration of the ions in the pore solution, the formation processes of M-S-H gel can be further understood.

- Scanning electron microscopy (SEM) could be carried out to investigate the microstructure of the cement to give a better understanding of the morphology of the cement and distribution of the elements. SEM images can also provide information on the formation mechanism and how the accelerated reaction occurred, helping to understand the M-S-H system further.

- The results suggest that the formation of hydromagnesite as intermediates may be one of the key factors for the acceleration effect of $NaHCO_3$ addition. Therefore, it may be useful to study the system with direct addition of hydromagnesite and $NaHCO_3$, or use hydromagnesite to substitute part of the brucite as raw materials. By carrying out such experiment, the acceleration mechanism of the alkali carbonates could possibly be further understood.

- As suggested in chapter 6, the Mg/Si/Al ratio may be important in M-S-H formation as well as the strength development of the products. In the purpose of using metakaolin for M-S-H cement production, it is worth testing the samples with various Mg/Si/Al ratio to study the compositional effects and identify an optimum proportion for the fast reaction and high strength.

- The measurement of the compressive strength only provides general information of the strength. To further understand the effect of the water content and superplasticizers on the cement, mercury intrusion porosimetry (MIP) method can be applied on the cement to measure the porosity of the cement, which can help to gain further insight into the effects of water and superplasticizers, through the correlation between the microstructure and strength.

Chapter 9. References

1. Environment, U.N., et al., *Eco-efficient cements: Potential economically viable solutions for a low-CO2 cement-based materials industry.* Cement and concrete Research, 2018. **114**: p. 2-26.
2. Walling, S.A. and J.L. Provis, *Magnesia-based cements: a journey of 150 years, and cements for the future?* Chemical reviews, 2016. **116**(7): p. 4170-4204.
3. Andrew, R.M., *Global CO2 emissions from cement production.* Earth Syst. Sci. Data, 2018. **10**(1): p. 195-217.
4. Unluer, C. and A. Al-Tabbaa, *The role of brucite, ground granulated blastfurnace slag, and magnesium silicates in the carbonation and performance of MgO cements.* Construction and Building Materials, 2015. **94**: p. 629-643.
5. Taylor, M.G. and D. Collins, *Novel cements: low energy, low carbon cements.* Fact Sheet, 2006. **12**.
6. Wilson, A.D., *The chemistry of dental cements.* Chemical Society Reviews, 1978. **7**(2): p. 265-296.
7. Seehra, S.S., S. Gupta, and S. Kumar, *Rapid setting magnesium phosphate cement for quick repair of concrete pavements—characterisation and durability aspects.* Cement and Concrete Research, 1993. **23**(2): p. 254-266.
8. Lu, X. and B. Chen, *Experimental study of magnesium phosphate cements modified by metakaolin.* Construction and Building Materials, 2016. **123**: p. 719-726.
9. Gardner, L.J., *Assessment of magnesium potassium phosphate cements for radioactive waste encapsulation.* 2016.
10. Nied, D., et al., *Properties of magnesium silicate hydrates (MSH).* Cement and Concrete Research, 2016. **79**: p. 323-332.
11. Brew, D.R.M. and F.P. Glasser, *Synthesis and characterisation of magnesium silicate hydrate gels.* Cement and Concrete Research, 2005. **35**(1): p. 85-98.
12. Temuujin, J., K. Okada, and K.J.D. MacKenzie, *Formation of layered magnesium silicate during the aging of magnesium hydroxide–silica mixtures.* Journal of the American Ceramic Society, 1998. **81**(3): p. 754-756.
13. Bernard, E., et al., *Formation of magnesium silicate hydrates (MSH).* Physics and Chemistry of the Earth, Parts A/B/C, 2017. **99**: p. 142-157.
14. Li, Z., et al., *Characterization of reaction products and reaction process of MgO–SiO2–H2O system at room temperature*. 2016.
15. Zhang, T., et al., *Characterization of magnesium silicate hydrate (MSH) gel formed by reacting MgO and silica fume.* Materials, 2018. **11**(6): p. 909.
16. Lothenbach, B., et al., *Magnesium and calcium silicate hydrates.* Cement and Concrete Research, 2015. **77**: p. 60-68.
17. Kalousek, G.L. and D. Mui, *Studies on formation and recrystallization of intermediate reaction products in the system magnesia - silica - water.* Journal of the American Ceramic Society, 1954. **37**(2): p. 38-42.

18. Yang, J.C.S., *The System Magnesia-Silica-Water Below 300° C.: I, Low-Temperature Phases from 100° to 300° C. and Their Properties.* Journal of the American Ceramic Society, 1960. **43**(10): p. 542-549.
19. Bernard, E., et al., *Characterization of magnesium silicate hydrate (MSH).* Cement and concrete research, 2019. **116**: p. 309-330.
20. Bernard, E., et al., *Alkali binding by magnesium silicate hydrates.* Journal of the American Ceramic Society, 2019. **102**(10): p. 6322-6336.
21. Jin, F. and A. Al-Tabbaa, *Thermogravimetric study on the hydration of reactive magnesia and silica mixture at room temperature.* Thermochimica acta, 2013. **566**: p. 162-168.
22. Yang, N., et al., *Properties of magnesium based cements.* 2017.
23. Batchelor, B., *Overview of waste stabilization with cement.* Waste Management, 2006. **26**(7): p. 689-698.
24. Walling, S., et al., *Structure and properties of binder gels formed in the system Mg(OH)2-SiO2-H2O for immobilisation of Magnox sludge*. Vol. 44. 2015.
25. Unluer, C. and A. Al-Tabbaa, *Enhancing the carbonation of MgO cement porous blocks through improved curing conditions.* Cement and Concrete Research, 2014. **59**: p. 55-65.
26. Zhang, T., C.R. Cheeseman, and L.J. Vandeperre, *Development of low pH cement systems forming magnesium silicate hydrate (M-S-H).* Cement and Concrete Research, 2011. **41**(4): p. 439-442.
27. Zhang, T., L.J. Vandeperre, and C.R. Cheeseman, *Magnesium-silicate-hydrate cements for encapsulating problematic aluminium containing wastes.* Journal of Sustainable Cement-Based Materials, 2012. **1**(1-2): p. 34-45.
28. Kinoshita, H., et al., *Corrosion of aluminium metal in OPC- and CAC-based cement matrices.* Cement and Concrete Research, 2013. **50**: p. 11-18.
29. Sandberg, B. and T. Mosberg. *USE OF MICROSILICA IN BINDER SYSTEMS FOR ULTRA-LOW CEMENT CASTABLES AND BASIC,'CEMENT-FREE' CASTABLES*.
30. Myhre, B., C. Ødegård, and H. Feldborg. *Periclase castables based on the bond MgO− SiO2− H2O*.
31. Odegard, C., H. Feldborg, and B. Myhre. *Magnesia-silica-hydrate bonded MgO castables*.
32. Liao, J. and M. Senna, *Mechanochemical dehydration and amorphization of hydroxides of Ca, Mg and Al on grinding with and without SiO2.* Solid State Ionics, 1993. **66**(3-4): p. 313-319.
33. Gartner, E. and T. Sui, *Alternative cement clinkers.* Cement and Concrete Research, 2018. **114**: p. 27-39.
34. Szczerba, J., et al., *Influence of time and temperature on ageing and phases synthesis in the MgO–SiO2–H2O system*. Vol. 567. 2013. 57-64.
35. Iler, R.K., *Chemistry of Silica--Solubility, Polymerization, Colloid and Surface Properties, and Biochemistry.* 1979.

36. Salomão, R. and V.C. Pandolfelli, *Microsilica addition as an antihydration technique for magnesia-containing refractory castables.* American Ceramic Society Bulletin, 2007. **86**(6): p. 9301-9306.
37. Zhang, F.H.D., *Magnesium oxide based binders as low-carbon cements.* 2013.
38. Temuujin, J., K. Okada, and K.J.D. MacKenzie, *Role of Water in the Mechanochemical Reactions of MgO–SiO2Systems.* Journal of Solid State Chemistry, 1998. **138**(1): p. 169-177.
39. Jin, F. and A. Al-Tabbaa, *Strength and hydration products of reactive MgO–silica pastes.* Cement and Concrete Composites, 2014. **52**: p. 27-33.
40. Vandeperre, L.J. and A. Al-Tabbaa, *Accelerated carbonation of reactive MgO cements.* Advances in Cement Research, 2007. **19**(2): p. 67-79.
41. Bernard, E., et al., *Effect of carbonates on the formation of magnesium silicate hydrates.* Materials and Structures, 2022. **55**(7): p. 183.
42. Dung, N.T. and C. Unluer, *Development of MgO concrete with enhanced hydration and carbonation mechanisms.* Cement and Concrete Research, 2018. **103**: p. 160-169.
43. Shah, V. and A. Scott, *Use of kaolinite clays in development of a low carbon MgO-clay binder system.* Cement and Concrete Research, 2021. **144**: p. 106422.
44. Bernard, E., et al., *Effect of aluminate and carbonate in magnesia silicate cement.* Cement and Concrete Composites, 2023. **139**: p. 105010.
45. Bernard, E., B. Lothenbach, and D. Rentsch, *Influence of sodium nitrate on the phases formed in the MgO-Al2O3-SiO2-H2O system.* Materials & design, 2021. **198**: p. 109391.
46. Wei, J., et al., *Reaction products of MgO and microsilica cementitious materials at different temperatures.* Journal of Wuhan University of Technology-Mater. Sci. Ed., 2011. **26**(4): p. 745-748.
47. Zhang, T., L.J. Vandeperre, and C.R. Cheeseman, *Formation of magnesium silicate hydrate (M-S-H) cement pastes using sodium hexametaphosphate.* Cement and Concrete Research, 2014. **65**: p. 8-14.
48. Jia, Y., et al., *Role of sodium hexametaphosphate in MgO/SiO2 cement pastes.* Cement and Concrete Research, 2016. **89**: p. 63-71.
49. Wang, L., et al., *Novel synergy of Si-rich minerals and reactive MgO for stabilisation/solidification of contaminated sediment.* Journal of hazardous materials, 2019. **365**: p. 695-706.
50. Iler, R.K., *The chemistry of silica, Solubility, Polymerization.* Colloid and Surface Properties, and Biochemistry, 1979. **866**.
51. Behnood, A., K. Van Tittelboom, and N. De Belie, *Methods for measuring pH in concrete: A review.* Construction and Building Materials, 2016. **105**: p. 176-188.
52. Suzuki, Y., et al., *Uniformly Porous MgTi2O5 with Narrow Pore-Size Distribution: XAFS Study, Improved In Situ Synthesis, and New In Situ Surface Coating.* Advanced Engineering Materials, 2012. **14**(12): p. 1134-1138.
53. Fertani-Gmati, M. and M. Jemal, *Thermochemistry and kinetics of silica dissolution in NaOH aqueous solution.* Thermochimica acta, 2011. **513**(1-2): p. 43-48.

54. Sheila, D., *Thermal analysis studies on the decomposition of magnesite.* International journal of mineral processing, 1993. **37**(1-2): p. 73-88.
55. Ren, H., et al., *Thermal characterization and kinetic analysis of nesquehonite, hydromagnesite, and brucite, using TG–DTG and DSC techniques.* Journal of Thermal Analysis and Calorimetry, 2014. **115**(2): p. 1949-1960.
56. Hartman, M., et al., *Thermal dehydration of the sodium carbonate hydrates.* Chemical Engineering Communications, 2001. **185**(1): p. 1-16.
57. Vermilyea, D.A., *The dissolution of MgO and Mg (OH) 2 in aqueous solutions.* Journal of the Electrochemical Society, 1969. **116**(9): p. 1179.
58. Tonelli, M., et al., *Effect of phosphate additives on the hydration process of magnesium silicate cements: Thermal and spectroscopic characterization.* Journal of Thermal Analysis and Calorimetry, 2019. **138**: p. 3311-3321.
59. Li, Z., et al., *Performance of magnesium silicate hydrate cement modified with dipotassium hydrogen phosphate.* Construction and Building Materials, 2022. **323**: p. 126389.
60. Zhao, H., et al., *Acceleration of M-S-H gel formation through the addition of alkali carbonates*. 2019, *Proceedings of the 15th International Congress on the Chemistry of Cement (ICCC 2019)* . Sheffield.
61. Thieme, C., *Sodium carbonates.* Ullmann's Encyclopedia of Industrial Chemistry, 2000.
62. Mitsuda, T. and H. Taguchi, *Formation of magnesium silicate hydrate and its crystallization to talc.* Cement and Concrete Research, 1977. **7**(3): p. 223-230.
63. Dewitte, C., et al., *Chemical and Microstructural Properties of Designed Cohesive MSH Pastes.* Materials, 2022. **15**(2): p. 547.
64. Yamamoto, G.-i., et al., *In situ and ex situ studies on thermal decomposition process of hydromagnesite Mg 5 (CO 3) 4 (OH) 2· 4H 2 O.* Journal of Thermal Analysis and Calorimetry, 2021. **144**: p. 599-609.
65. Yamamoto, G.-i., A. Kyono, and S. Okada, *Thermal decomposition process of dypingite Mg5 (CO3) 4 (OH) 2· 5H2O.* Materials Letters, 2022. **308**: p. 131125.
66. Vágvölgyi, V., et al., *Controlled rate thermal analysis of hydromagnesite.* Journal of Thermal Analysis and Calorimetry, 2008. **92**(3): p. 893-897.
67. Oh, K.-R., et al., *Syntheses of MgCO3 and Na2Mg (CO3) 2 through solid-gas reactions mediated by alkali nitrates.* Journal of Solid State Chemistry, 2018. **263**: p. 224-230.
68. Diao, T., et al., *Characterization of DMSO Coordination to Palladium(II) in Solution and Insights into the Aerobic Oxidation Catalyst, Pd(DMSO)2(TFA)2.* Inorganic Chemistry, 2012. **51**(21): p. 11898-11909.
69. Yu, P., et al., *Structure of calcium silicate hydrate (C-S-H): Near-, Mid-, and Far-infrared spectroscopy.* Journal of the American Ceramic Society, 1999. **82**(3): p. 742-748.
70. Hidalgo, A., et al., *Microstructural changes induced in Portland cement-based materials due to natural and supercritical carbonation.* Journal of Materials Science, 2008. **43**: p. 3101-3111.
71. Zhong, Y., et al., *Chemical structure of Si–O in silica fume from ferrosilicon production and its reactivity in alkali dissolution.* Isij International, 2019. **59**(6): p. 1098-1104.

72. Manni, A., et al., *Magnesite and dolomite micro-particles: preparation, physical properties and application in bio-based polymer composite.* Polymer Bulletin, 2021: p. 1-23.
73. Zhang, Z., et al., *Temperature-and pH-dependent morphology and FT− IR analysis of magnesium carbonate hydrates.* The journal of physical chemistry B, 2006. **110**(26): p. 12969-12973.
74. Montes-Hernandez, G., et al., *Rapid precipitation of magnesite microcrystals from Mg (OH) 2-H2O-CO2 slurry enhanced by NaOH and a heat-aging step (from∼ 20 to 90° C).* Crystal growth & design, 2012. **12**(11): p. 5233-5240.
75. Gautier, Q., et al., *Hydromagnesite solubility product and growth kinetics in aqueous solution from 25 to 75 C.* Geochimica et Cosmochimica Acta, 2014. **138**: p. 1-20.
76. Perry, D.L., *Handbook of inorganic compounds*. 2016: CRC press.
77. Bernard, E., *Research progress on magnesium silicate hydrate phases and future opportunities.* RILEM Technical Letters, 2022. **7**: p. 47-57.
78. Debure, M., et al., *Borosilicate glass alteration driven by magnesium carbonates.* Journal of Nuclear Materials, 2012. **420**(1-3): p. 347-361.
79. Khawam, A. and D.R. Flanagan, *Solid-state kinetic models: basics and mathematical fundamentals.* The journal of physical chemistry B, 2006. **110**(35): p. 17315-17328.
80. American Chemical, S. and R. American Chemical Society. Committee on Analytical, *Reagent Chemicals: Specifications and Procedures : American Chemical Society Specifications, Official from January 1, 2006*. An American Chemical Society Publication. 2006: American Chemical Society.
81. Ballirano, P., et al., *Phase transitions in the MgCO2H2O system and the thermal decomposition of dypingite, Mg5 (CO3) 4 (OH) 2· 5H2O: Implications for geosequestration of carbon dioxide.* Chemical Geology, 2013. **340**: p. 59-67.
82. Xing, Z., et al., *Synthesis of MgCO3 microcrystals at 160° C starting from various magnesium sources.* Materials Letters, 2010. **64**(12): p. 1401-1403.
83. Ding, Y., et al., *The role of sodium compound fluxes used to synthesize Gd 2 O 2 S: Tb 3+ by sulfide fusion method.* Journal of Materials Science: Materials in Electronics, 2017. **28**: p. 2723-2730.
84. Ni, X., et al., *A new type of fire suppressant powder of NaHCO3/zeolite nanocomposites with core–shell structure.* Fire safety journal, 2009. **44**(7): p. 968-975.
85. Felmy, A.R., et al., *Reaction of water-saturated supercritical CO2 with forsterite: Evidence for magnesite formation at low temperatures.* Geochimica et cosmochimica acta, 2012. **91**: p. 271-282.
86. Ulrich, M., et al., *Dissolution–precipitation processes governing the carbonation and silicification of the serpentinite sole of the New Caledonia ophiolite.* Contributions to Mineralogy and Petrology, 2014. **167**: p. 1-19.
87. Kursun, H. and U. Ulusoy, *Influence of shape characteristics of talc mineral on the column flotation behavior.* International Journal of Mineral Processing, 2006. **78**(4): p. 262-268.
88. Tang, Q., et al., *Study on pore distribution and formation rule of sepiolite mineral nanomaterials.* Journal of Nanomaterials, 2012. **2012**: p. 2-2.

89. Pokrovsky, O.S., J. Schott, and A. Castillo, *Kinetics of brucite dissolution at 25 C in the presence of organic and inorganic ligands and divalent metals.* Geochimica et Cosmochimica Acta, 2005. **69**(4): p. 905-918.
90. Dumas, A., et al., *Phyllosilicates synthesis: a way of accessing edges contributions in NMR and FTIR spectroscopies. Example of synthetic talc.* Physics and Chemistry of Minerals, 2013. **40**: p. 361-373.
91. Lin, Y., et al., *Thermogravimetric analysis–mass spectrometry (TGA–MS) of hydromagnesite from Dujiali Lake in Tibet, China.* Journal of Thermal Analysis and Calorimetry, 2018. **133**: p. 1429-1437.
92. McIntosh, R.M., J.H. Sharp, and F.W. Wilburn, *The thermal decomposition of dolomite.* Thermochimica Acta, 1990. **165**(2): p. 281-296.
93. Hsieh, K.C. and H. Kinoshita, *The Effect of $NaHCO_3$ and Na_2CO_3 on the Reactivity of $Mg(OH)_2$ and SiO_2 for the Formation of M-S-H gel*. 2021: dissertation submitted to the Department of Materials Science and Engineering, University of Sheffield.
94. Bernard, E., *Magnesium silicate hydrate (MSH) characterization: temperature, calcium, aluminium and alkali.* 2017.
95. Bakera, A.T. and M.G. Alexander, *Use of metakaolin as supplementary cementitious material in concrete, with focus on durability properties.* RILEM Technical Letters, 2019. **4**: p. 89-102.
96. Aiswarya, S., G. Prince Arulraj, and C. Dilip, *A review on use of metakaolin in concrete.* Engineering Science and Technology, 2013. **3**(3): p. 592-597.
97. Mehta, A. and D.K. Ashish, *Silica fume and waste glass in cement concrete production: A review.* Journal of Building Engineering, 2020. **29**: p. 100888.
98. Khan, M.I. and R. Siddique, *Utilization of silica fume in concrete: Review of durability properties.* Resources, Conservation and Recycling, 2011. **57**: p. 30-35.
99. Bernard, E., et al., *Aluminum incorporation into magnesium silicate hydrate (MSH).* Cement and concrete research, 2020. **128**: p. 105931.
100. Geddes, D., *A Study of the Suitability of Metakaolin-based Geopolymers for the Immobilisation of Problematic Intermediate Level Waste.* 2020.
101. Satsangi, P.G. and S. Yadav, *Characterization of PM 2.5 by X-ray diffraction and scanning electron microscopy–energy dispersive spectrometer: Its relation with different pollution sources.* International Journal of Environmental Science and Technology, 2014. **11**: p. 217-232.
102. Al-Jaroudi, S.S., et al., *Use of X-ray powder diffraction for quantitative analysis of carbonate rock reservoir samples.* Powder Technology, 2007. **175**(3): p. 115-121.
103. Booster, J.L., et al., *Characterization of hydroxyl-bearing magnesium fluoride containing physically bound water.* Powder Diffraction, 2002. **17**(2): p. 112-118.
104. Miyata, S., *The syntheses of hydrotalcite-like compounds and their structures and physico-chemical properties—I: the systems Mg 2+-Al 3+-NO 3−, Mg 2+-Al 3+-Cl−, Mg 2+-Al 3+-ClO 4−, Ni 2+-Al 3+-Cl− and Zn 2+-Al 3+-Cl−.* Clays and Clay Minerals, 1975. **23**: p. 369-375.
105. Provis, J.L., *Alkali-activated materials.* Cement and concrete research, 2018. **114**: p. 40-48.

106. Vespa, M., et al., *Structural characterisation of magnesium (sodium) aluminium silicate hydrate (M-(N)-ASH) phases by X-ray absorption near-edge spectroscopy.* Applied Geochemistry, 2020. **123**: p. 104750.
107. Vandeperre, L.J., M. Liska, and A. Al-Tabbaa, *Microstructures of reactive magnesia cement blends.* Cement and Concrete Composites, 2008. **30**(8): p. 706-714.
108. Vandeperre, L.J., M. Liska, and A. Al-Tabbaa, *Hydration and mechanical properties of magnesia, pulverized fuel ash, and portland cement blends.* Journal of materials in civil engineering, 2008. **20**(5): p. 375-383.
109. Dung, N.T. and C. Unluer, *Improving the carbonation of reactive MgO cement concrete via the use of NaHCO 3 and NaCl.* Journal of Materials in Civil Engineering, 2018. **30**(12): p. 04018320.
110. Geng, H., et al., *Effect of pre-dispersing metakaolin in water on the properties, hydration, and metakaolin distribution in mortar.* Frontiers in Materials, 2019. **6**: p. 99.
111. Yahyaoui, R., et al., *Synthesis, characterization and combined kinetic analysis of thermal decomposition of hydrotalcite (Mg6Al2 (OH) 16CO3· 4H2O).* Thermochimica Acta, 2018. **667**: p. 177-184.
112. Swanson, E.J., et al., *Directed precipitation of hydrated and anhydrous magnesium carbonates for carbon storage.* Physical Chemistry Chemical Physics, 2014. **16**(42): p. 23440-23450.
113. Tran, H.M. and A. Scott, *Strength and workability of magnesium silicate hydrate binder systems.* Construction and Building Materials, 2017. **131**: p. 526-535.
114. Aïtcin, P.-C., et al., *Retardation effect of superplasticizer on different cement fractions.* Cement and Concrete Research, 1987. **17**(6): p. 995-999.
115. Sonat, C. and C. Unluer, *Development of magnesium-silicate-hydrate (M-S-H) cement with rice husk ash.* Journal of Cleaner Production, 2019. **211**: p. 787-803.
116. Ojovan, M.I. and W.E. Lee, in *An Introduction to Nuclear Waste Immobilisation (Second Edition)*. 2014, Elsevier: Oxford.